PL-TR-96-2294

INVESTIGATION OF Lg BLOCKAGE AND THE TRANSPORTABILITY OF REGIONAL DISCRIMINANTS IN THE MIDDLE EAST

Douglas Baumgardt

ENSCO, Inc
5400 Port Royal Road
Springfield, VA 22151-2388

11 November 1996

Scientific Report No. 1

19970422 101

This technical report has been reviewed and is approved for publication.

DELAINE R. REITER
Contract Manager
Earth Sciences Division

JAMES F. LEWKOWICZ
Director
Earth Sciences Division

DISCLAIMER NOTICE

THIS DOCUMENT IS BEST QUALITY AVAILABLE. THE COPY FURNISHED TO DTIC CONTAINED A SIGNIFICANT NUMBER OF COLOR PAGES WHICH DO NOT REPRODUCE LEGIBLY ON BLACK AND WHITE MICROFICHE.
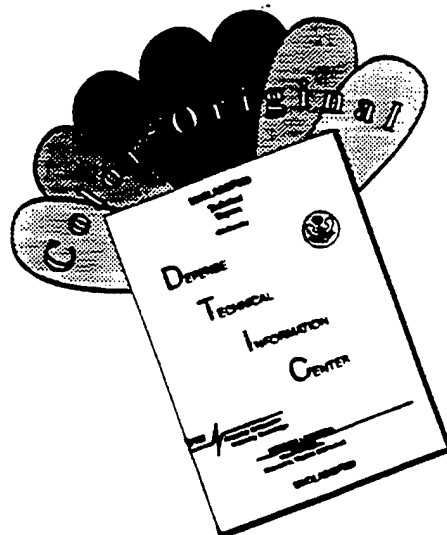
REPORT DOCUMENTATION PAGE

Form Approved
CMB No. 0704-0188

1. AGENCY USE ONLY (Leave Blank)	2. REPORT DATE 11 November 1996	3. REPORT TYPE AND DATES COVERED Scientific No. 1

4. TITLE AND SUBTITLE

Investigation of Lg Blockage and the Transportability of Regional Discriminants to the Middle East

6. AUTHOR(S)

Douglas Baumgardt

5. FUNDING NUMBERS

PE 69120H

PR DENN TA GM WU AQ

F19628-95-C-0203

7. PERFORMING ORGANIZATION NAME(S) AND ADDRESS(ES)

ENSCO, Inc.
5400 Port Royal Road
Springfield, VA 22151-2388

8. PERFORMING ORGANIZATION REPORT NUMBER

9. SPONSORING/MONITORING AGENCY NAME(S) AND ADDRESS(ES)

Phillips Laboratory - Monitoring
29 Randolph Road
Hanscom AFB, MA 01731-3010

Contract Manager: Delaine Reiter/GPE

10. SPONSORING/MONITORING AGENCY REPORT NUMBER

PL-TR-96-2294

11. SUPPLEMENTARY NOTES This research was sponsored by the Department of Energy, Office of Non-Proliferation & National Security, Washington, DC 20585

12a. DISTRIBUTION/AVAILABILITY STATEMENT

Approved for public release; distribution unlimited

12b. DISTRIBUTION CODE

13. ABSTRACT *(Maximum 200 words)*

To investigate nuclear explosion monitoring in the Middle East, the characteristics of regional phase propagation and regional discriminants have been investigated for events and propagation-paths in Israel, Jordan, Lebanon, Syria, Egypt, and Iran. Mostly earthquake recordings from stations in the Middle East, including Iranian Long Period Array (ILPA) and Mednet and IRIS stations, have been studied with the goal of relating regional characterization of events in the Middle East to discrimination in the region. Pg and Lg propagation blockages have been noted for paths crossing the Levantine Basin of the Eastern Mediterranean and the Southern Caspian Basin north of Iran. However, Pn and Sn phases are often well observed for these paths which suggests that there may be a shear-wave energy balance for seismic events which is conserved. Examples of attenuated Sn have been observed for the Red Sea region and may be correlated with high heatflow in this region. Analysis of Zagros thrust events in Iran recorded at two stations show significant variations in Pn/Lg ratios that may either be caused by propagation or source radiation-pattern effects. Comparison of regional P/S ratios for Middle-East earthquakes with those in other regions shows that Pn/Sn and Pn/Lg ratios are interchangeable as discriminant features and usually can discriminate Middle Eastern earthquakes from mine blasts and nuclear explosions in other regions of Eurasia. Future studies should address the regional tectonic effects on regional discriminants to support inter-regional comparisons with explosions outside the Middle East, since it is unlikely the calibration explosions will be forthcoming within the Middle East.

14. SUBJECT TERMS

Seismic , Discrimination, Earthquakes, Nuclear Explosions, Lg Blockage, Sedimentary Basins, Attenuation, Heatflow, Middle East

15. NUMBER OF PAGES
84

16. PRICE CODE

17. SECURITY CLASSIFICATION OF REPORT Unclassified	18. SECURITY CLASSIFICATION OF THIS PAGE Unclassified	19. SECURITY CLASSIFICATION OF ABSTRACT Unclassified	20. LIMITATION OF ABSTRACT SAR

NSN 7540-01-280-5500

Standard Form 198 (Rev. 2-89)
Prescribed by ANSI Std. Z39-18
298-102

TABLE OF CONTENTS

1. INTRODUCTION

1.1 Issues in Discriminant Transportability

Recent seismological discrimination studies (e.g., Ryall, et al, 1996; Baumgardt, 1995) have demonstrated that certain waveform feature measurements can be used to identify very small seismic events. The most commonly studied discriminant is the regional *P/S* amplitude ratio, where *P* can be *Pn* or *Pg* and *S* is typically *Lg* or *Sn*. Generally, these ratios are smaller for earthquakes than nuclear explosions. Mine blasts tend to have higher ratios than earthquakes but not as high as nuclear explosions. Sometimes, "earthquake like" *Pn/Lg* ratios have been observed for mine blasts (e.g., Baumgardt, 1995).

Small event discrimination with waveform discriminants will be a required capability for monitoring a small or zero-yield Comprehensive Test Ban Treaty (CTBT). Typically, such events will have seismic local magnitudes as low as 2.5 that may be too small to be recorded teleseismically at a large number of stations, and perhaps only one or two stations will detect the event at regional distances. Because small events may have poorly constrained locations and depths due to the small number of detecting stations, waveform features from single-station recordings at regional distances may be the only information available for the identification of small events.

The approach to worldwide event identification in the development of the Intelligent Seismic Event Identification System (ISEIS) (Baumgardt, et al, 1991) has been to systematically measure many different waveform features for seismic events recorded in different regions of the world and to save the features in an Oracle database. Then, when new events from these regions or new regions of the world need to be identified, the old features from the previously studied known events can be called up from the database and compared with the new features.

This method of "inter-region" event feature comparisons for event identification is usually considered to be severely affected by differences in the geology of the propagation paths and the tectonics of the regions and

1

perhaps site effects under the different sensors. The issue of "discriminant transportability" (Baumgardt and Der, 1995; Baumgardt, 1995) concerns whether or not one can use discriminants trained in one region, recorded at seismic stations in that region, to identify events in other regions with perhaps completely different stations. In spite of the differences in stations and propagation paths, inter-region comparisons have revealed strong similarity of regional P/S amplitude ratio waveform features between events of the same source type but in different regions recorded at different stations. This indicates that these discriminants may be very robust when transported from one region to another.

This report describes continued investigation of discriminant transportability with application to seismic discrimination in the Middle East. Understanding regional phase propagation and discriminants for seismic events in the Middle East poses a major challenge to developing the capability for monitoring the Comprehensive Test Ban Treaty (CTBT) and Non-Proliferation Treaty (NPT). Seismic monitoring of events in the Middle East may be more complicated than in other regions because of two difficulties: (1) The extreme geologic and tectonic complexity of regional propagation paths in the region needs to be understood and calibrated in order to use seismic waveform features for discrimination. (2) Although earthquakes occur in abundance in the tectonic belts of the Middle East, discrimination studies in this region are necessarily limited by the paucity of known explosive sources in the region.

The approach to the first problem has been to assemble a database of seismic events, consisting mostly of earthquakes, for the key countries of interest (Egypt, Jordan, Israel, Iran, Iraq) and to investigate the characteristics of regional phase propagation in the region. Of key interest in this study is the variation of excitation of high-frequency regional shear waves, principally Sn and Lg, relative to regional compressional waves, mainly Pn and Pg. Variations and anomalies in these features are interpreted in terms of geological characteristics of the propagation path. Of particular interest has been the observation of the blockage of Lg, a key regional phase for a number of different discriminants.

To address the second problem, seismic waveform-feature discriminants have been extracted, using the ISEIS discrimination system, for presumed earthquakes recorded at stations in the Middle East. As much as possible, these features are compared with those for known or presumed explosions in the region. However, because only limited numbers of such events, in particular, nuclear explosions, are available for the region, the earthquake features must be compared with the same features for explosions in other regions which have been stored in the ISEIS database.

1.2 Data Sources

The data-collection effort for this study has primarily focused on earthquakes in Israel, Jordan, Egypt, Iran, and Iraq. An Oracle database of seismic waveforms has been collected from the following data sources:

(1) Iranian Long-Period Array (ILPA) - This array operated during the 1970s and included broadband borehole KS36000 seismometers (Texas Instruments, 1977). A database assembled by Lori Grant of Multimax (Grant et al, 1996), and analyzed by Flori Ryall to identify the principal regional phases, has been imported into the ISEIS database. The initial focus has been on seismic events in the Caspian region, in particular, propagation paths which cross known Lg-blockage region of the South Caspian Basin. The characteristics of other paths within and around Iran have also been investigated.

(2) Single station data from Mednet and IRIS Stations - The key Mednet station of interest has been Kottamya, Egypt (KEG) because of its proximity to the planned location of the LUXESS array in eastern Egypt. This station is in an advantageous location to record events in many different regions of interest in the Middle East. Signals at this station are also compared with those recorded at the IRIS station at Alibek, Turkmenistan (ABKT) for common events in the Zagros Mountains region of Iran.

(3) Previously computed data for Scandinavian Arrays and WMQ - All the events studied in the Middle East are earthquakes. For discrimination studies, the features for these events can be compared with those previously computed for mine blasts in Scandinavia, recorded at the ARCESS array, and earthquakes in China and nuclear explosions in Russia recorded at Urumchi (WMQ).

1.3 Report Overview

Section 2 reviews the problem of *Lg* blockage, with an analysis of data from the Caspian region recorded at the IR1 sensor of ILPA. First, observations of *Lg* blockage in the Barents Sea are discussed, which Baumgardt (1991) originally explained as being caused by "sedimentary basin capture" of the *Lg* shear waves within the Barents sedimentary basin. The ready availability of crustal-structure data for Eurasia from geographic information systems (GIS) (Fielding et al, 1993) allows comparative interpretation of individual propagation-path cross sections for blocked- and unblocked-*Lg* propagation paths, and this analysis clearly shows that the perturbation of the crustal "granitic layer" by sedimentary basins in the continents results in partial and complete *Lg* blockage. This same analysis is also applied to propagation paths across the Caspian Sea to the IR1 sensor, which shows that the "sedimentary basin capture" mechanism may explain the well-known *Lg* blockage in the Caspian Sea region.

Section 3 presents the result of the characterization study of Middle Eastern earthquakes recorded at the Mednet station at Kottyama, Egypt (KEG) and Alibek, Turkmenistan (ABKT). Earthquakes in the Jordan/Dead Sea transform region are well recorded at the KEG station and augment the local database for Galilee for stations inside Israel (Grant et al, 1996). This study of these events reveals the presence of *Lg* blockage in the Levantine sedimentary basin of the Mediterranean Sea and an apparent tradeoff in the blockage of *Sn* and *Lg*. Also, earthquakes in the Gulf of Aqaba and Sinai are well recorded at KEG. Gulf of Aqaba earthquakes show evidence of water-column reflections which may be considered as another method for identifying shallow earthquakes beneath water-covered areas. Events to the south in Ethiopia and in the Red Sea region are also recorded at KEG but with limited bandwidth interpreted in terms of high heatflow in the region. Finally, recordings of *Pn* and *Lg* at KEG and ABKT are compared for common events in the Zagros Mountains of Iran, which reveal interesting patterns in *Pn/Lg* ratio which may be caused by either propagation path differences or source mechanism radiation pattern effects.

Finally, Section 4 presents the summary and conclusions, including plans for future research.

2. CONTINUED INVESTIGATION OF LG BLOCKAGE

Lg "blockage" is defined as the sudden disappearance of the phase along a particular propagation path that is not explainable by anelastic attenuation or geometric spreading. The regional phase, *Lg*, propagates in the continents and is blocked when it crosses continent/ocean margins (Zhang and Lay, 1995) and does not propagate in ocean basins. However, *Lg* also has been known to suddenly disappear in certain continental regions (Baumgardt, 1990; Baumgardt, 1991). It is important to understand the causes of *Lg* blockage in continental cratons because of the importance of the regional phase in test-ban treaty monitoring, particularly in seismic event identification.

To explain *Lg* blockage in the continents, lateral heterogeneities in crustal structure, particularly variations in the thickness of the crust (e.g., Kennett, 1986), presence of oceanic crust (e.g., Kadinski-Cade, et al, 1981), or strong anelastic attenuation (Ruzaikin, et al, 1977; Ni and Barazangi, 1983) are often invoked. This section presents observational evidence that high-frequency *Lg* may propagate primarily in the upper part of the continental crust and that lateral heterogeneities in shallow structure can explain *Lg* blockage. In the case of the Eurasian continental craton, *Lg* blockages appear to be associated with deep sedimentary basins (Baumgardt, 1991). As an explanation for *Lg* blockage in sedimentary basins, Baumgardt (1991) proposed an explanation called **basin capture**. Ray tracing experiments show that much of the *Lg* wavetrain can be modeled as SV type waves reverberating at near critical angles in the continental granitic layer. If the granitic layer is partly or completely replaced by an enclosed low-velocity sedimentary basin, the SV waves, composing *Lg*, coming out of the granitic layer into the basin are refracted to steeper angles and reverberate many times in the basin. This extends the *Lg* wave train, delays the arrivals, and essentially kills them by attenuation caused by the multiple bounces in the basin and possibly low-Q in the sediments. *Lg* blockage of this kind has been observed in the Barents Sea, the north and south Caspian Basins, the Timan-Pechora Basin, and basins around the Urals (Baumgardt, 1991).

Two regions of *Lg* blockage in Eurasia, the Barents Sea Basin and Caspian Basins, are studied and interpreted in terms of the sedimentary basin blockage model of Baumgardt (1991) as an explanation for *Lg* blockage in these regions. The method is to examine crustal cross sections, derived from the on-line GIS databases for Eurasia made available by Cornell (Fielding, et al, 1992), for the blocked and unblocked paths, and to look for differences between the two paths. This method assumes that the primary energy of regional phases propagates in the diametral plane from source to receiver and that the crustal cross sections along the source-receiver path, obtained from the GIS databases, are accurate representations of the crustal structure along these paths. This analysis shows that the main difference between blocked and unblocked paths for many of these regions resides in the upper crust, and *Lg* blockage in these continental regions can be explained by shallow crustal heterogeneity.

2.1 *Lg* Blockage in the Barents Sea Revisited

The *Lg* blockage the Barents Sea for nuclear explosions on Novaya Zemlya, recorded in Norway, was first identified by Baumgardt (1990) and studied in more detail by Baumgardt (1991). To demonstrate the blockage explicitly, two paths are compared in the region from a Kola Peninsula Soviet PNE detonated in the 1972 and recorded at the NORSAR array with a Novaya Zemlya explosion detonated in 1988 recorded at the ARCESS array. **Figure 1(a)** shows the propagation paths for these two explosions superimposed on an image map basement depth produced using data from the Cornell GIS database for Eurasia (Fielding et al, 1992). **Figure 1(b)** shows the cross sections for the two paths.

These two paths are very similar in that they are in the same region and cover about the same distance. There are some variations in Moho depths in the region in that the crust thickens by about 10 km along the Kola-to-NORSAR path. The most significant difference in the two paths, as most evidenced in **Figure 1(b)**, is the presence of the Barents Sea in the path from Novaya Zemlya to ARCESS. The Barents Sea contains a water layer and an enclosed sedimentary basin with sediment thicknesses reaching 15 to 20 km.
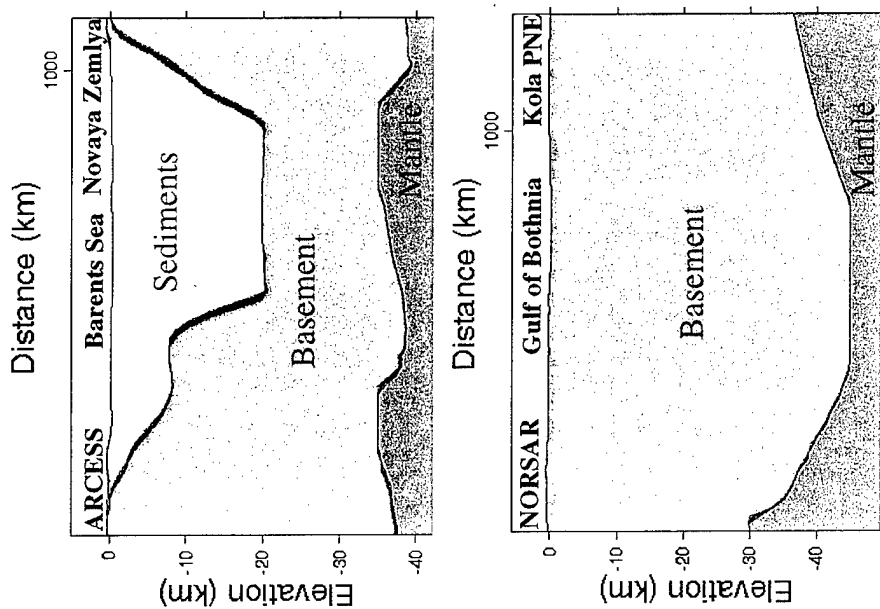
Figure 1: Comparison of NZ-ARCESS and Kola-NORSAR propagation paths. (a) Great circle propagation paths plotted on a contour image of sediment thickness map for Scandinavia. (b) Crustal cross sections for the NZ to ARCESS path (top) and the Kola-PNE to NORSAR path.

Figure 2 shows a comparison of the ARCESS (top) and NORSAR (bottom) waveforms for the two events. Both traces have been bandpass filtered from 0.6 to 3.0 Hz to eliminate noise and differences in the NORSAR and ARCESS recording instrumentation. The ARCESS recording has no apparent *Lg* at the expected arrival time for the 3.5 km/sec *Lg*. However, a strong *Lg* was recorded from the Kola Peninsula PNE.

Figure 3 compares the same two waveforms but after filtering in the 6 to 8 Hz band. This comparison reveals that the *Sn* is well recorded at high frequency coming from the Novaya Zemlya nuclear explosion recorded at ARCESS but considerably weaker for the Kola PNE recording at NORSAR. The strength of the *Sn* waves from Novaya Zemlya at high frequency is remarkable given the fact that the event is a nuclear explosion, although the *Pn* energy is still much greater. For example, in a study of the 31 December 1993 Novaya Zemlya event (Baumgardt, 1993; Ryall, et al, 1996), Novaya Zemlya explosions could be easily discriminated from earthquakes and mine blasts because of their high *Pn/Sn* ratios at high frequency. In theory, nuclear explosions are pure explosive sources and should excite little intrinsic shear wave energy other than that derived from *P*-to-*S* mode conversions. The large shear waves produced by the Novaya Zemlya nuclear explosions may have resulted from induced tectonic effects, such as block motions or tectonic release, or from strong P-to-S mode conversions from the complex topography of the island. Later, an alternative shear-wave energy balance hypothesis will be discussed as a possible cause of large *Sn* waves for paths where *Lg* is blocked.

The cause of the *Lg* blockage for Novaya Zemlya explosions may be found in the comparison of the crustal characteristics for the blocked and the unblocked paths. **Figure 1(b)** shows a comparison of the crustal cross sections for the two paths taken from the Cornell database (Fielding, et al, 1993). The path from Novaya Zemlya to ARCESS, shown at the top, crosses the Barents Sea which contains deep sediments with depths reaching 20 km. The path from the PNE to NORSAR crosses a relatively uniform crust although the Moho deepens by about 15 km. As originally suggested by Baumgardt (1990), the *Lg* blockages commonly observed from Novaya

Comparison of December 4, 1988 NZ and September 4, 1972 Kola Explosions
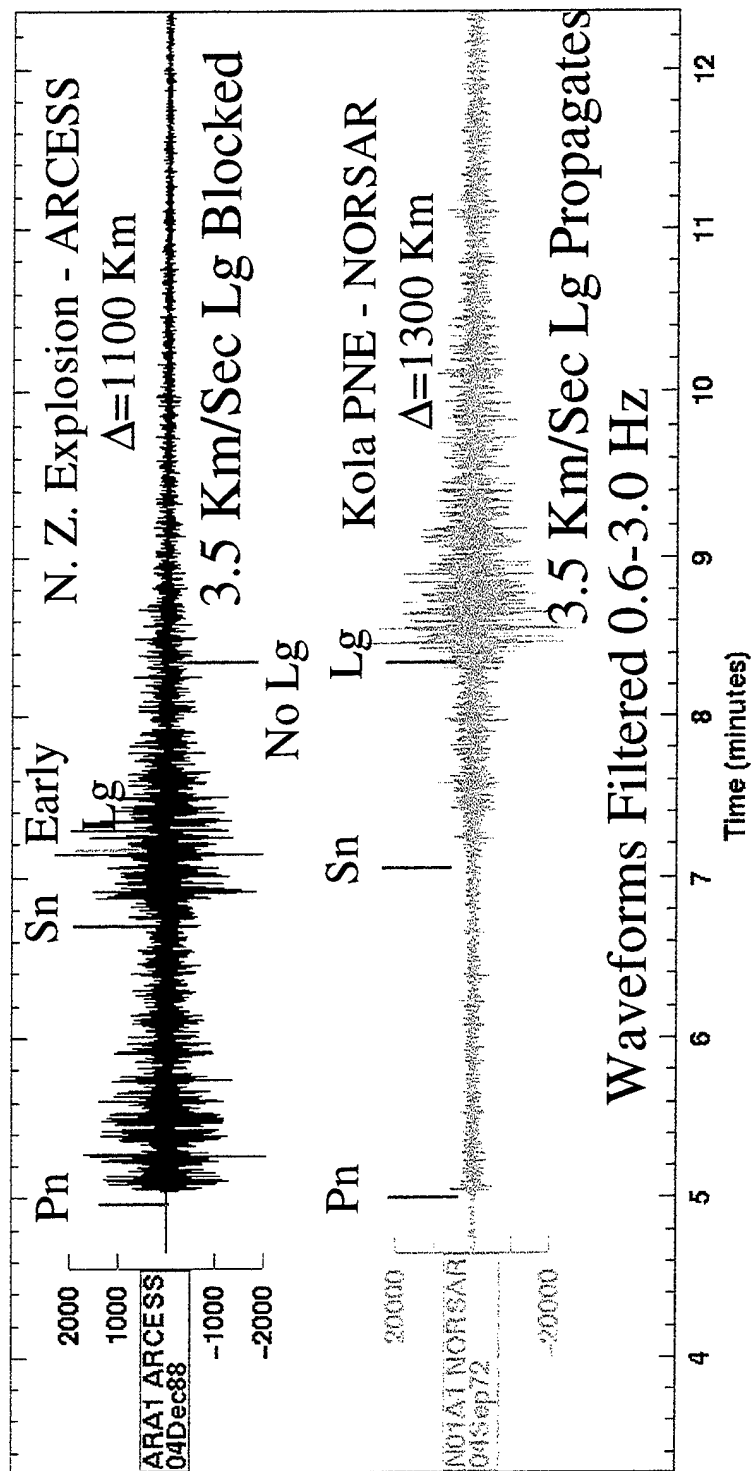
Figure 2: Comparison of waveforms, filtered in the 0.6 to 3.0 Hz band, for the NZ-ARCESS (top) and Kola PNE-NORSAR paths shown in Figure 1. The top plot shows that the Lg is apparently blocked along the path that crosses the Barents Sea. The bottom plot shows that in Lg wave appears to propagate efficiently across Norway.
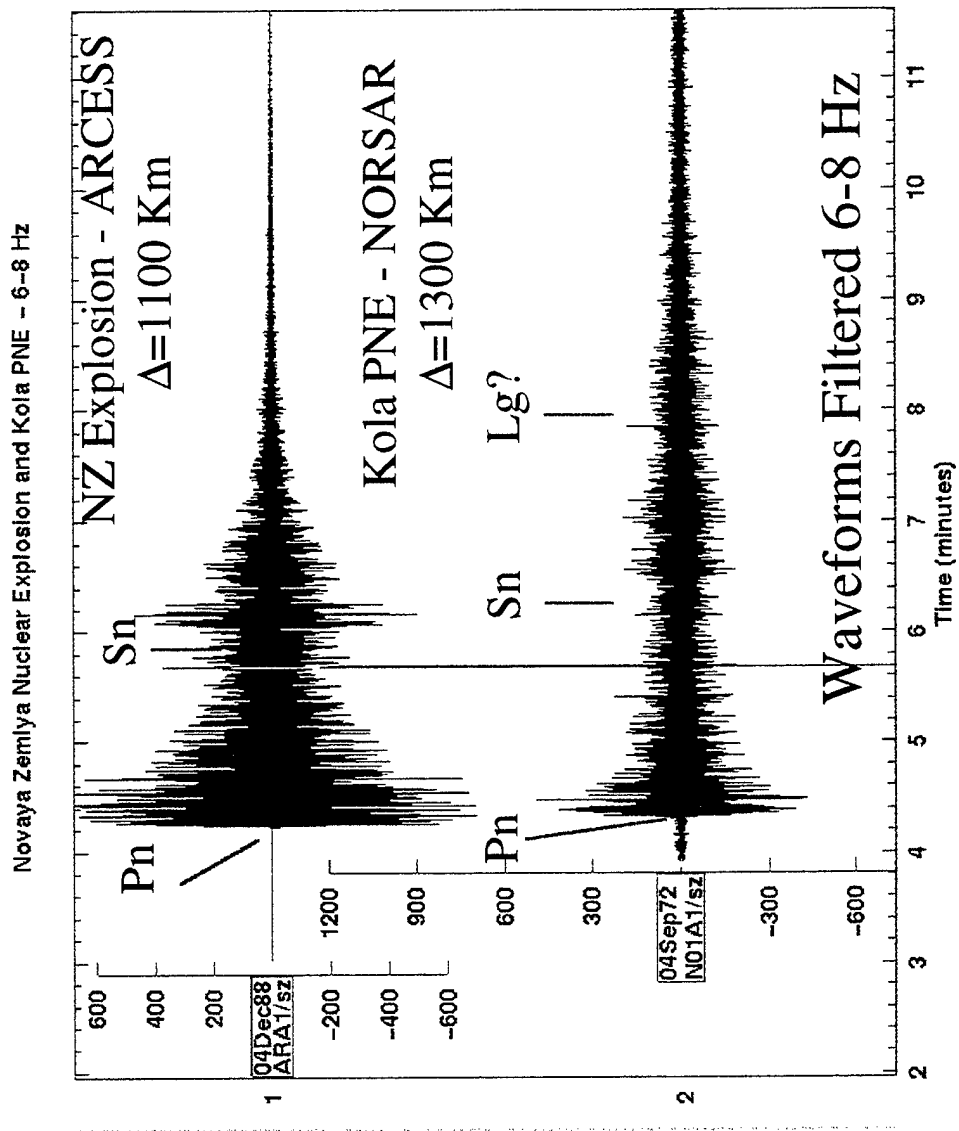
Figure 3: Same waveforms as in Figure 1 except that they have been filtered in the 6 to 8 Hz band. Notice that at high frequency, Sn is strong from the NZ event but weak from the Kola PNE.

Zemlya at ARCESS appear to be related to the presence of the sedimentary basin.

Baumgardt (1991) showed how this blockage could result using raytracing experiments. Teng and Kuo (1993) have modeled the blockage by means of finite element method to synthesize full-wave Lg waveforms. They showed that an enclosed basin of low velocity sediments in the granitic layer of the crust was sufficient to block Lg. Jih (1995) considered a variety of models, including sedimentary basin/crustal pinchout models like that shown in **Figure 1(b)**, and theoretically demonstrated not only Lg blockage but also the Sn-to-Lg mode conversion (early Lg) which was also observed associated with Lg blockage (Baumgardt, 1991). Therefore, Lg waves will be partially or completely blocked along paths crossing an enclosed basin containing thick low-velocity sediments.

2.2 Caspian-Sea Lg Blockage - Evidence from the ILPA Data Set

A new data set has recently been made available by Lori Grant of Multimax of seismic events recorded at the Iranian Long Period Array (ILPA), for seismic events in the region of the Southern Caspian Sea (Grant et al, 1996). The KS36000 seismometers of ILPA were primarily designed for long-period seismic recording. However, ILPA also recorded in the short-period band to 10 Hz Nyquist (Texas Instruments Report, 1977). This region was previously studied by Sikharulidzhe (1964), as reported by Shishkevish (1979), who observed no propagation of Lg for paths across the central and southern parts of this region. Kadinsky-Cade et al (1981) attributed Lg blockage in this region to the presence of deep oceanic crust in the region. However, the basin-capture idea discussed earlier can also explain the blockage.

Figure 4(a) shows locations of seismic events with Lg propagation paths to ILPA which cross the central and southern Caspian Basin. A record section of vertical component waveforms from the first ILPA channel (IR1) is plotted in **Figure 5**. The 18 December 1978 event, at a distance near 1400 km, is a nuclear explosion in the Azgir region north of

12

Pri Caspian Events Recorded at ILPA – Blocked Lg Paths
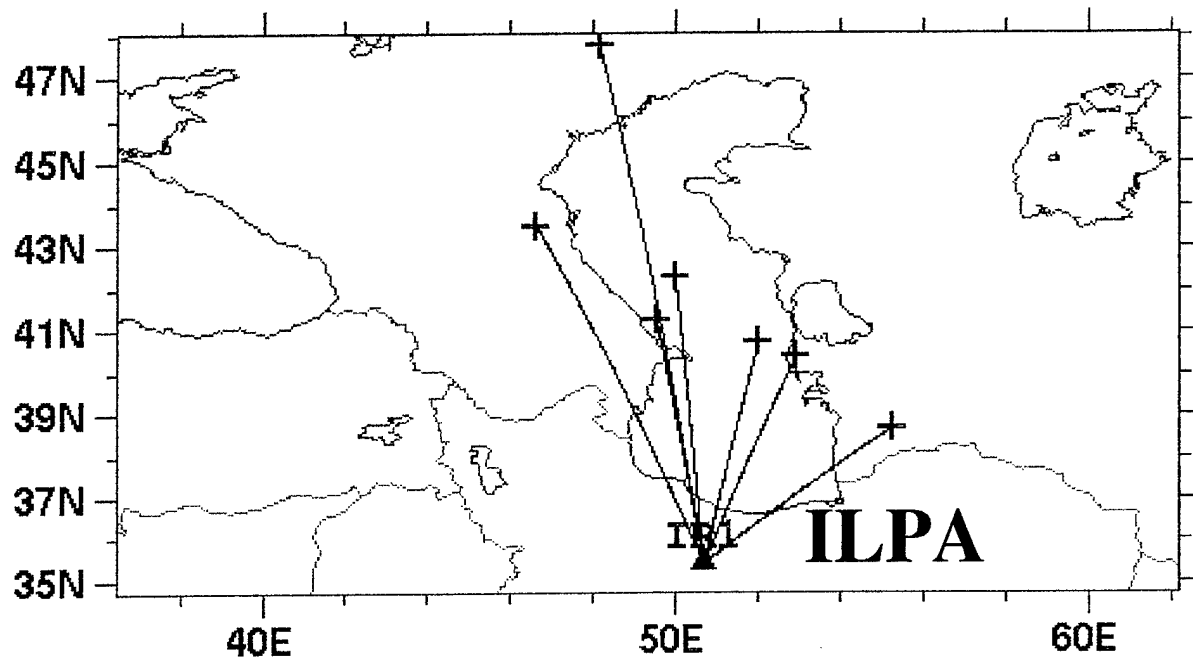
(a)

Caucasus–Black Sea Events Recorded at ILPA – Unblocked Lg Paths
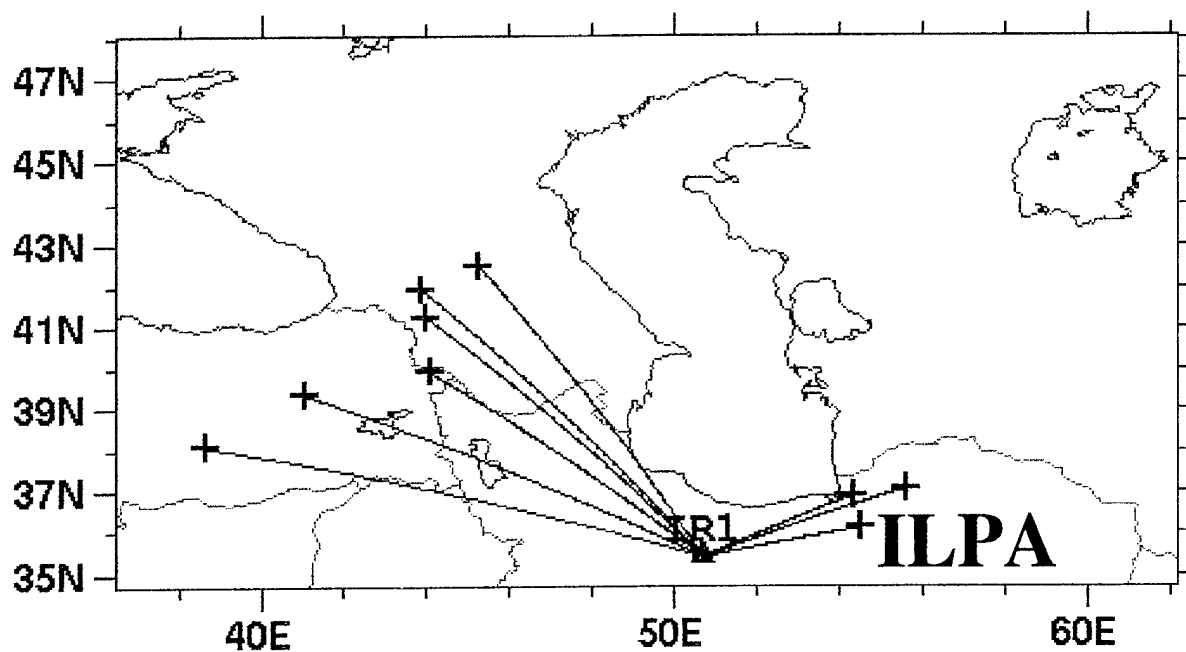
(b)

Figure 4: Maps showing progation paths for events around the Caspian Sea recorded at sensors in the ILPA array. (a) Events whose propagation paths cross the South Caspian Sea Basin. (b) Caucasus and Northern Iran Events whose path do not cross the South Caspian Sea Basin.

13
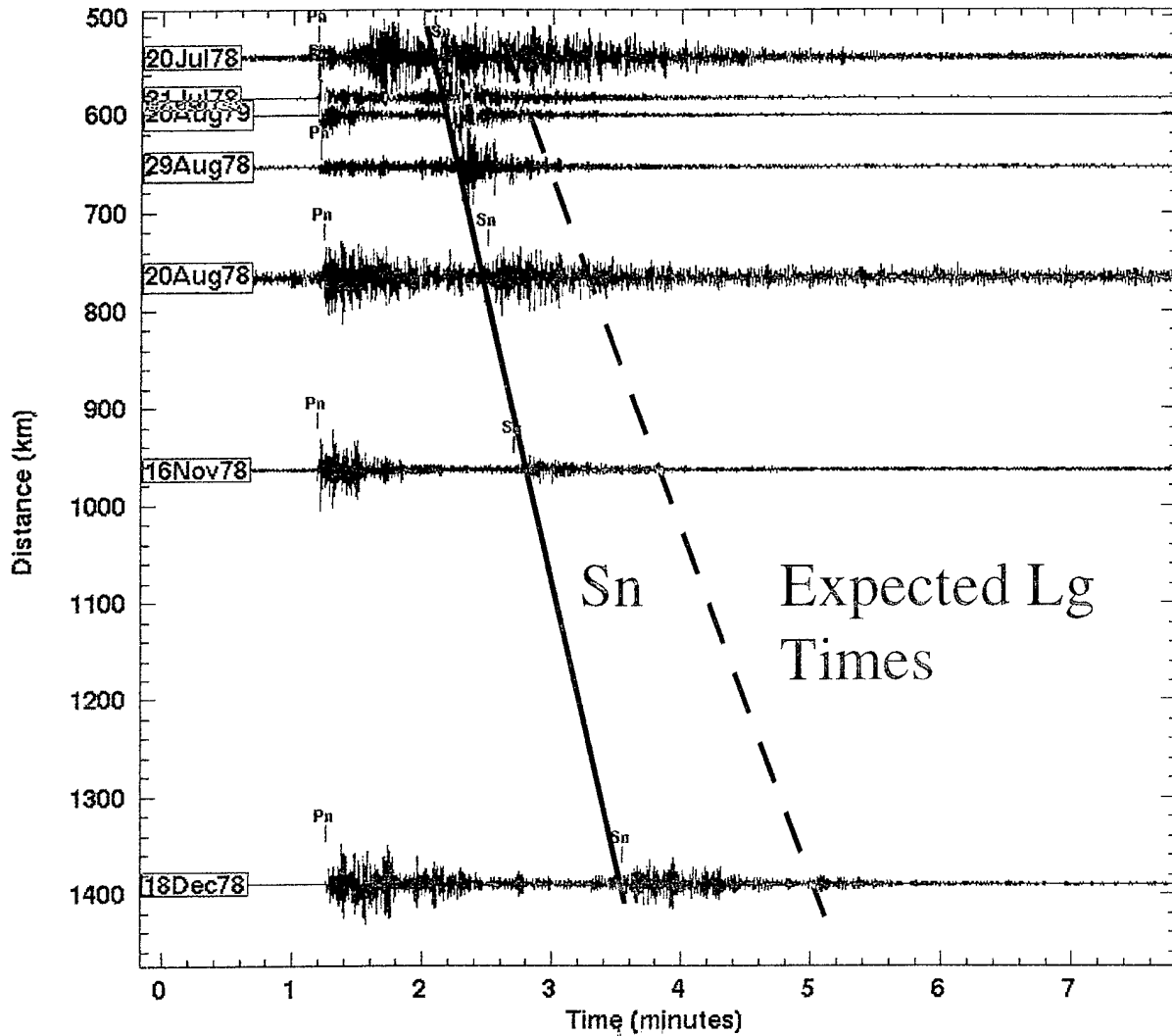
Figure 5: Record section for events whose Lg propagation paths cross the South Caspian Basin. For these events, Pg and Lg are evidently blocked but Pn and Sn are well observed. Note that the 18 December 1978 event at the bottom is a known nuclear explosion at Azgir and the 16 November 1978 event may also be an explosion.

the Caspian Sea. Also, the 16 November 1978 event looks explosion-like because it has a large *Pn* wave and a small *Sn* wave, although there is no record that this event is an explosion. The other events appear to be earthquakes because they are located in the Caspian Sea and generally have larger *Sn* waves than *Pn* waves.

The waveforms in **Figure 5** contain *Pn* and *Sn* arrivals. The dashed line in **Figure 5** indicates the expected arrival time of the *Lg* but no clear arrivals are apparent at the indicated time of *Lg*. For these paths, *Lg* propagation has been blocked.

Figure 4(b) shows paths for other events, recorded at ILPA, but which do not cross the Caspian Sea. **Figure 6** shows the record section of the ILPA (IR1) recordings of these events. These waveforms are distinctly different than those in **Figure 5** in that they contain significant energy at the expected arrival time of *Lg*. Also, these events produced much stronger *Pg* and coda waves than the events in **Figure 5**. The greater complexity of these waveforms may be due to the increased complexity of the propagation paths, since many of the paths cross the Caucasus and the thrust belts of northern Iran.

To explore more closely the differences in the blocked and un-blocked paths, **Figure 7** shows a comparison of waveforms for two such events and the crustal cross sections for the two propagation paths. The West Caspian earthquake (16 November 1978) is the event with the blocked path and the South Caucasus earthquake (22 August 1978) is the unblocked path.

Figure 8 shows a black-and-white rendering of a color image of the topography (top), basement depth (middle), and Moho depth (bottom). The white areas on these maps indicate large values. It can be seen clearly that the southern Caspian is underlain by an enclosed sedimentary basin with sedimentary thicknesses approaching 30 km. This region also has thickened crust, to 50 km, as well as the regions of thicker crust to the west and south of the Caspian.

ILPA Recordings of Caucasus–Black Sea Earthquakes – 0.6–4.5 Hz Filter
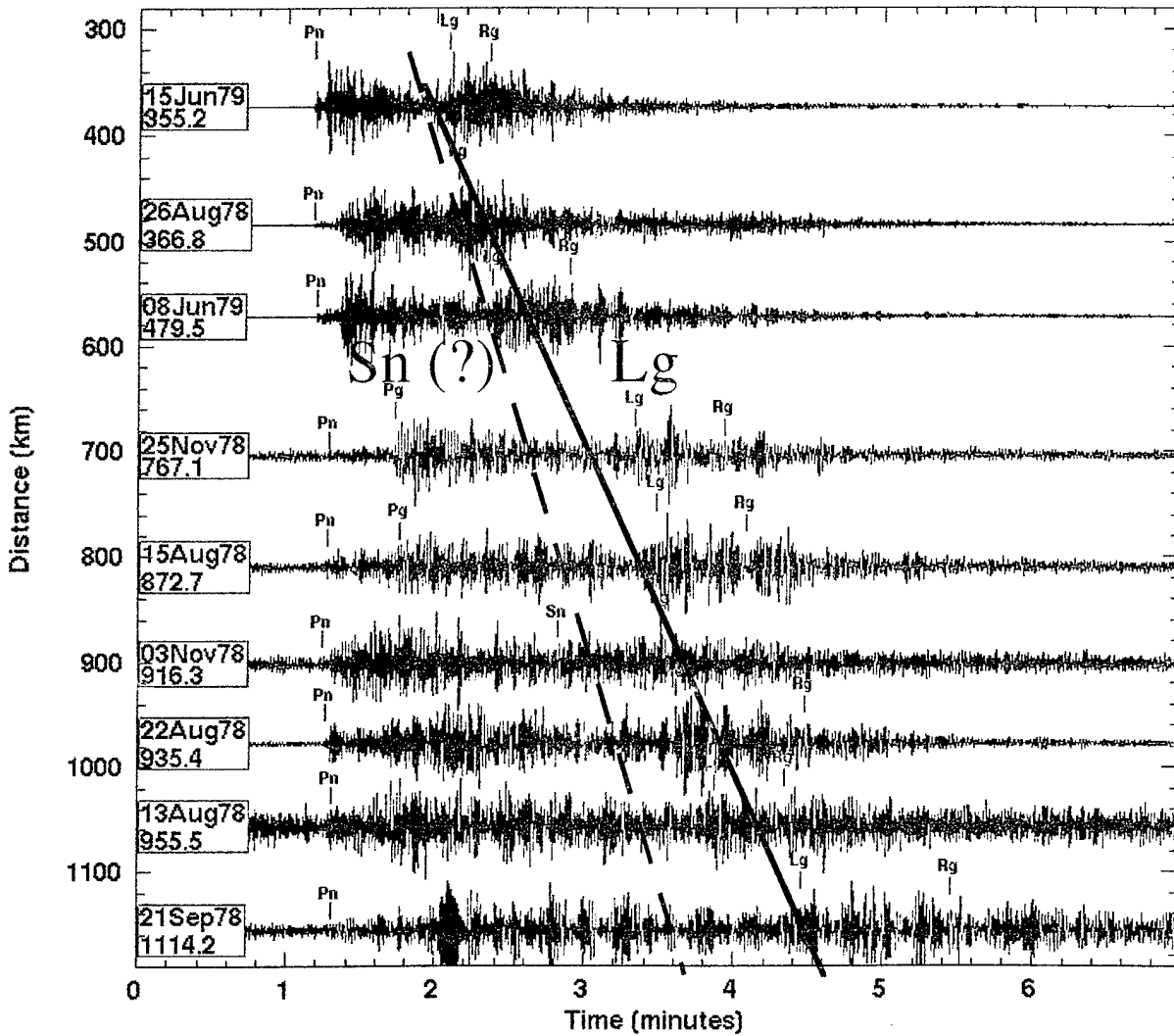
Record Section Aligned to Pn

Figure 6: Record section for events in the Caucasus mountains and Northern Iran whose Lg propagation paths do not cross the South Caspian Basin. For these paths, both Pg and Lg are strong, but Pn is emergent and Sn is usually not oberved.
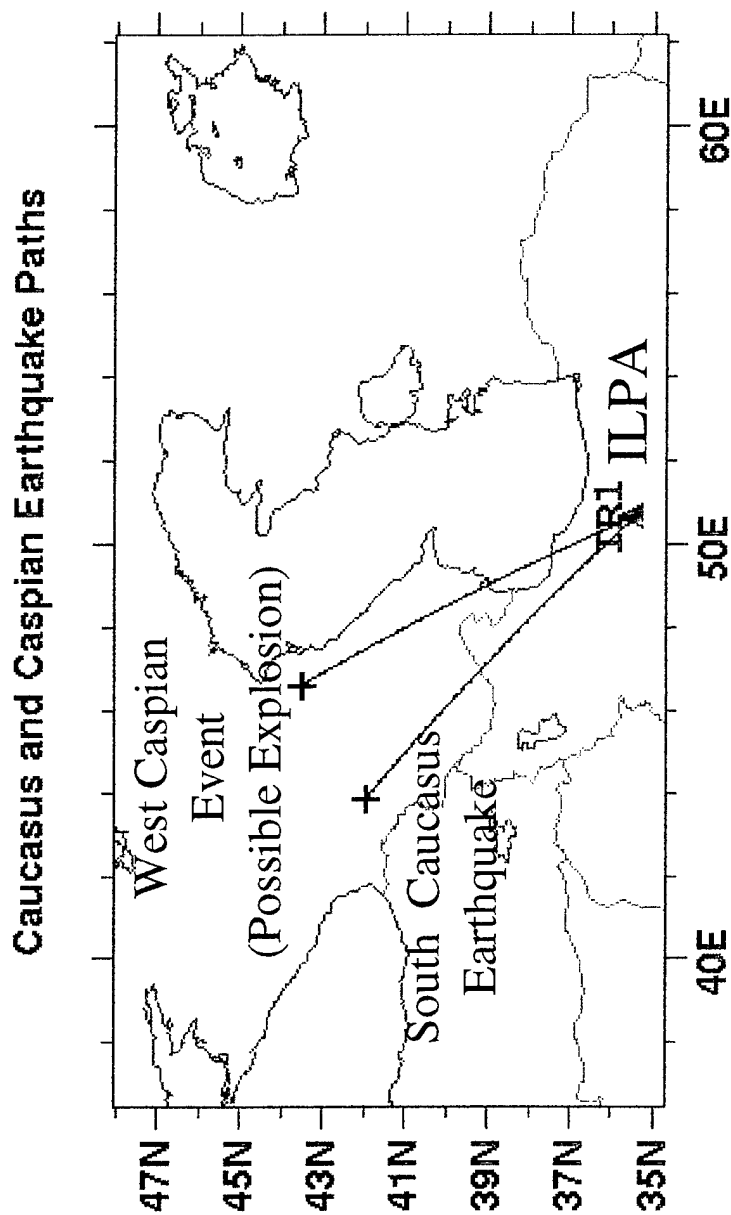
16

Figure 7: Direct comparison of Northern Iran Propagation Paths to ILPA for the blocked (West Caspian event) and unblocked Lg (South Causasus earthquake) propagation paths to ILPA.
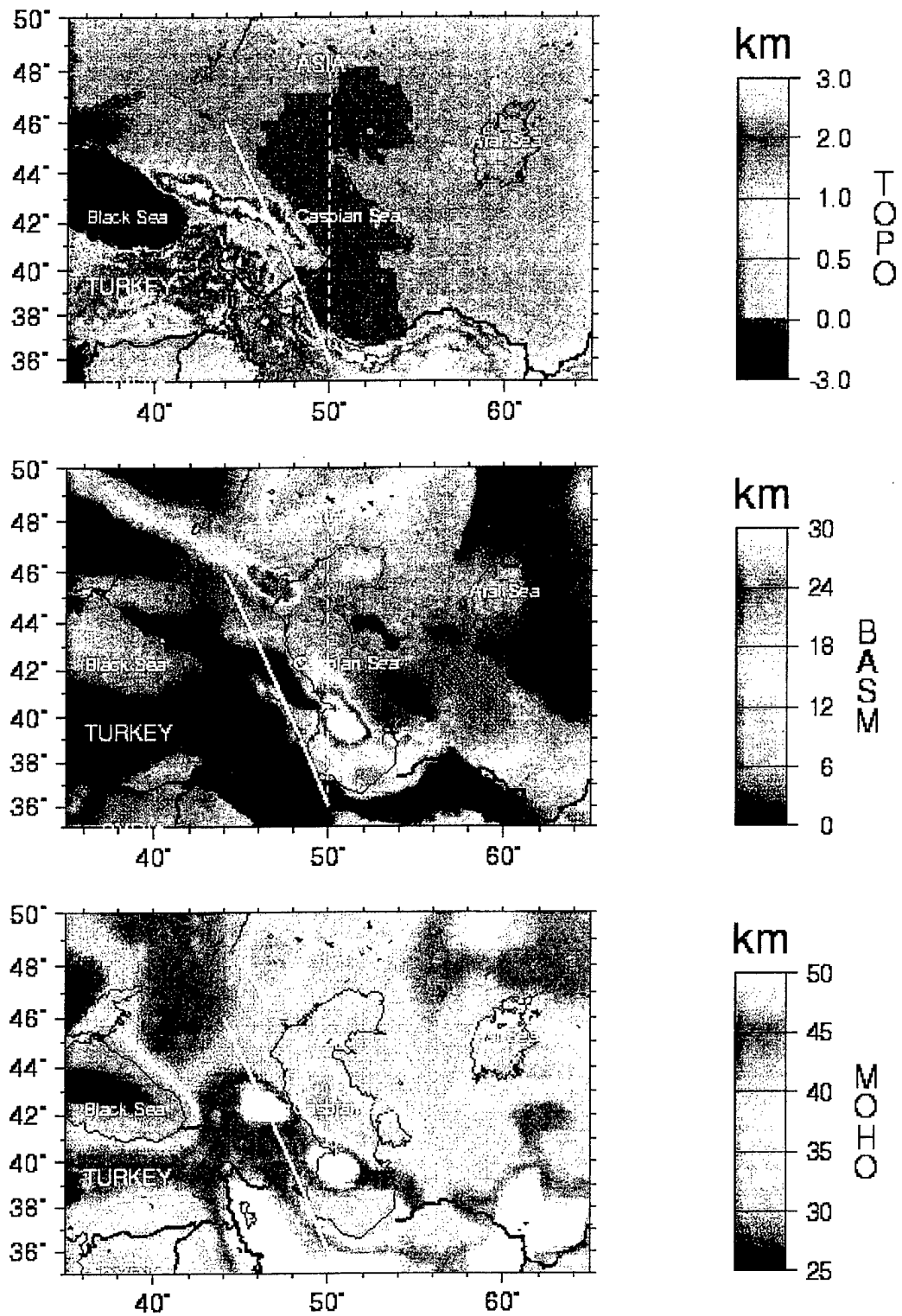
Figure 8: Maps of topography (top), basement depth (middle), and Moho depth (bottom) for the Caspian region. The two lines correspond to the cross section shown in Figure 9.

Figure 9 shows a comparison of the cross sections and waveforms for the blocked and unblocked paths. Note that the blocked path from the West Caspian earthquake just skirts the western edge of the southern Caspian Basin that is an enclosed sedimentary basin, with sediments reaching 12 km thickness in this region. The unblocked path clearly misses the sedimentary basin.

2.3 Caspian Region Earthquakes and Explosions

Finally, the differences between the only known nuclear explosion in this data set, the December 18, 1978 nuclear blast, an earthquake and the unusual November 16, 1978 event in **Figures 6** and **9** will be examined.

Figure 10 shows a bandpass filter analysis applied to the data for the Caucasus Earthquake of August 22, 1978 discussed above. The path for this event is the dashed line shown in **Figure 8**. This event has signals in the unfiltered or low frequency seismograms, but the signals die off quickly with frequency above 3 to 4 Hz. The *Lg* is obviously low frequency, since it does not appear at all on filtered traces above 2 Hz. In contrast, the filtered nuclear explosion, shown in **Figure 11**, has strong signals at frequencies up to the 6-to-8 Hz band. Also, notice that the *Sn* phase has significant energy at frequencies up to 4 to 6 Hz.

Thus, even though *Lg* is blocked along this path, shear-wave energy is clearly produced by the explosion and propagates in the form of *Sn* waves. As was observed in the case of nuclear explosions in Russia (Kola Peninsula and Novaya Zemlya) recorded in Scandinavia at ARCESS, where *Lg* waves are also blocked by a sedimentary basin, large *Sn* signals are apparent at high frequency. However, in contrast to earthquakes, the nuclear-explosion *Pn* amplitude exceeds the *Sn* amplitude at all frequencies but especially at high frequency. So, even for blocked *Lg* paths, nuclear explosions and earthquakes can be discriminated using high-frequency *Pn/Sn* amplitude ratios.

Finally, **Figure 12** shows the bandpass filter analysis applied to the November 16, 1978 event, shown as the "blocked *Lg*" example in **Figure 9**. By all accounts, this event appears to be an earthquake. Two catalogs,
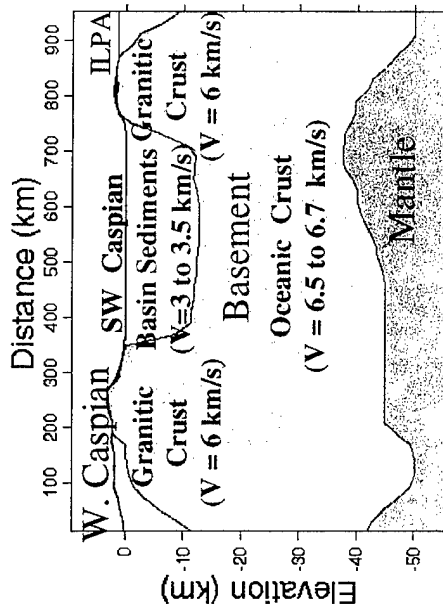
19
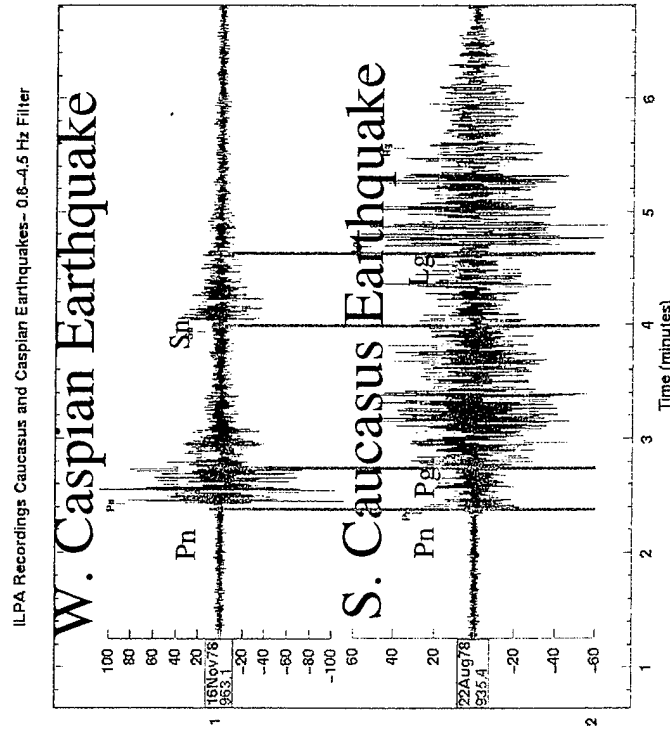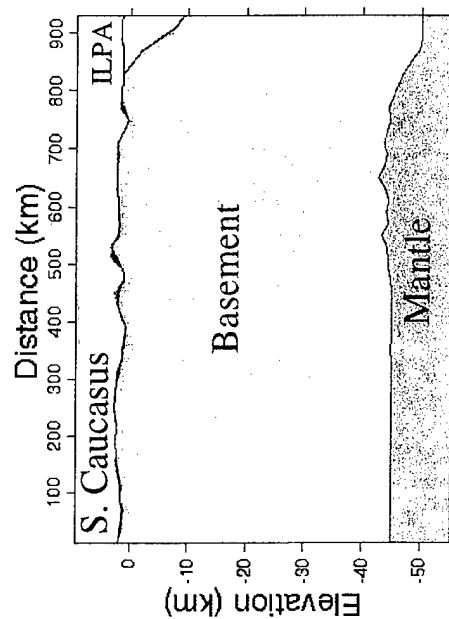
Figure 9: Comparison of blocked and unblocked waveform propagation paths cross sections (left) and the waveforms for the two paths. The top cross section and waveform is for the blocked path and the bottom for the unblocked path.

20

Figure 10: Bandpass filter analysis of the Caucasus Region Earthquake Recorded at ILPA. Note the lack of energy at frequencies above the 2 to 4 Hz band.

Figure 11: Bandpass filter analysis of the known Azgir Nuclear explosion recorded at ILPA IR1 channels. Strong Pn and Sn is apparent through the entire frequency band. At the higher frequencies, Sn decays rapidly compared with Lg, as expected.
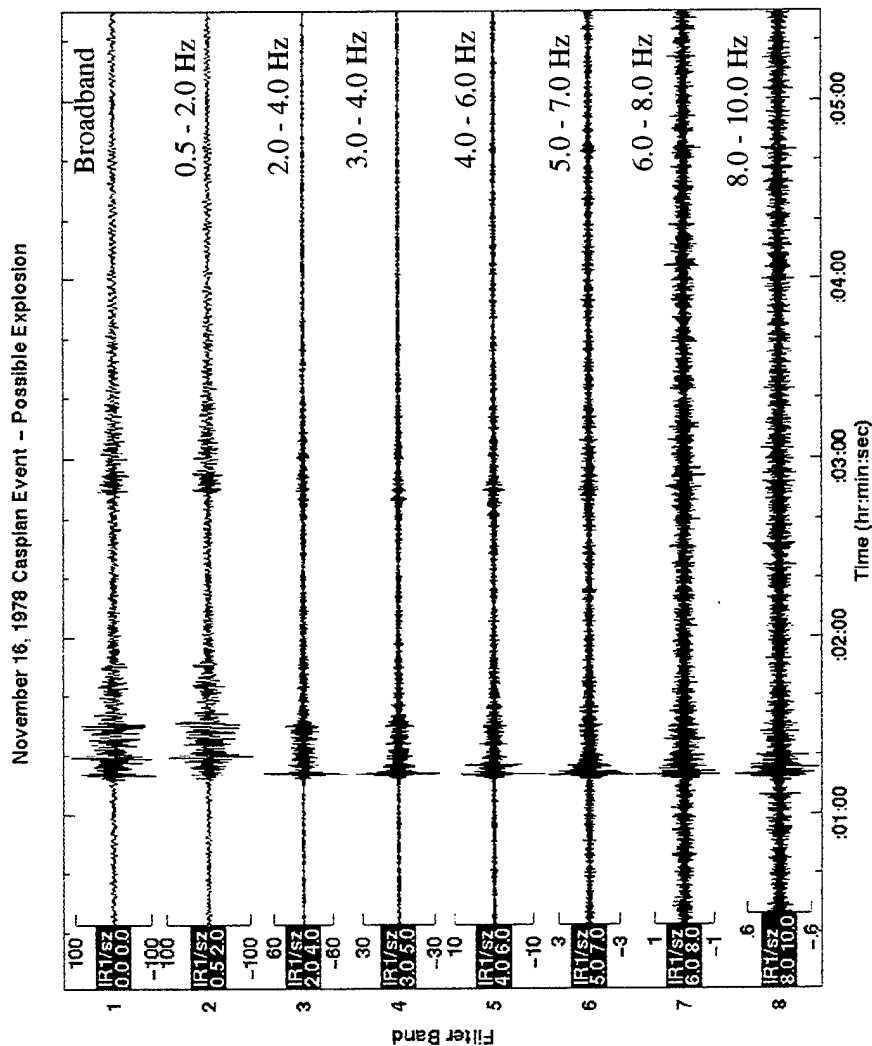
Figure 12: Bandpass filter analysis of the West Caspian event recorded at the ILPA array IR1 element. Note that strong Pn at high frequency and decay of the Sn amplitude with increasing frequency, like that shown in Figure 10. This event appears to be an explosion, although no known nuclear explosion has been reported for the region.

NEIS and the Soviet Earthquake Catalog (SEC) (provided by William Leith), report the source parameters for this event on November 16, 1978, as follows:

NEIS   Latitude - 43.499N, Longitude - 46.623 E, Origin Time - 5:46:9.48, mb = 3.9

SEC   Latitude - 43.6 N, Longitude - 47.0 E, Origin Time - 5:46:15, K = 9.

These two locations appear to be for the same event, and since the Soviet catalog only reports earthquakes, the November 16, 1978 event has been identified as an earthquake. However, the filter analysis shows a very similar pattern to that in **Figure 11** for the nuclear explosion, notably the strong Pn energy compared with the Sn energy at the higher frequencies. Pn can even be observed in the 8 to 10 Hz band. This "lonesome Pn" observation at high frequency is a characteristic signature of an explosion. However, there is no known record of a nuclear explosion on that day, and no known nuclear explosions have occurred in that region west of the Caspian. Although the accuracy of the event's location may be questionable, the Pn-to-Sn time interval is clearly shorter for the November 16 event than the December 18 Azgir explosion, so the November 16 event must be at a closer distance than the Azgir region north of the Caspian.

Because this event is on the western edge of the south Caspian basin, which is near mining districts and gas fields, the event may actually be a large chemical blast or an unannounced PNE. The fact that it was reported in the Soviet Earthquake Catalog means that it probably was not a Soviet explosion. However, waveform P/S amplitude ratio discriminants would have identified the event as an explosion. Perhaps this is a radiation pattern effect for the earthquake or perhaps it is an unknown mine blast. However, without other data for this event, it remains a very questionable and enigmatic event for discrimination.

2.4 Discussion

The crustal structure and deep sedimentary basins in the Caspian have been explained as remnants of a much larger marginal seas which were buried during the Mesozoic collision of the Arabian promontory and the Eurasian margin (e.g., Zonenshain and Le Pichon, 1986). As revealed by Russian DSS studies, the sediments in the basin have low velocity (about 3.5 km/sec) which overlie the basement rocks of much higher velocity (6.5 km/sec), the latter associated with the oceanic crust of the buried (Tethys) ocean. The basement rocks on either side of the basin appear to have normal granitic velocities (6.0 km/sec) (Berberian, 1983).

The structure is the same as the Barents Sea and that the basin capture theory can explain the *Lg* blockage across this region. Whether or not there is oceanic crust beneath the sedimentary basin is immaterial to the *Lg* blockage. The large velocity contrast between the sediments of the contained sedimentary basin and the surrounding crust, whether continental or oceanic, results in the *Lg* waves being trapped in the basin and explains the blockage of *Lg* across the southern Caspian Sea.

Also, this analysis suggests that a "crustal pinchout", like those that appear in the models of Kennett (1996) and Jih (1995), are not apparent in the Barents Sea and Caspian Sea cross sections in **Figures 1** and **9**. Although there are in fact perturbations in the Moho depth in these cross sections, which may in some way be related to the thick overlying sediments, a substantial elevation of the Moho does not exist. Therefore, the *Lg* blockage appears to originate primarily from the strong velocity perturbation in the upper crust caused by the presence of the low-velocity sediments in the Barents and South Caspian Basins along the path. The lower crust has little effect in this region since it is comparatively less laterally heterogeneous than the upper crust.

This study has indicated that the strength of recordings of the *Sn* and *Lg* phases may be governed by a "shear-wave energy balance" condition that seems to be conserved even in the case of *Lg* blockage or strong *Sn* attenuation. This can best be seen in the comparison of **Figures 5** and **6**. Whenever *Lg* is blocked, *Sn* appears to be strong (**Figure 5**) whereas the

reverse holds true when *Lg* waves are not blocked (**Figure 6**). This suggests that seismic events produce a certain amount of shear-wave energy that propagates either as *Sn* or *Lg*, depending on the complexity of the path. One possible mechanism for this is that when the shear waves propagate into an enclosed sedimentary basin and are captured, they may be directed into steeper paths closer to the vertical in the basin and the shear-wave energy gets diverted downward into the lower crust to become *Sn* or *Sn*-coda waves.

Also, these comparisons reveal that the same patterns exist for the amplitudes of *Pg* and *Pn* which follow the patterns of *Lg* and *Sn*. That is, *Pg* is blocked when *Lg* is blocked and *Pn* is strong and impulsive as is *Sn*. When *Lg* is strong, *Pg* is also strong and *Pn* is weak and emergent when *Sn* is weak or nonexistent. Usually, *Pn* is always observed, especially at high frequency, which is also often the case for *Sn*. However, *Sn* arrives in the higher-noise environment of the *Pg* coda which may explain why *Sn* is apparently missing when *Pg* is strong.

Other studies (e.g., Kadinski-Cade et al, 1981) have argued that the *Sn* phase is not observed for paths crossing these regions west, east, and south of the Caspian Sea because of high anelastic attenuation (low Q). Because low Q in the mantle may be thermally activated by high temperatures near the melting point solidus (Sato et al, 1989), there may be a correlation between high *Sn* attenuation and measurements of high surface heatflow.

To investigate this, a rasterized heatflow database has been produced for the study region around the Caspian Sea from the data for Pollack et al (1993). **Figure 13(a)** shows the point heatflow measurements plotted on a topographic map of the Caspian region. In **Figure 13(b),** this data has been rasterized into an image using the "near neighbor" function of Generic Mapping Tools (GMT) package (Wessel and Smith, 1995). **Figure 13(c)** shows the cross sections through the rasterized heatflow database for blocked (solid line) and unblocked (dashed line) *Lg* paths shown in **Figure 13(b)**. Portions of both paths show high heatflow, generally above the continental average of 65 mW m^{-2}, for the parts of the paths in the Caucasus and especially those which cross the middle part of the Caspian Sea. However, for the "weak *Sn* " paths, the heatflow values never
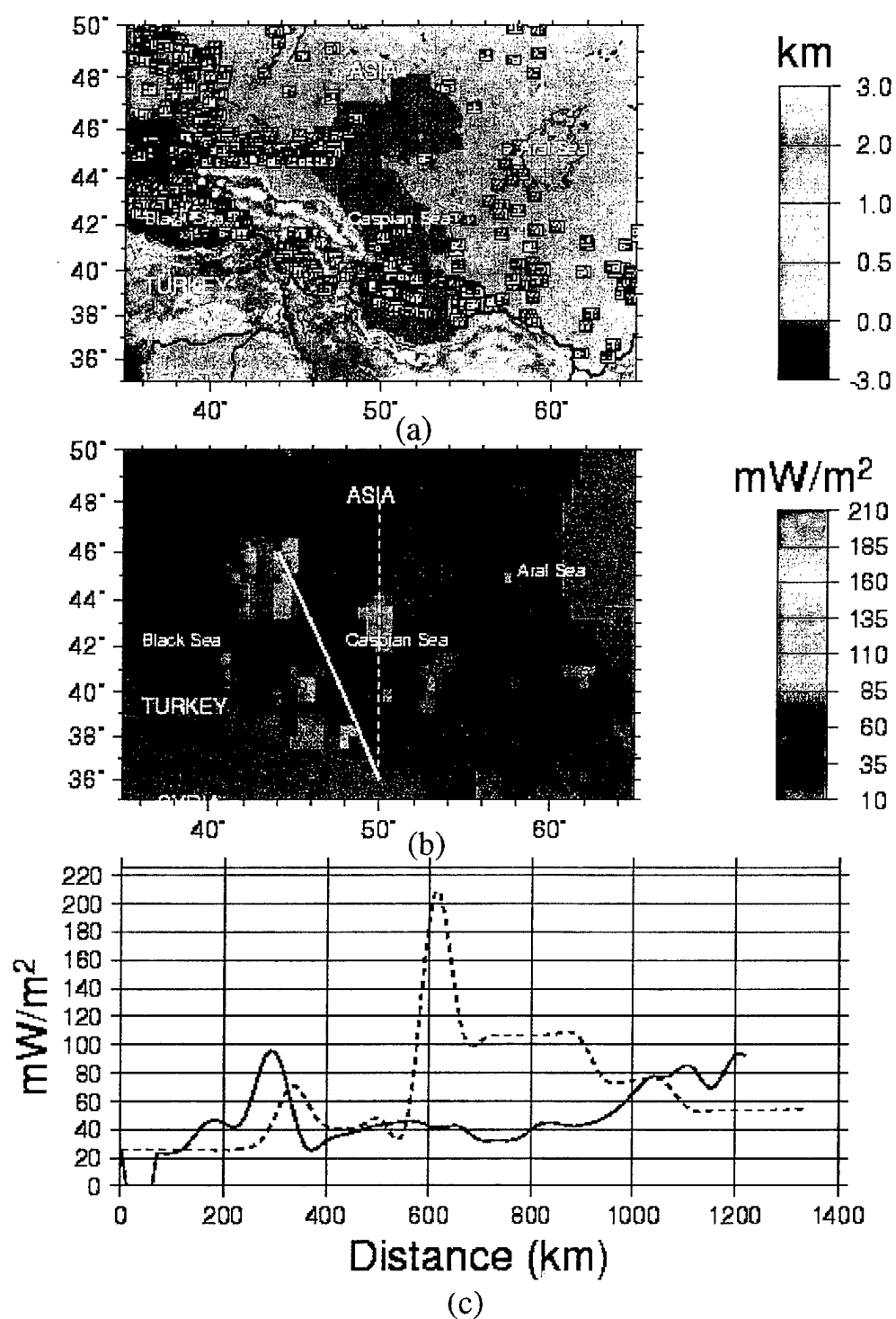
Figure 13: Maps of topography (a), heat flow (b), and heat flow cross sections (c) for the comparison event in Figure 9.

exceed 100 mW m^{-2}. However, extreme high values in excess of 100 mW m^{-2} for heatflow are found for the Caspian Sea path which is the same path where *Sn* propagates efficiently. These heatflow values may be anomalous and may be of variable quality, as pointed out by Pollack et al (1993). Ignoring the extreme high values of heatflow along the Caspian path, the average heatflow along the dashed-line path (efficient *Sn*) is not much different than that alone the solid-line path. Thus, in this region, high surface heatflow does not seem to correlate with regions of weak *Sn*.

These results suggest that the presence or absence of *Sn* in the Caspian Sea region is controlled more by the energy balance between *Sn* and *Lg* due to the propagation path blockage effects and to the strength of the *Pg* coda level. Attenuation appears to be uniformly high for all phases for paths from the Caucasus region as evidenced by the lack of high frequency energy in the bandpass filter analysis of the Caucasus earthquake **in Figure 10**. However, there appears to be no strong evidence of unusually high attenuation, due to high heatflow, which might explain the inefficient *Sn* propagation for paths around the Caspian. The lack of observed *Sn* energy may be due to how the total shear-wave energy budget of the seismic sources is partitioned between the *Sn* and *Lg* modes of propagation. For the Caucasus paths, the shear-wave energy balance goes mainly into *Lg*. The lack of *Sn* may be caused by the fact that all the shear-wave energy propagates as *Lg* rather than *Sn*. For paths which cross the Caspian Basin, the energy balance concentrates the energy into *Sn*, since the *Lg* waves are blocked.

The overall conclusion regarding discrimination is that earthquakes and explosions are distinguishable on the basis of region *P/S* ratios, even in cases when either *Sn* or *Lg* is blocked since they are not blocked at the same time. Future research might be directed towards developing a total compressional to shear wave energy ratio, such as for example, *Pn+Pg/Sn+Lg* ratios, rather than just ratios involving one or the other phase.

3. CHARACTERIZATION OF REGIONAL PHASE PROPAGATION IN THE MIDDLE EAST

The Middle East is a region of the world of key interest in monitoring a CTBT or NPT. Countries in this region are believed to either have untested nuclear weapons (Israel) or are aspiring to be nuclear nations (Iran, Iraq, Pakistan). Although the primary motivation of the nonproliferation treaties would be to prevent the development of nuclear weapons to the test stage, the monitoring system must be capable of detecting and identifying any potential "first test" which might occur.

Seismic identification in the Middle East is complicated by the fact that, although there are many seismically active regions, there are no known nuclear explosion tests, except for the close by Russian PNEs north of the Caspian Sea which have been recorded by stations in the Middle East. However, identification in the key regions of North Africa, the Levant east of the Mediterranean Sea, and regions in Mesopotamia and the Persian Gulf, must rely on the characterization of earthquakes and hypothetical characterizations of potential nuclear explosions in the region. Theoretical modeling has been proposed as a method for accomplishing this (Goldstein, et al, 1996) although this would be problematic because there would be no way to directly validate models for explosions in the regions of the Middle East.

The approach taken in this study has been to empirically characterize earthquake sources in the region with the intent of understanding the propagation and source effects on recorded waveform features, in particular, regional *P/S* amplitude ratios. For discrimination purposes, the waveform features are compared with those from explosions in other regions of the world which may have similar propagation paths to those in the Middle East.

This section presents preliminary analysis of selected seismograms from earthquakes in key regions of the Middle East recorded at the Mednet station KEG and the IRIS station ABKT. The main focus has been on earthquakes alone the Jordan-Dead Sea transform, Gulf of Aqaba and Sinai, Red Sea, and the Zagros thrust zone in western Iran. For the Mednet sta-

tion KEG, waveforms were collected from the IRIS Data Center and were only available for the years 1991 through 1994. The station ABKT came on line in 1994. So, for some events in the Zagros, data was collected from the IRIS Data Center for the same events recorded in 1994 at both KEG and ABKT

3.1 *Lg* Propagation Barriers in the Levant

Figure 14 shows a map of propagation paths from a number of earthquakes in Syria, Jordan, Israel, and Lebanon recorded at the Mednet station KEG. Most of these events were located along a region defined by the Jordan-Dead Sea transform fault system which separates the Arabian and Sinai plates. Tectonically, the Dead Sea transform system has evolved since mid-Cenozoic time as a result of the breakup of the Arabian plate from the African plate (Ambraseys and Barazangi, 1989). The system includes the pull-apart basins of the Sea of Galilee and the Dead Sea and extends as far north to the Ghab and Yammouneh faults in Syria and south into the Gulf of Aqaba. The faulting processes along the system are basically left-lateral strike-slip although the fault movements are quite variable from north to south (Walley, 1988; Ben-Avraham and Lyakhovsky, 1992).

The crustal structure in the region shown in **Figure 14** is also known be quite variable since the region formed from the convergence of a number of displaced terranes (Ben-Avraham and Ginzburg, 1990). The eastern Mediterranean Sea is underlain by the quaternary Levantine sedimentary basin. Seismic refraction surveys of the basin (Ginzburg and Folkman, 1980) have inferred seismic velocities of 1.5 to 2.1 km/sec in the sediments in the eastern part of the basin extending to depths of 8 to 10 km depth underlain by velocities of 4.1 to 4.5 km/sec. The adjoining Galilee-Lebanon, Samaria, and Negev regions have very different crustal structures, perhaps thinner crust, and the seismic velocities in the upper crust range from 3.7 to 6.2 km/sec. As shown in **Figure 14**, all the events occurred east of the Levantine Basin, but the great-circle propagation paths from the northern events in Syria and Lebanon to KEG cross the eastern part of the Levantine Basin.
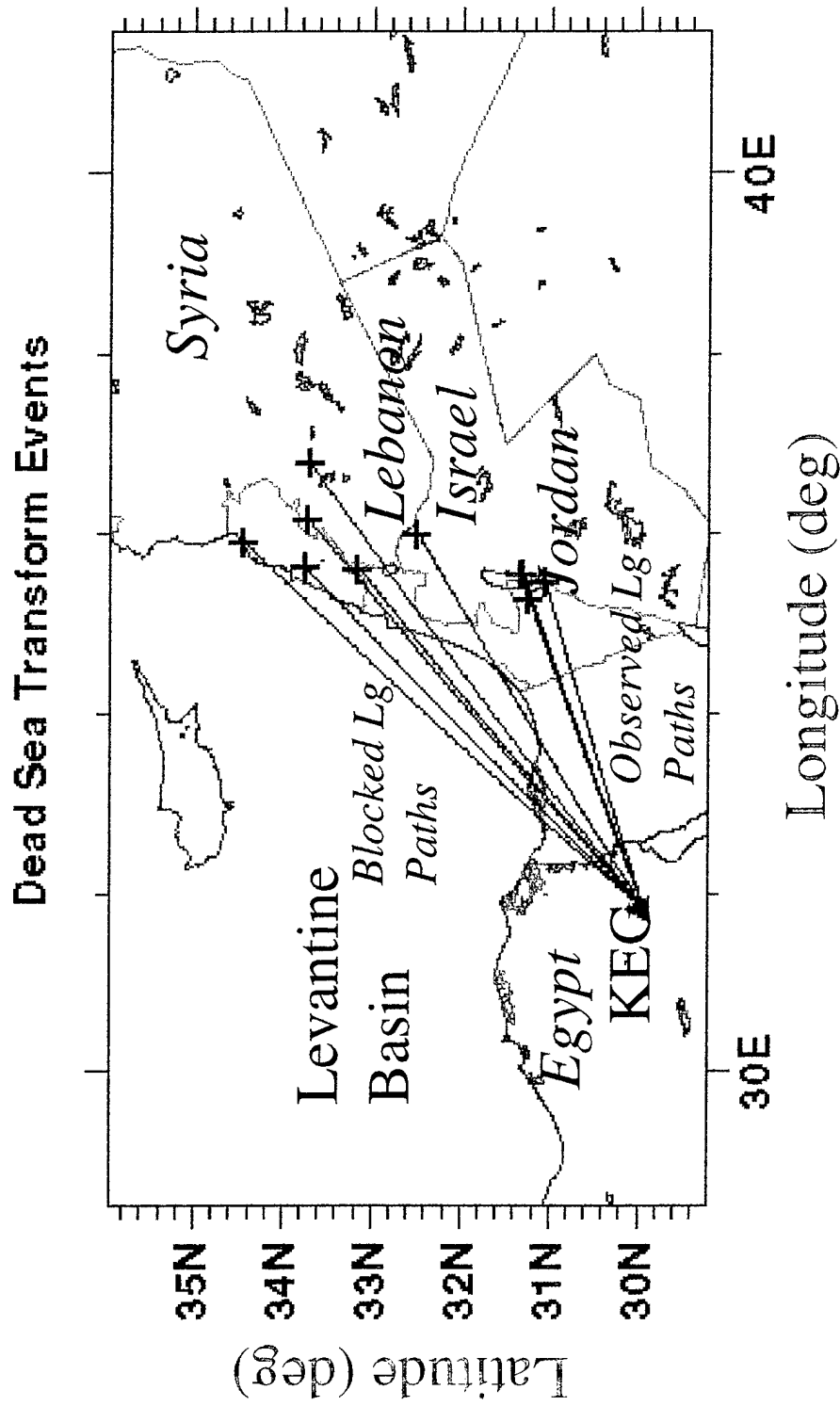
Figure 14: Map showing the propagation paths to the Mednet station at Kottamya, Egypt (KEG) from Dead Sea Transform events.

Record sections for these events, with both filtered broadband (0.6 to 6 Hz) and high frequency (8 to 10 Hz) waveforms, are shown in **Figure 15** and **16**, respectively. The most notable observation in these plots is the apparent blockage of *Lg* between 388 km and 488 km distance from KEG. The blocked paths are associated with the paths that cross the Levantine Basin, as shown in **Figure 14**. Both plots show that *Sn* is non existent for the shorter distance where *Lg* is observed but is strong at the greater distances where *Lg* is blocked. Also, *Pg* apparently disappears when *Lg* does and the *Pn* is more impulsive for the paths where *Sn* is strongest.

In this study, only events with NEIS magnitudes in excess of 3.5 were recorded with observable signals at KEG. The 11 events shown in **Figures 14** through **16** were the only events which produced observable signals at KEG from 1991 to 1993. The high detection threshold may be a result of low instrument magnification at KEG. **Figure 15** shows that high frequency regional signals propagate efficiently across these paths, except for the blocked paths where *Pg* and *Lg* is not observed. However, even along blocked paths, high-frequency *Pn* and *Sn* phases propagate with high signal-to-noise ratio which indicates that attenuation is not extremely high in this region.

These results are consistent with the observation in the Barents Sea and Caspian Sea basins. The *Pg, Lg* blockage is associated with paths which cross the sedimentary basin, and there is a tradeoff in energy between *Pn, Sn* phases and *Pg, Lg* phases. Thus, basin capture, not high attenuation, may be the cause of the blockages in this region. In spite of the blockages, however, *Pn* and *Sn* phases are recorded at high frequency which means regional *P/S* ratio discriminants can still be used in these regions.

3.2 Regional Phase Propagation from the Gulf of Aqaba/Suez/Northern Egypt Events

Figure 17 shows propagation paths for a set of events in the Gulf of Aqaba and Suez recorded at KEG. These paths generally cross northern Egypt and the Sinai. As discussed above, earthquakes in the Gulf of Aqaba are part of the southern extension of the Jordan-Dead Sea transform fault zone. This part of the fault zone is much more active than the northern part
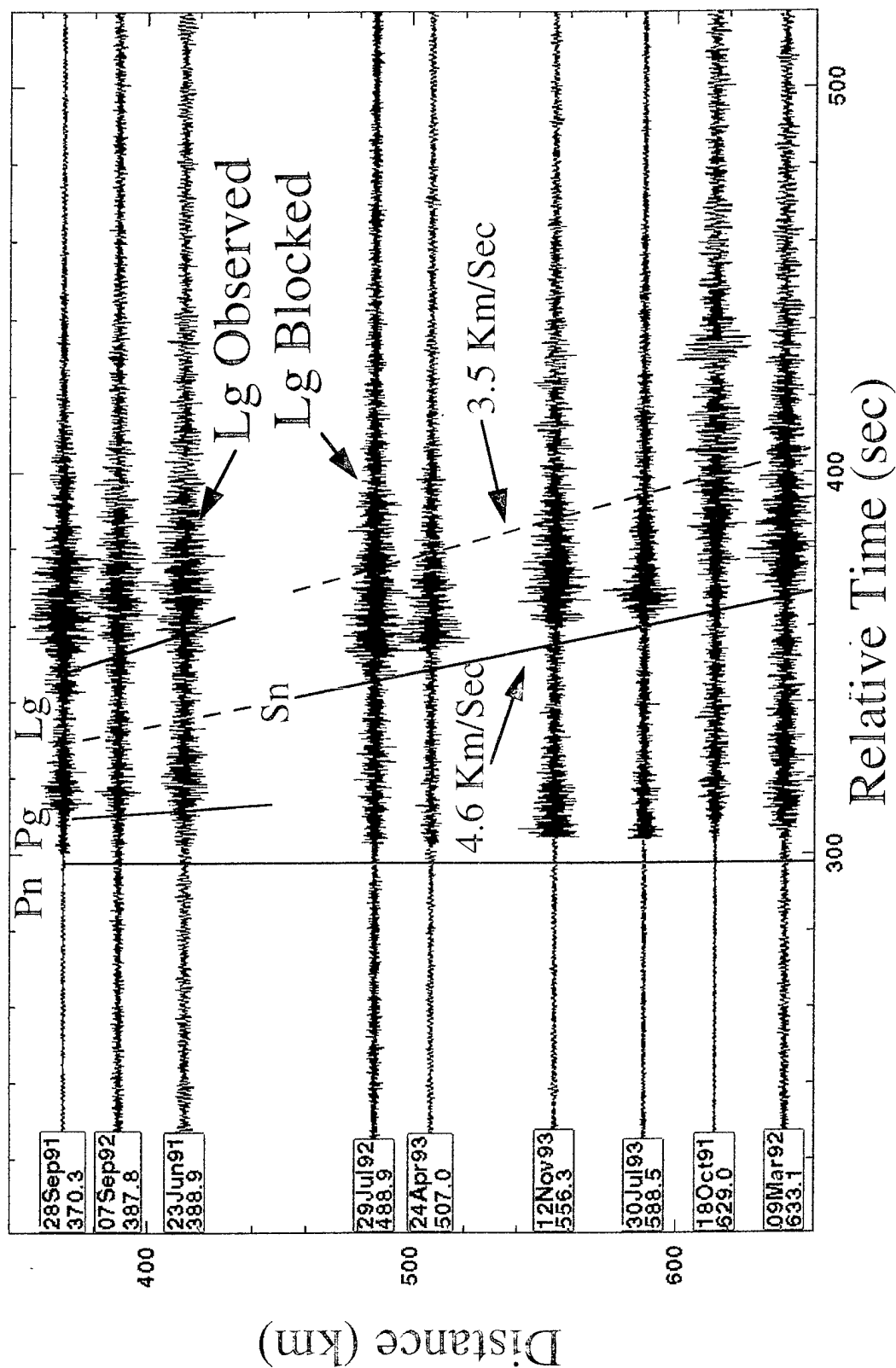
Figure 15: KEG record section for Dead Sea Transform Events - 0.5-4.0 Hz filter. The Lg blockage beginning about 480 km is apparent.
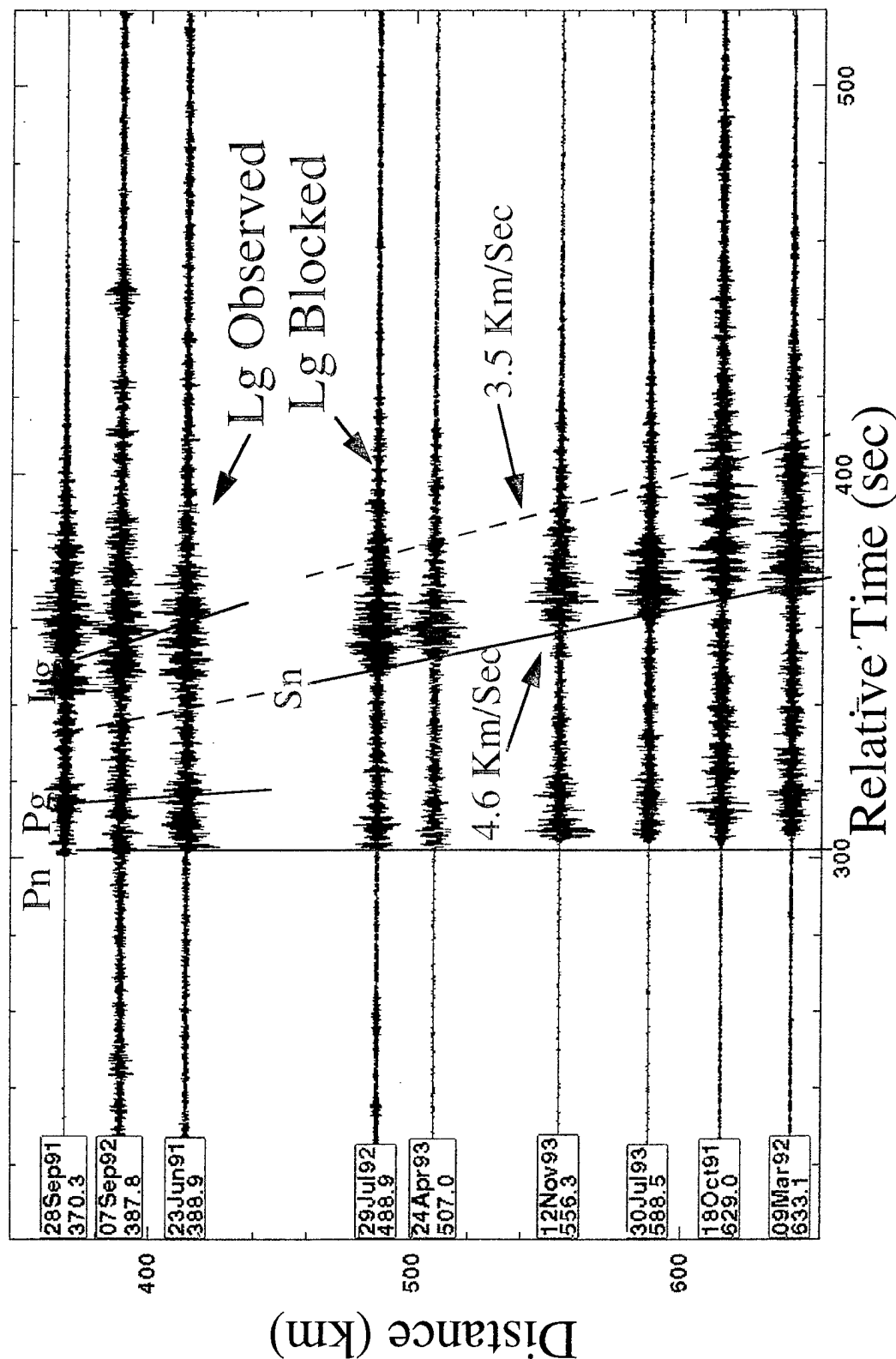
33

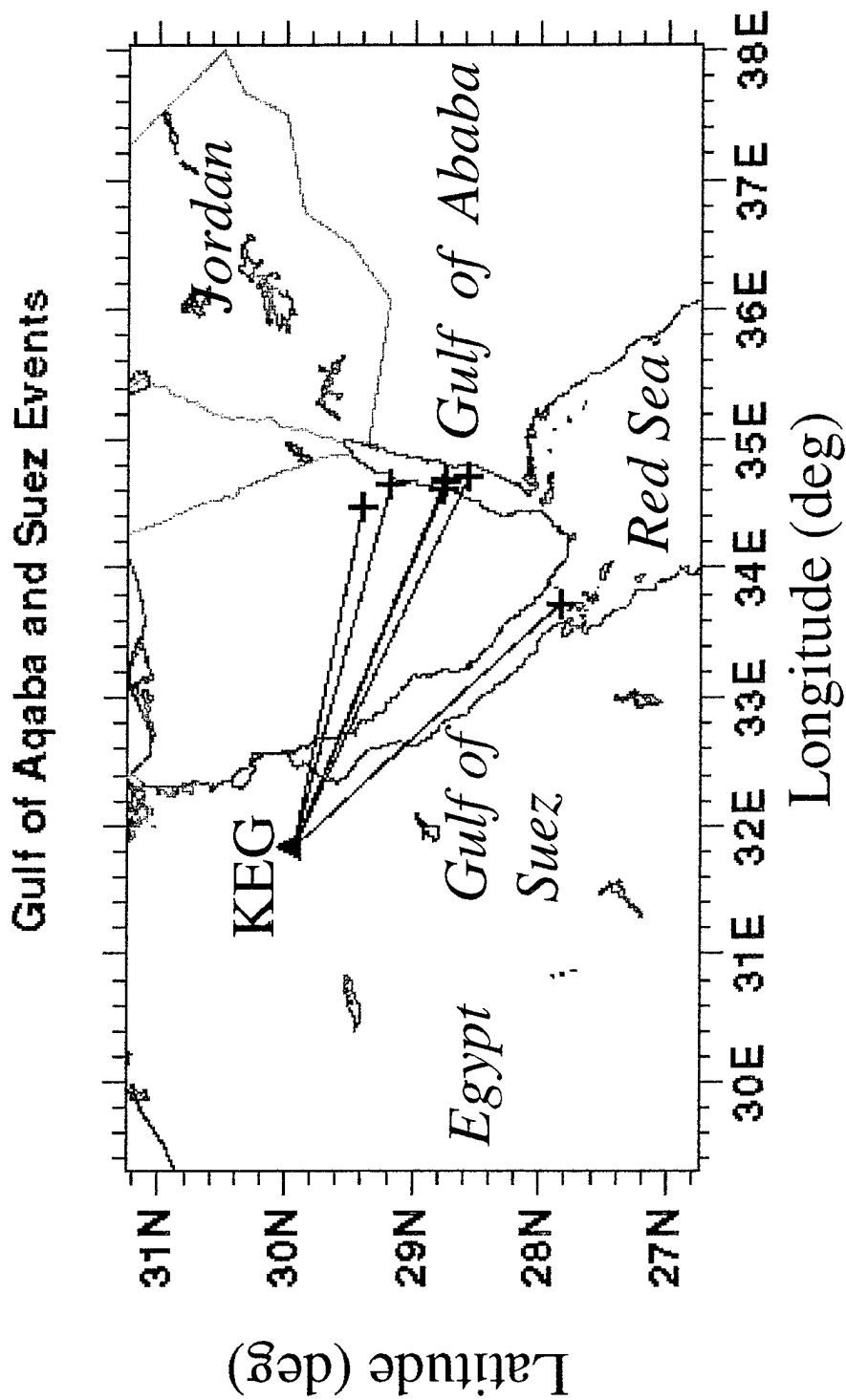Figure 16: KEG record section for Dead Sea Transform events - 8.0-10.0 Hz filter.

Figure 17: Propagation paths for Gulf of Aqaba and Suez Events recorded at KEG.

and over 20 events were obtained from one year (1993) with body-wave magnitudes between 3.7 and 4.7. The events plotted in **Figure 17** are a sample of events from this region.

Figures 18 and **19** show record sections of the waveforms in the 0.6 to 6 Hz and 8 to 10 Hz bands, respectively, for the earthquakes in **Figure 16**. The distances in this region range from 260 to 330 km. The seismograms show strong Lg and Pg signals, emergent Pn signals, and no apparent Sn signals. As in the case of the southern paths from the events to the north of KEG in **Figure 14**, the seismic energy in this region propagates primarily as Pg and Lg modes at very high frequency. The observation of high-frequencies in the region indicates relatively low attenuation overall. However, the lack of Sn energy may be because the total energy budget for shear waves propagates as Lg and little or no energy is partitioned into the Sn phase.

3.3 Water Column Bounces in the Gulf of Aqaba

One interesting observation for many of the events in the Gulf of Aqaba is that their spectra show evidence of spectral scalloping in the Pn and Pg phase but not so much in the Lg phase. **Figures 20** shows examples of spectra for two earthquakes which exhibit this character. **Figure 21** shows cepstra computed from the spectra which exhibit cepstral peaks associated with the spectral scalloping. The time delay for this peak is about 0.3 seconds and may be caused by reflections in the water column of the Gulf of Aqaba. As shown, a two-way travel time of 0.3 seconds is consistent with a water column depth of about 228 meters, which is close to the actual value from the bathymetry data for the Gulf of Aqaba.

Spectral scalloping features like this are often observed in mine blasts on land and are caused by ripple firing (Baumgardt and Ziegler, 1988). Also, spectral scalloping has been observed in presumed underwater
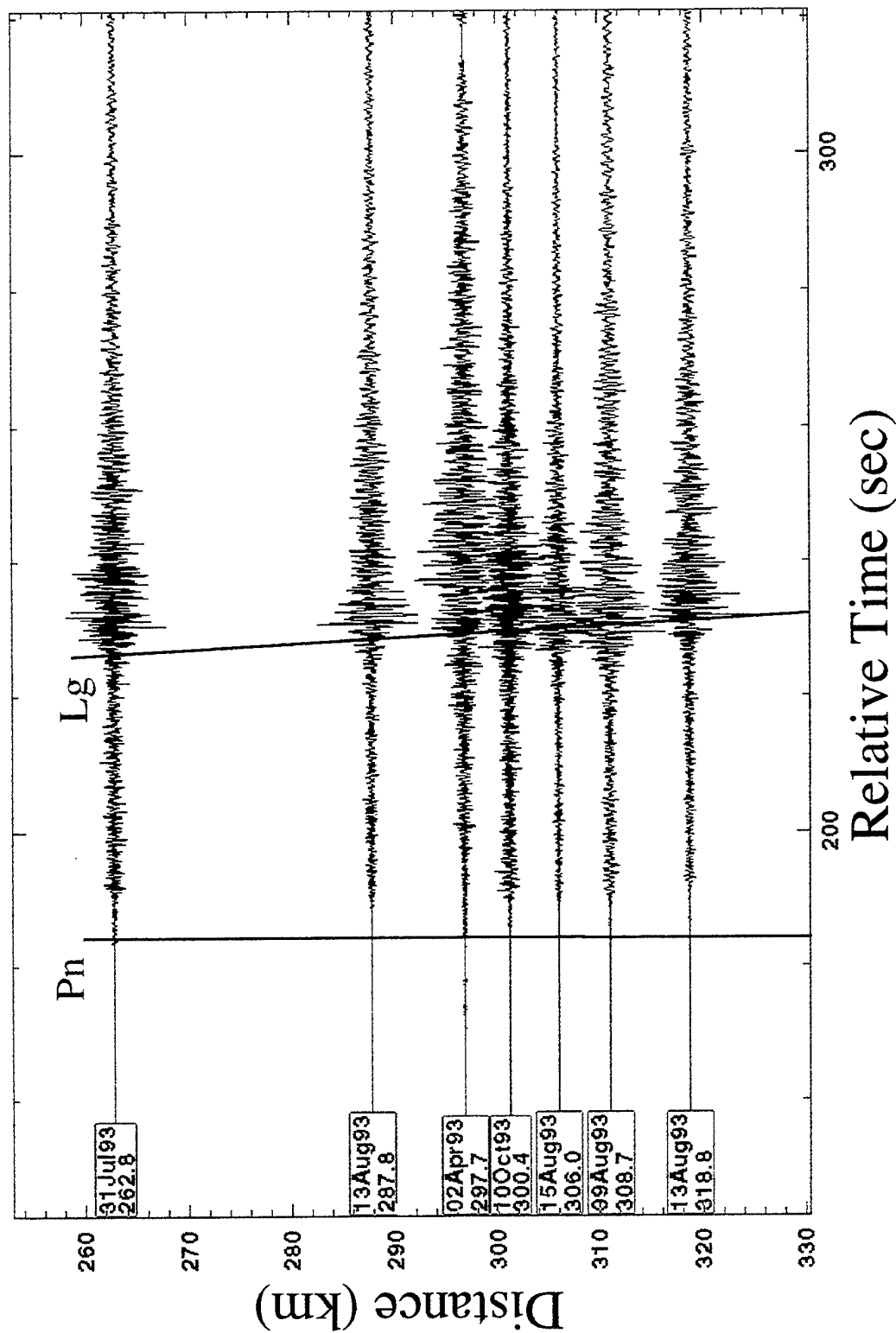
Figure 18: KEG record section of Gulf of Aqaba/Suez events - 0.5-4.0 Hz filter.
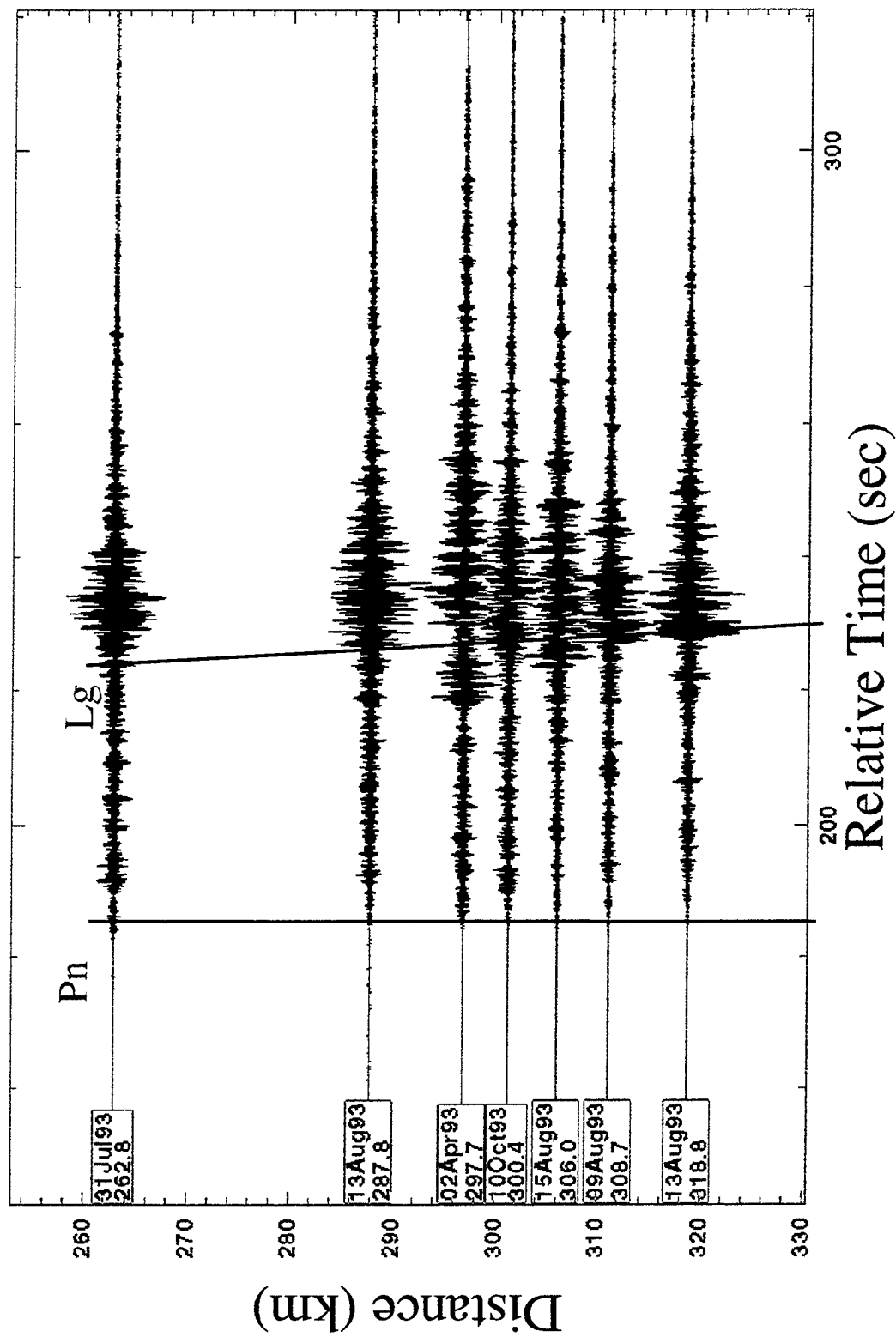
Figure 19: KEG record section of Gulf of Aqaba/Suez events - 8.0-10 Hz filter.
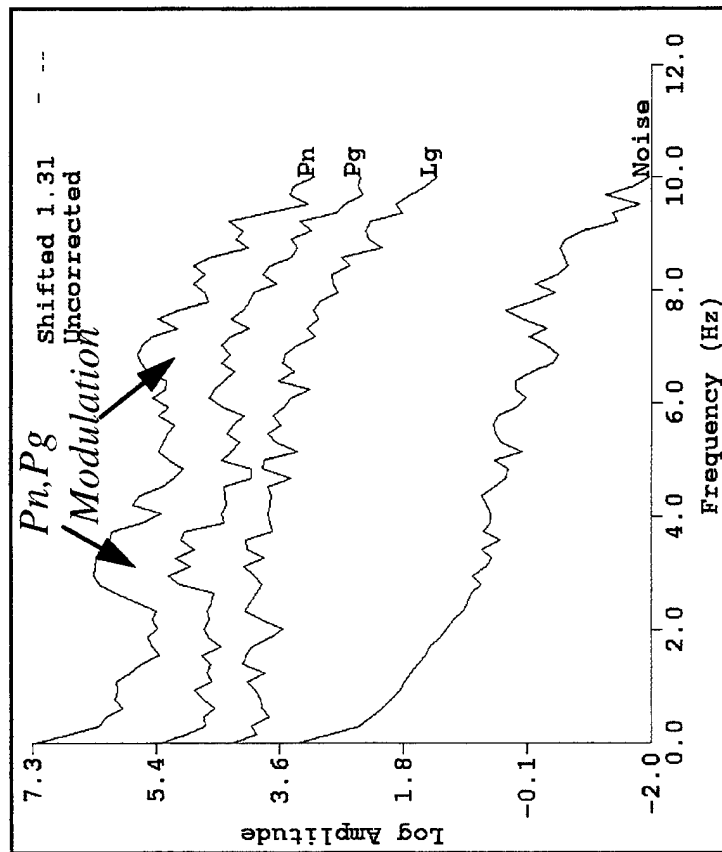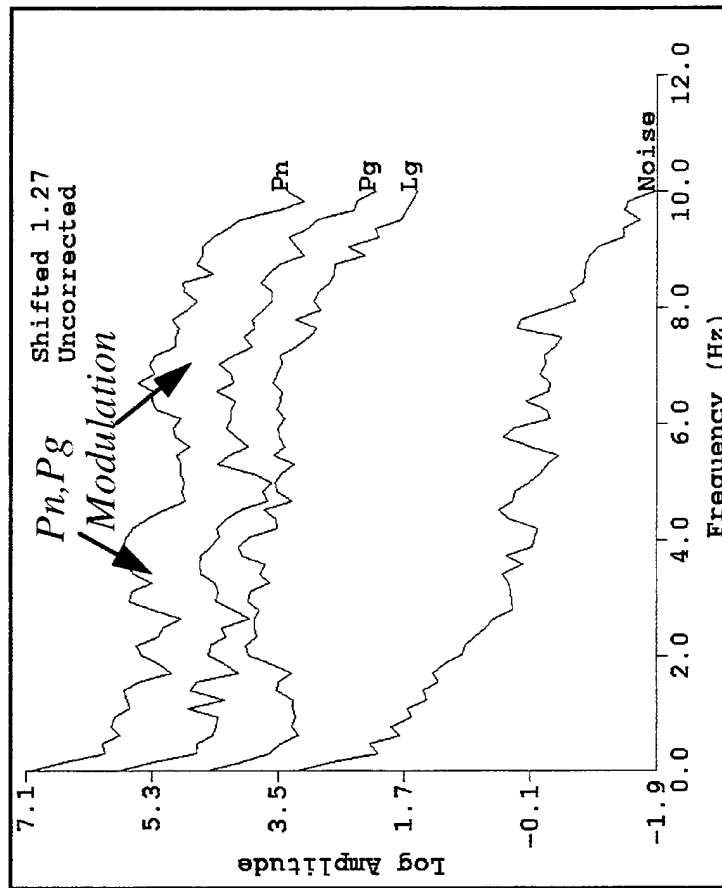
Figure 20: KEG spectra for the Gulf of Aqaba events. Spectral modulations in Pn and Pg Spectra may be scalloping caused by acoustic water-column reflections.

39
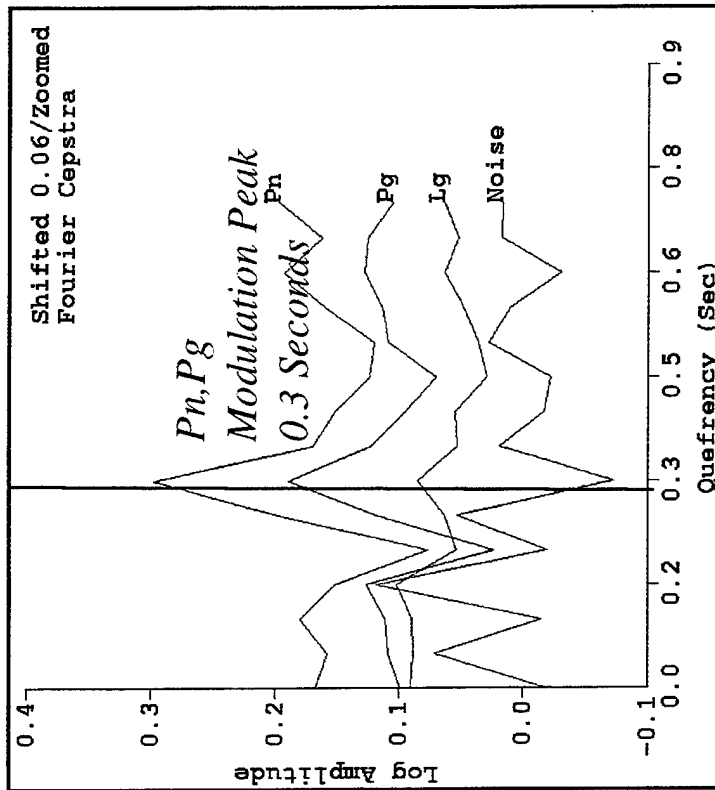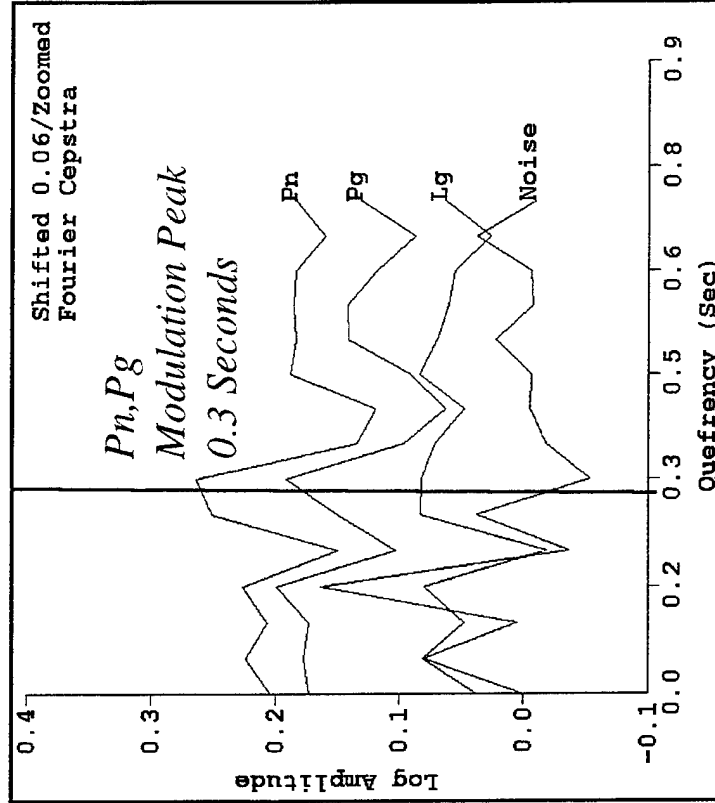
Figure 21: KEG cepstra for Gulf of Aqaba events. Cepstral peaks in *Pn* and *Pg* cepstra indicate water reverberations in water 228 m deep, which is consistent with the bathymetry of the Gulf of Aqaba.

blasts by Gitterman and Shapira (1993) and Baumgardt and Der (1996). In these studies, spectral scalloping was observed in all phases from the blasts, including *Lg*. The fact that spectral modulations are observed for earthquakes in the Gulf of Aqaba is interesting and significant in that this feature has usually been regarded as an indication of ripple fired mineblasts and underwater explosions.

The fact that the spectral scalloping is mainly observed in the region *P* phases, and not the *Lg*, might be explained by the way in which these phases are generated. The earthquakes are presumed to be crustal and immediately below the region covered with water. Thus, the upgoing *P* waves, both *Pn* and *Pg*, couple directly into the water column as acoustic waves, and the water column reflections would couple in directly to the *Pn* to *Pg* coda. The *S* type phases do not, except by mode conversion to *P*. Since all this occurs in the source region, and *Lg* primarily builds up along the path, the near source water reflections appear primarily in the early arriving *Pn* and *Pg* type phases.

In terms of discrimination, features of this kind would be an indication of underwater earthquakes and can be distinguished from underwater blasts by the lack of spectral scalloping in the *Lg* phase. In future research, the degree to which these features show up for the Gulf of Aqaba earthquakes (i.e., the number of events, where they are located) will be investigated more fully. Moreover, it may be possible to more precisely estimate the location and the depth of shallow earthquakes in this region, given knowledge of the bathymetry of the Gulf, by estimating the depth of the water column over the earthquake.

3.4   Red Sea/Ethiopia Earthquakes

**Figure 22** shows the locations of seismic events, located in Ethiopia and the southern Red Sea region, whose propagation paths to the station KEG cross the Red Sea region. A total of seven events could be obtained from the IRIS Data Center with observable signals at KEG in the 1991 and 1994 time frame. The body wave magnitudes for the events ranged from 4.1 to 5.4. Generally, no events with magnitudes less than 4.0 produced observable signals at KEG.
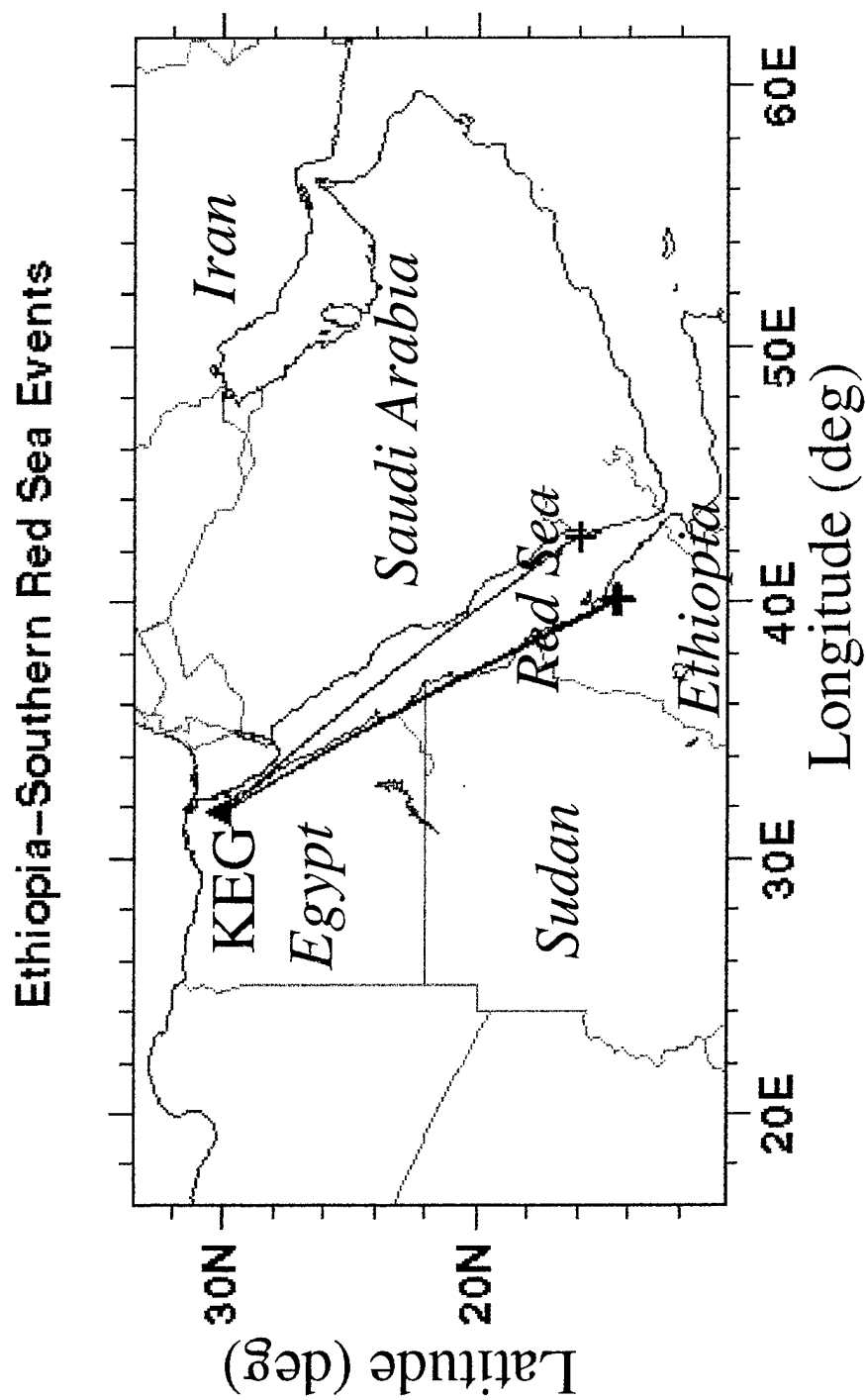
Figure 22: Southern Red-Sea earthquake propagation paths to KEG.

Geologically, the Red Sea region is known to be an incipient spreading center, and studies of distant events crossing this region have indicated weak *Sn* propagation. It has been generally assumed that high attenuation in the region would kill the propagation of *Sn*, and probably *Lg*. Regions of upwelling from the aesthenosphere have been inferred from gravity data (Makris et al, 1991), and Barazangi et al (1996) have inferred a low density aesthenosphere under the region which they suggest explains why no *Sn* or *Lg* phase crosses the Red Sea.

Figure 23 shows a broadband filtered (0.4-4.5 Hz) record section of the waveforms recorded from the earthquakes in **Figure 22**. The distance ranges for these events are quite large ranging between 1898 to 1921 km. In spite of the large distances and the fact that the paths for these event either cross or pass near the Red Sea to the west, strong *Lg* energy was recorded for all the events. Also *Pn* is observed although it is much weaker than the *Lg*. No *Sn* was observed for these paths. Clearly, the *Lg* propagates at a velocity near 3.5 km/sec across the Red Sea as is observed in other continental region.

It should be emphasized that, although strong *Lg* signals do in fact propagate near and across the Red Sea, the signals are low-frequency. Above 1 Hz, the signals are below noise level. Moreover, the *Pn* signal observed in **Figure 23** is also very low frequency and is generally not observed above 0.5 Hz.

These results show that the crustal structure of the Red Sea does not impede *Lg* propagation. However, the low frequency character of the signals and the lack of *Sn* energy probably relates to high attenuation in the region. Also, high attenuation may explain the high detection threshold for events in the region. Thus, from the point of view of discrimination, large *Lg* waves can identify earthquakes in this region. Nuclear explosions in the same region would probably excite much stronger *Pn* energy, although it would likely be low frequency due to attenuation. High frequency *P/S* ratio
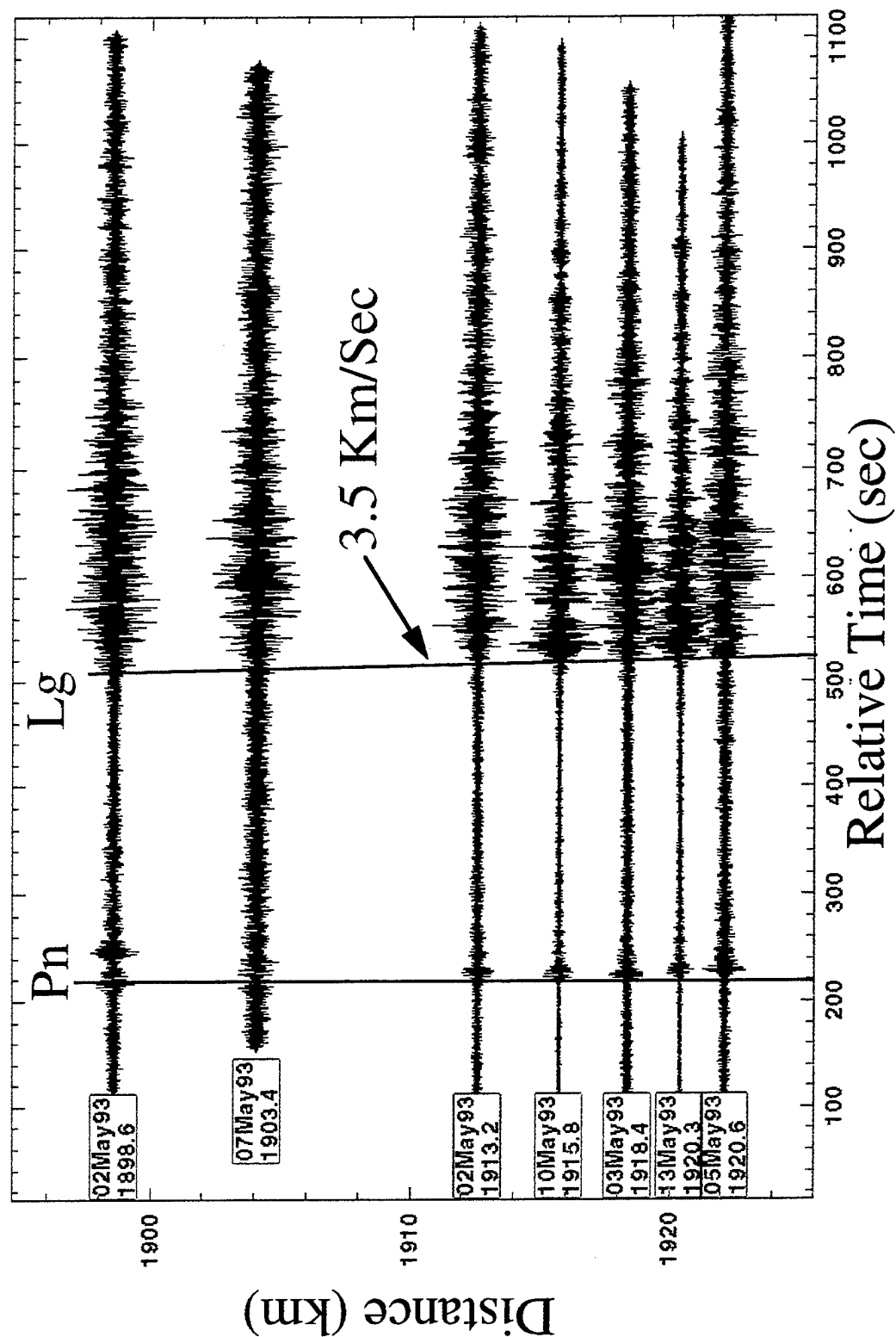
Figure 23: KEG record section for the Red Sea events shown in Figure 17 - 0.5- 4.0 Hz filter.

discriminants cannot be applied to events in this region using just the station KEG.

3.5 Observations of Zagros Earthquakes

Figure 24 shows the locations of earthquakes in the Zagros region that were recorded at the stations KEG and ABKT. As shown, many of the events were recorded at both stations. A total of 29 events were collected from IRIS for KEG between the dates for 1993 and 1994 and 54 events for ABKT between 1994 and 1995. The overlap year of 1994 when events were collected at both stations included a total of seven events. The body-wave magnitudes for these events ranged from 4.7 to 4.9. The lowest body-wave magnitude for which reasonable signals were recorded was about 4.7 for both KEG and ABKT.

The Zagros mountains has been characterized tectonically as collisional zone between the Arabian and Eurasian plates. The recent Miocene period of deformation in the collisional zone has been indicated by the presence of an active volcanic belt and numerous thrust mechanism earthquakes (Ni and Barazangi, 1986). Most of the events in **Figure 24** appear to be associated with the Zagros thrust belt.

Figure 25 shows a plot of the waveforms from the Zagros recorded at KEG in distance order. These waveforms have been prefiltered from 0.5 to 4.5 Hz. For most of the events in the distance range of 1500 to 2000 km, strong *Pn* and *Lg* waves were produced. No *Sn* energy above 0.5 Hz was apparently produced. As shown in **Figure 24**, the *Lg* wave seems to disappear beyond a distance of about 2000 km.

Recordings of waveforms at ABKT are shown in **Figure 26** in the form of a record section. The line shows the expected moveout of *Lg*. Strong *Pn* and coda waves are produced over the distance range of 1016 to 1262 km. However, *Lg* waves are relatively weak.

Comparison of **Figures 25** and **26** definitely shows differences in the relative excitation of *Pn* and *Lg*. Even though the distances from the Zagros earthquakes to the ABKT station are smaller than those to the KEG station, *Lg* appears to be stronger than *Pn* at KEG out to 2000 km whereas
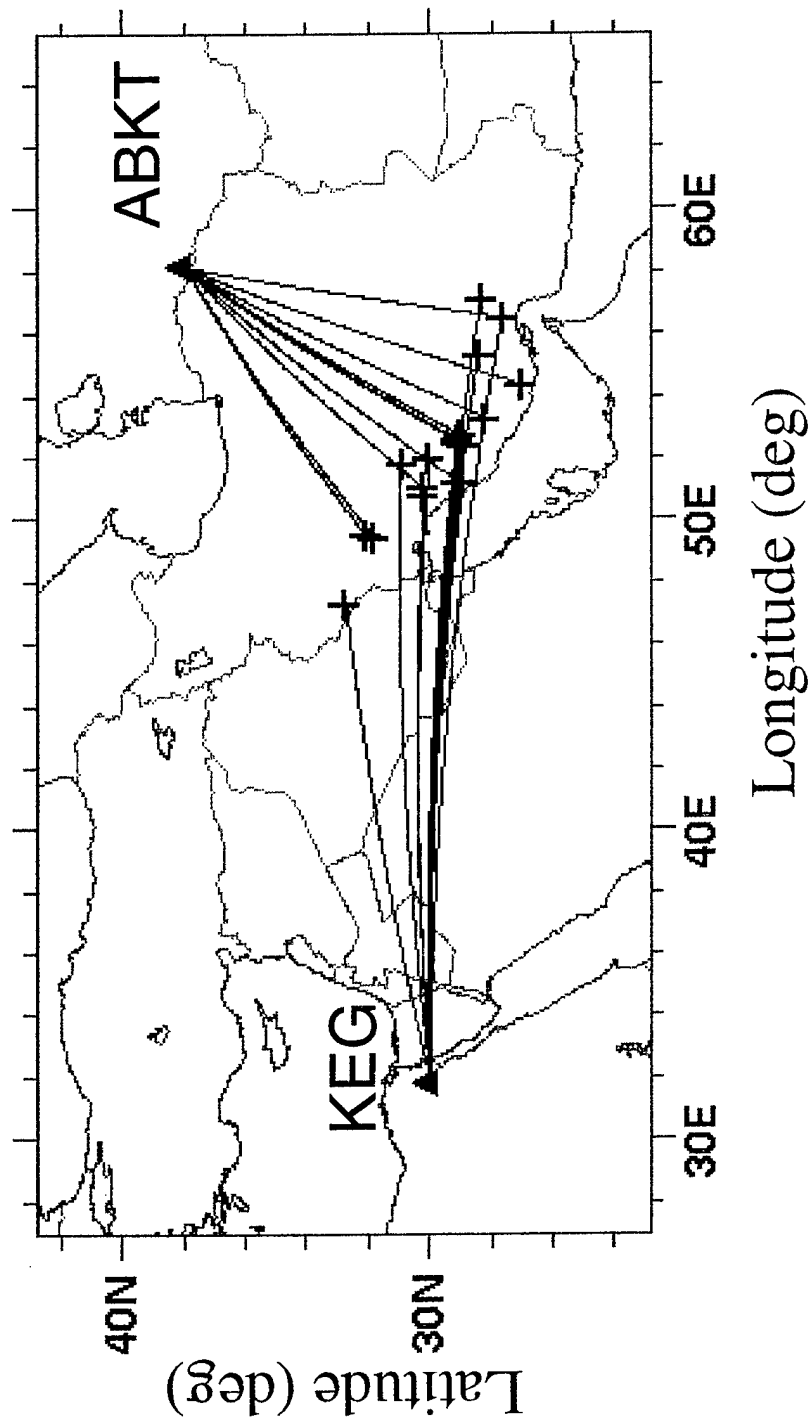
Figure 24: Propagation paths from Zagros Earthquakes to KEG and ABKT.
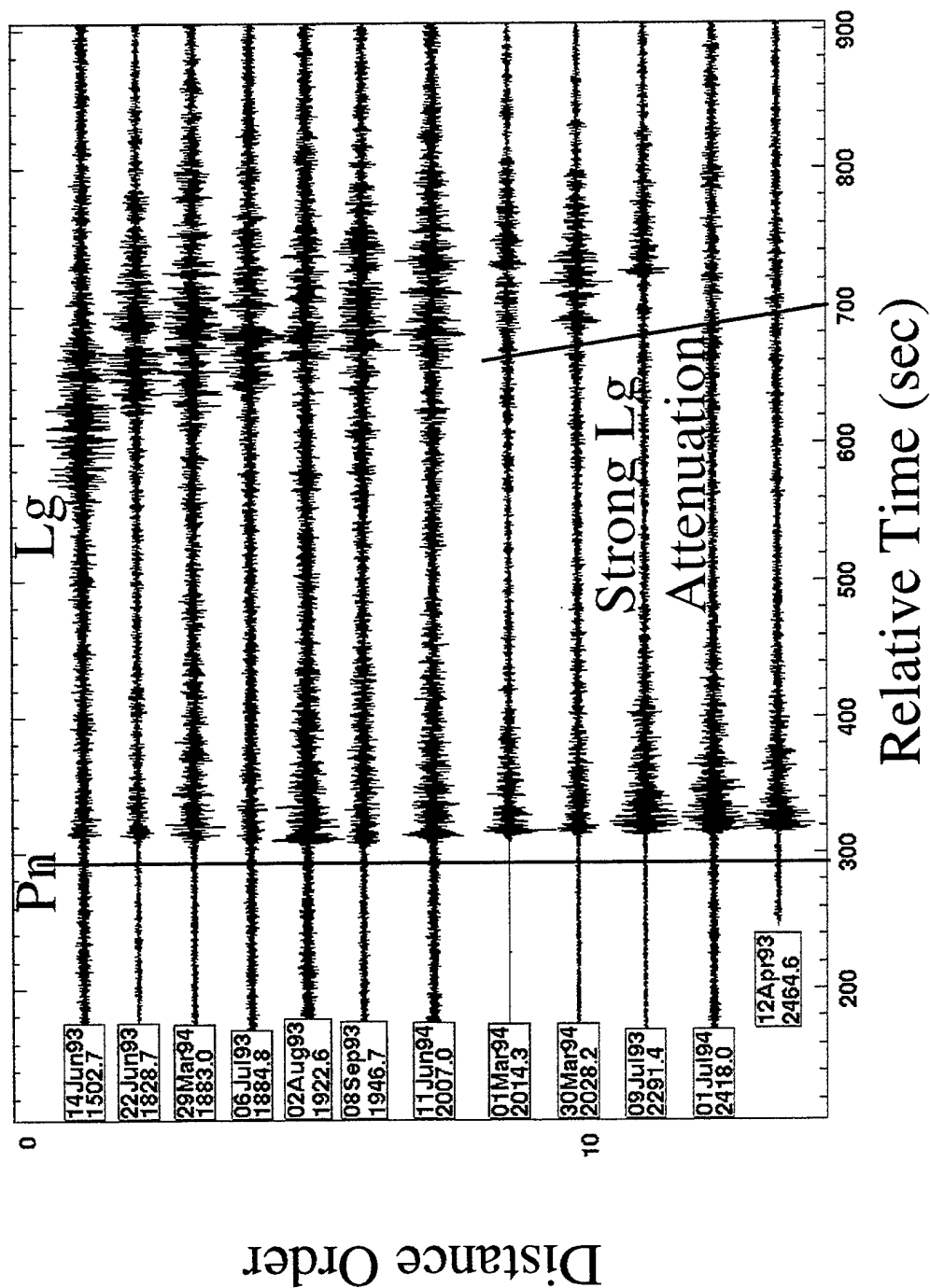
Figure 25: KEG recordings for Zagros Earthquakes - 0.5-4.5 Hz filter.
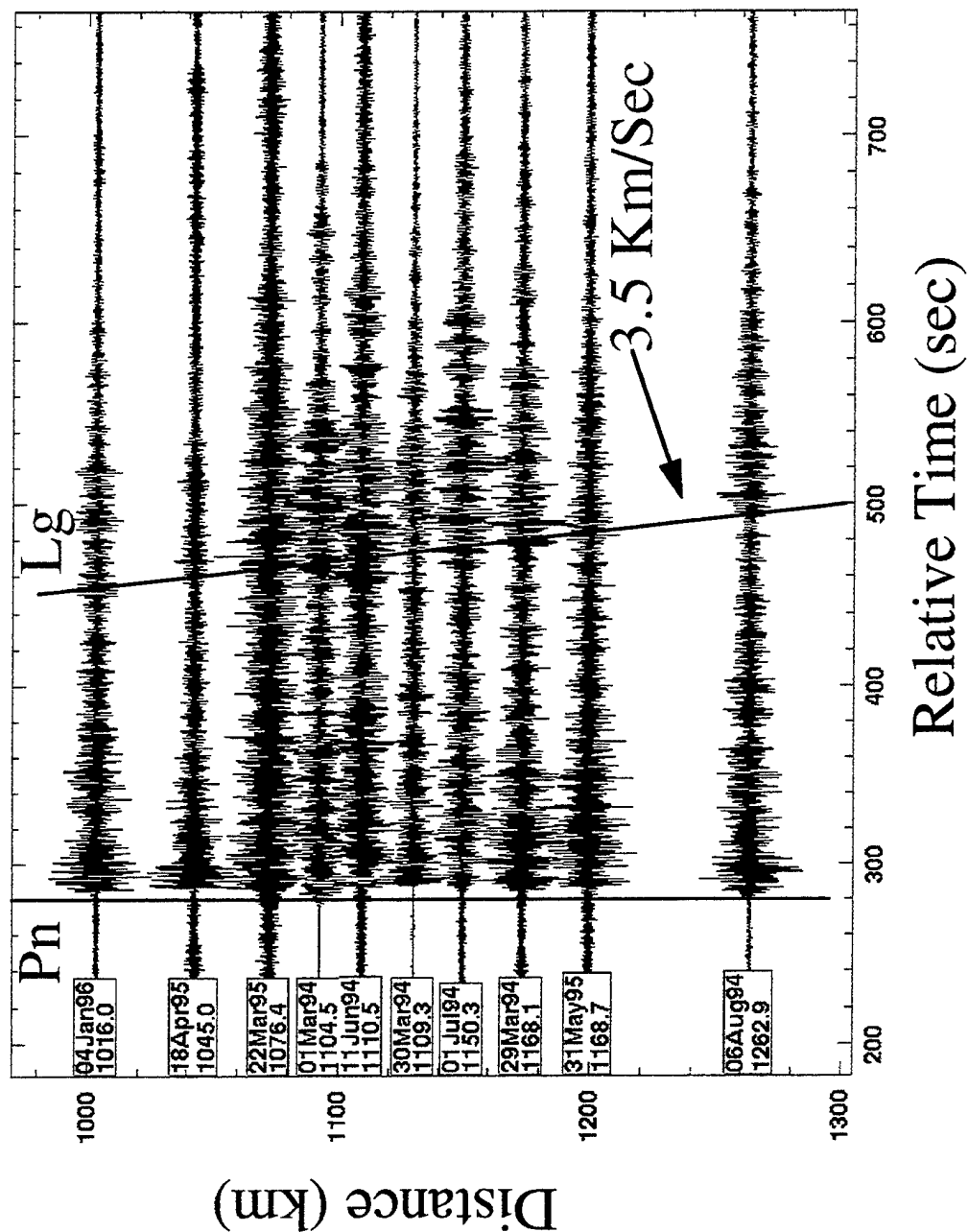
Figure 26: ABKT recordings for Zagros Earthquakes - 0.5-4.5 Hz filter.

48

the reverse is true for the ABKT station. A more direct illustration of this difference is shown in **Figure 27**, which shows two waveforms in record section from same event. The *Pn* -to-*Lg* amplitude ratio at ABKT at 1066 km distance exceeds 1 whereas at KEG, at the much greater distance of 1703 km, the *Pn* -to-*Lg* amplitude ratio is less than 1. KEG overall has a much lower signal-to-noise ratio than ABKT because of the greater propagation distance. However, the difference in the relative *Pn* and *Lg* amplitudes is quite striking and the reverse of what might be expected.

One possible conclusion of this study is that *Sn* is blocked to ABKT and *Lg* is partially blocked, and the variations in the *Pn/Lg* amplitude ratio for the paths to ABKT and KEG are due to propagation path differences. However, Rodgers et al (1996) have also studied propagation of *Sn* and *Lg* from Zagros events to ABKT and concluded that *Sn* propagates inefficiently along all paths but found mixed results for *Lg*. Some paths for *Lg* propagation through Iran were efficient, others inefficient, and often, efficient and inefficient paths overlapped. Similar mixed results for paths to other stations on Iran were reported by Kadinski-Cade et al (1981). These mixed results, and the azimuthal variations observed in this study, suggest that source effects might be an alternative explanation. These ideas are discussed in more detail in the next section.

3.6 Discussion - Causes of Regional Blockage and Attenuation in the Middle East

In the previous discussion of earthquakes in the Middle East recorded at KEG and ABKT, three major observations were made:

(1) *Lg* waves are blocked in the Eastern Mediterranean
(2) *Lg* propagates efficiently across southern Israel, Sinai, and northern Egypt
(3) Strong *Lg* waves are observed from the Red Sea region
(4) *Sn* and *Lg* relative excitation tradeoff. Also, *Pn* and *Pg* relative excitation tradeoff.
(5) Azimuthal difference in *Pn/Lg* relative excitation for Zagros Thrust events.
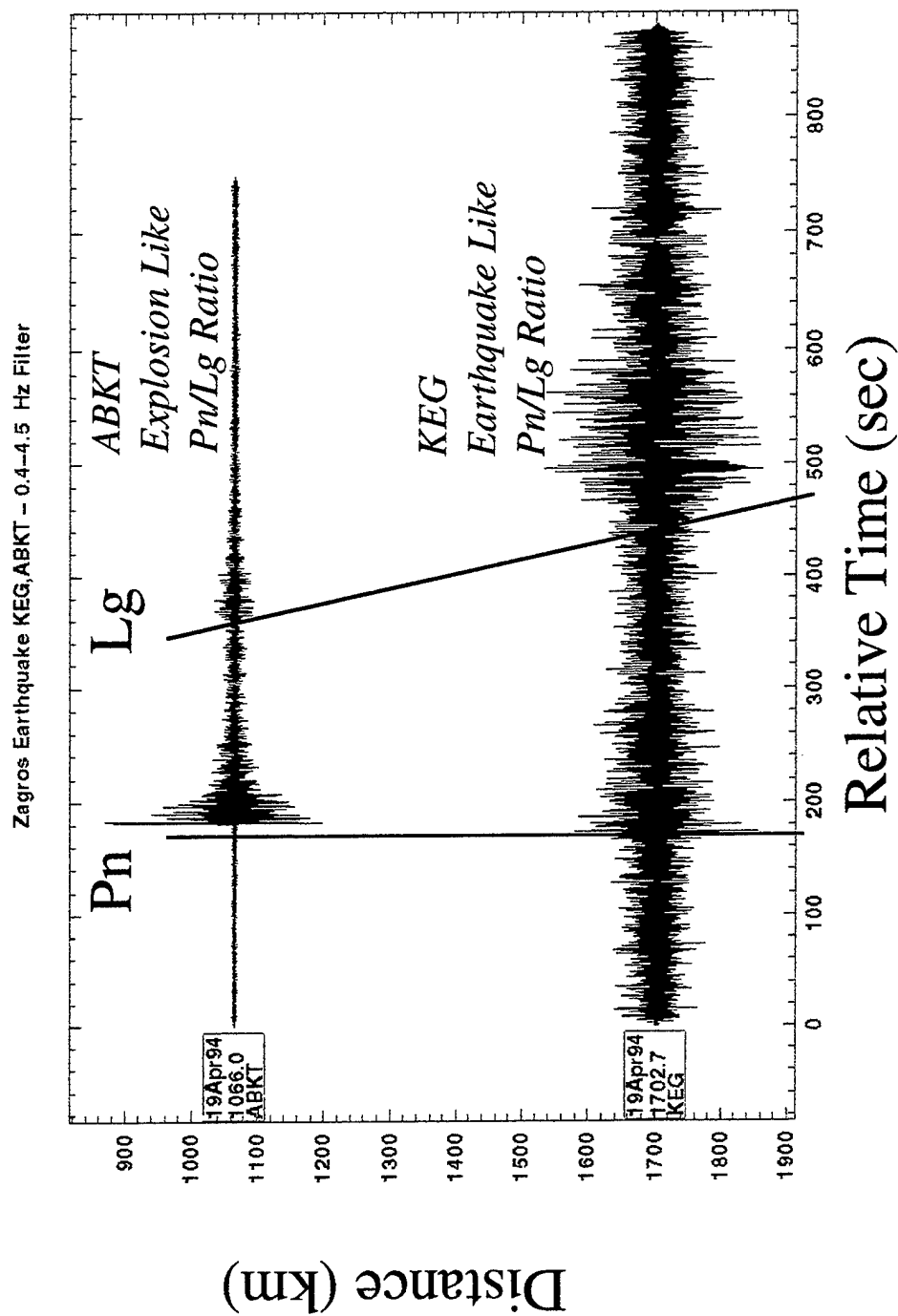
Figure 27: Comparison of ABKT and KEG recording of Zagros earthquake - 0.5-4.5 Hz filter.

This section discusses possible explanations for these observations, based on available information about the geology and geophysics of the region.

3.6.1 *Lg* Blockage By Basin Capture In the Levantine Basin

Figure 28 shows comparisons of propagation paths from events along the northern Jordan-Dead Sea transform (dashed white lines) and the southern extension of the transform in the Gulf of Aqaba (solid black lines). These paths are plotted on gray-scale contour maps of basement depth and Moho depth in **Figure 28(a)** and **(b)**, respectively. As shown, the eastern Mediterranean Sea, or the Levantine Basin, is underlain by thick sediments and a thinning of the crust.

Figure 29(a) and **(b)** shows a direct comparison of the cross sections for all the paths in **Figure 28(a)** and **(b)**. The dashed-line cross sections correspond to the dashed line northern paths in **Figure 29** and the solid-line cross sections correspond to the solid-line paths in **Figure 29**. The dashed-line cross sections show sediment depths extending to 15 km and Moho depths thinning from 35 km to 20 km. Underneath southern Israel, the Sinai, and northern Egypt, there are no sediments and the crustal thickness is relatively constant at about 35 km.

Thus, a very apparent "pinchout" in the crust exists in the Levantine Basin. As discussed above, the seismic velocities in the sediments of the Levantine basin are very low, ranging from 1.5 to 2.0 km/sec, and they overlie much higher velocities of the lower crust and upper mantle. This sharp velocity contrast between the lower velocities in sediments of the Basin and the surrounding higher velocity blocks, which include thinning crust, resemble the conditions observed in the Barents Sea and Caspian Sea Basins. Thus, the "basin capture" mechanism may explain the extinction of *Lg* for the northern paths to KEG which cross the Levantine Basin. Also, the "crustal pinchout" pattern, which was modeled by Jih (1995), also exists. However, the crustal pinchout may be secondary to the primary effect of the strong velocity contrasts in the upper crust and the basin capture mechanism.
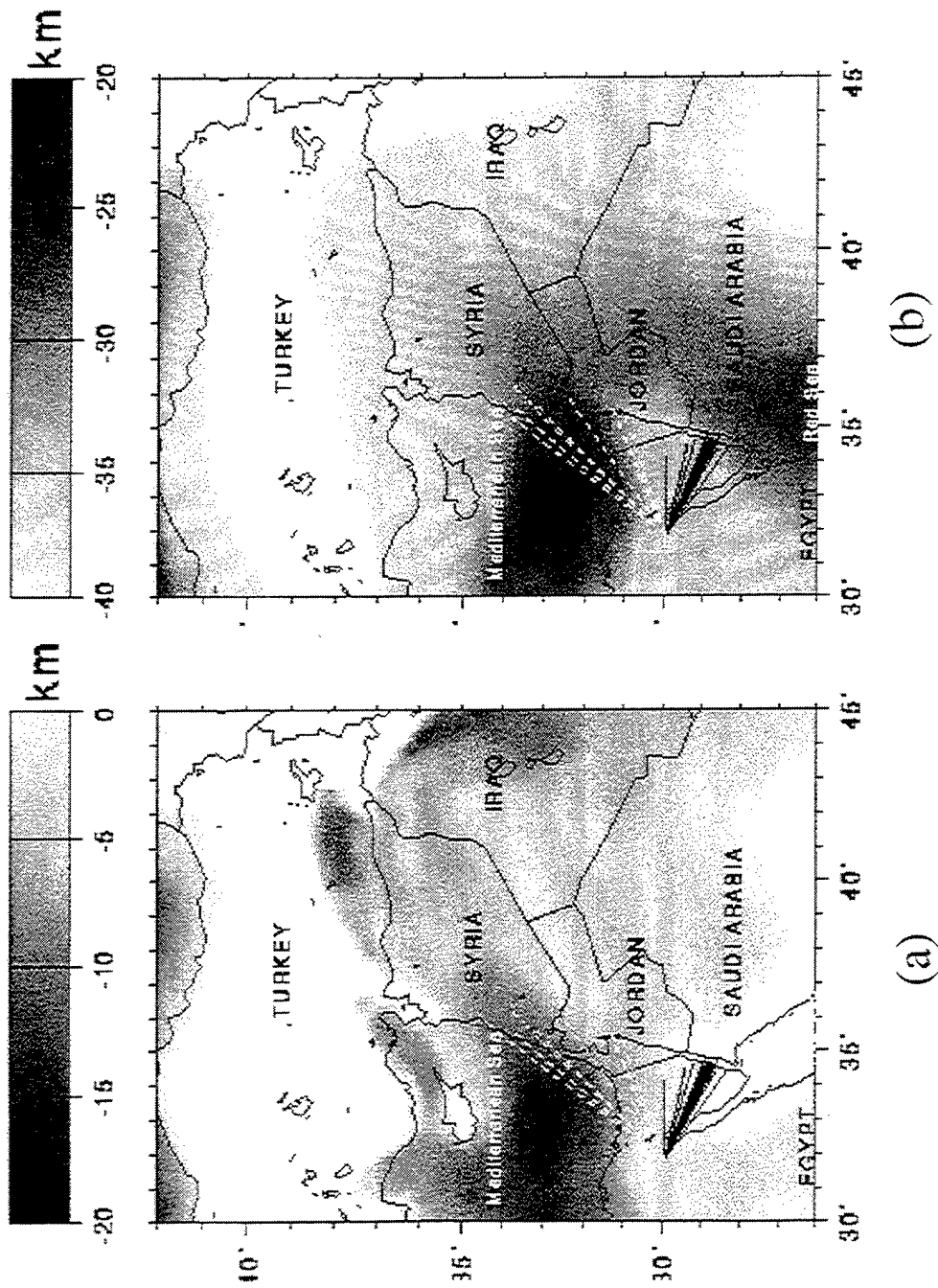
Figure 28: Propagation paths for events along the Jordan/Dead Sea Transform recorded at the Mednet station KEG. (a) Basement depth map. (b) Moho depth map.
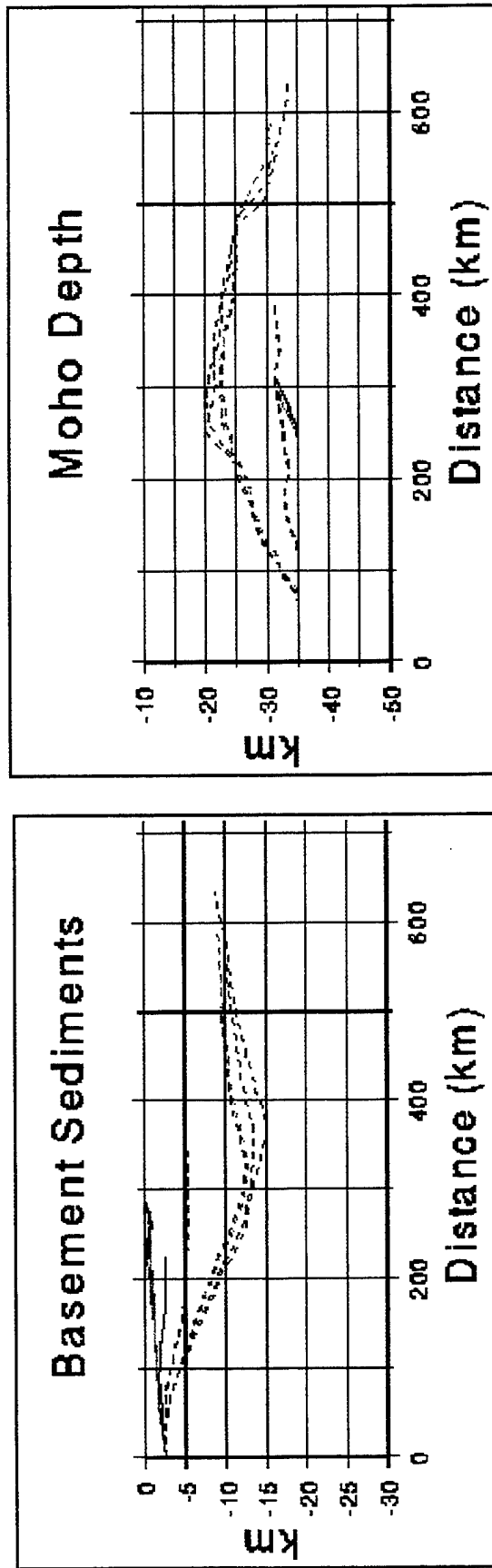
Figure 29: Comparison of the propagation-path cross sections for the various events shown in Figure 27(a). Depth-to-basement cross sections, (b) Depth-to-Moho cross sections.

53

Also, **Figures 15** and **16** may show additional evidence of the "shear-wave energy balance hypothesis" discussed earlier in connection with the Barents and Caspian Sea; i.e., strong *Sn* waves are observed when *Lg* is apparently blocked and visa versa. Moreover, the lack of strong *Sn* waves from the Gulf of Aqaba may be a further manifestation of this effect. Also, as we have pointed out earlier, there is a corresponding tradeoff in *Pn* and *Pg* excitation which accompanies the *Sn* and *Lg* tradeoff. These results again point to the possible development of a *Pn+Pg/Sn+Lg* amplitude ratio discriminant where the relative total compressional and shear wave energy budget should be used in discrimination.

3.6.2 Comparison of Heat Flow in the Levant and Red Sea Regions

Figure 30(a) shows a shaded relief map of the rasterized heatflow database for the Middle East taken from Pollack et al (1993). The same propagation paths to KEG from all the earthquakes Jordan/Dead-Sea/Gulf-of-Aqaba, as well as those which run adjacent to or cross the Red Sea, are plotted. **Figure 30(b)** shows heatflow cross sections for all the northern paths, and **Figure 30(c)** shows the heatflow cross sections for the paths near the Red Sea. For the northern paths, the dashed-line cross sections of heatflow are generally less than 75 mW/m^2, slightly above the global continental average of 65 mW/m^2. The Gulf of Aqaba paths seem to have somewhat higher heatflows, which range between 75 and 100 mW/m^2.

For the paths along the Red Sea, the heatflow values are much more variable, although the expected higher values are found. Generally, at distances closer than 400 km, the heatflow is less than 100 mW/m^2. However, beyond this distance, much higher heatflow values appear which are near the oceanic average heatflow of about 101 mW/m^2 (Pollack et al, 1993). The variations in the heatflows along these paths are probably not significant, given the uncertainties of the observed heatflow data which go into this database. However, the generally observed higher values of heatflow along these paths are consistent with the fact that the Red Sea is considered to be an incipient spreading center with associated upwelling of hot material into the crust from the aesthenosphere. Higher temperatures
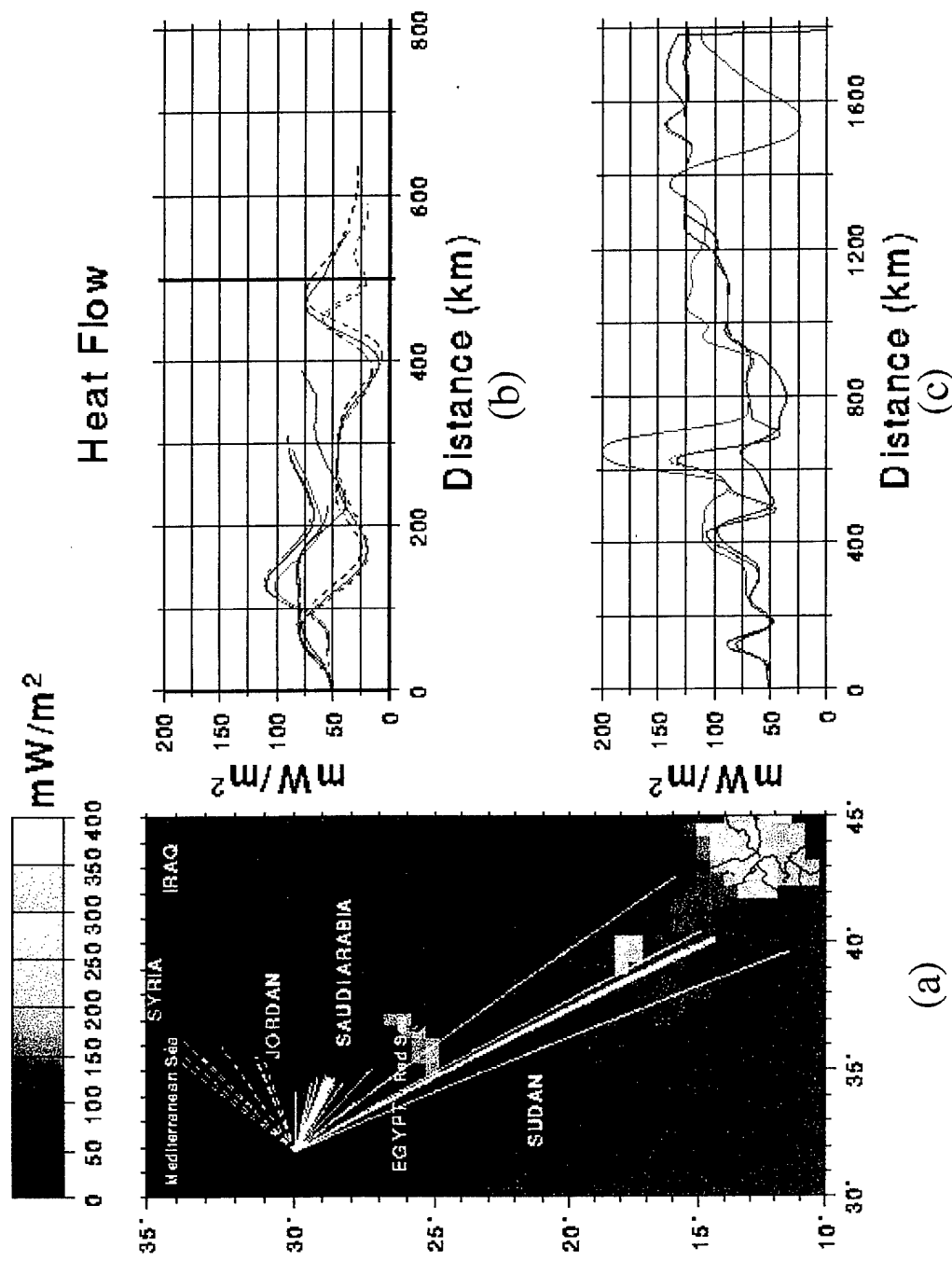
Figure 30: (a) Shaded map of the heatflow for the Middle East region studied in this report. (b) Cross sections of heatflow for the short paths from the Jordan-Dead Sea transform events to KEG. (c) Cross sections of heatflow from the longer paths along the Red Sea from the Southern Egypt events to KEG.

55

usually produce higher seismic Q, and this may explain the lack of high frequencies and the high magnitude detection thresholds for events whose paths cross this region.

We thus conclude overall that high heatflow regions cause high anelastic attenuation. However, this does not necessarily block Lg, at least not at low frequency (<1 Hz). The lack of Sn may be a direct result of the elevation of the aesthenosphere and the higher attenuation in the lower crust and upper mantle. However, for the paths crossing the Levantine Basin, where heatflows are relatively high, high attenuation does not kill Sn even though Lg is blocked. Again, the lack of Sn may be because all the shear-wave energy propagates as Lg.

3.6.3 Zagros Azimuthal Patterns - Propagation Difference or Radiation Patterns?

For the observation of the azimuthal differences in the excitation of Pn and Lg from the Zagros, two possible explanations are considered, propagation-path differences and source radiation patterns.

Figure 31 shows a comparison of the great-circle propagation paths for the signals shown in **Figure 27** from the common Zagros earthquake. The shaded maps in **Figure 31(a)** include the topography (top), depth to basement (middle), and depth to Moho (bottom), taken from the Eurasia data base from Cornell (Fielding et al, 1992). **Figures 31(b)** show the cross sections for the Zagros-to-KEG and Zagros-to-ABKT paths, respectively. The path to the ABKT stations crosses the central part of Iran, including the Lut depression (Giese et al, 1983) where there are fluctuations in both depth to basement and depth to Moho, although these variations are not extreme. The sediments in the Lut depression, for example, only reach 5 to 10 km, although there are sudden changes in sediment depth. The Moho depth shows little variation. The path from the Zagros to KEG also shows variations in depth to basement and depth to Moho, but the variations are more gradual. The underlying sediments of the Zagros mountains are mainly platform cover and shelf type (Berberian and King, 1981). To the west, the sedimentary rocks are thickest in the

Figure 31: Interpretation of propagation paths from the Zagros event, shown in Figure 25, to the two stations ABKT and KEG. (a) Shaded maps of elevation (top), depth to basement (middle) and depth to Moho (bottom) with white lines showing the paths. (b) Cross section for the path to KEG. (c) Cross section for the path to ABKT.

57

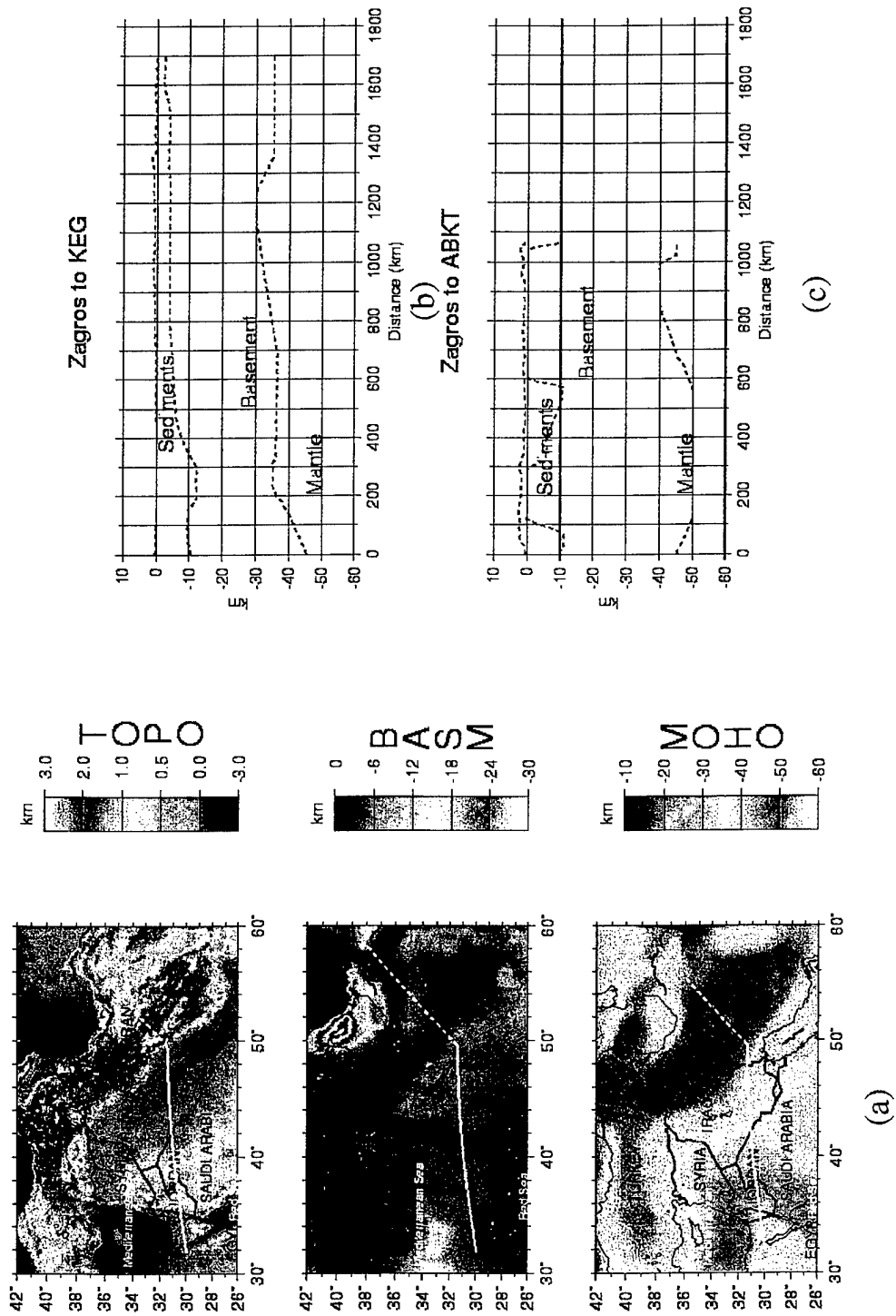Mesopotamian Fordeep, at about 13 km, and gradually thin to the west into the Arabian Shield, where there are no sediments (Beydoun, 1989). Also, for this path, the Moho depth exhibits little variation.

Comparison of these two propagation paths suggests that the path to ABKT has more complicated near-crustal variations in sediment thickness. The "basin capture" idea may be invoked for the Lut depression as an explanation for the "blockage" of Lg. The path to KEG passes through regions of thick sediments, but the sedimentary basin thins gradually to the west. Blockages of Lg are associated with propagation through completely contained basins, not gradually thinning basins like the Mesopotamian Fordeep.

An alternative explanation is that the differences in Pn/Lg ratio for the two paths may be due to differences in the compressional and shear wave radiation patterns from earthquakes in the region. This idea is illustrated in **Figure 32**. **Figure 32(a)** is a reproduction of **Figure 24** that shows the great-circle paths from all the earthquakes to the two stations. For comparison, **Figure 32(b)** shows source mechanisms for Zagros earthquakes studied by Ni and Barazangi (1986) plotted on a tectonic map of the Zagros thrust belt. Note that these are not the same events, i.e., the Ni and Barazangi (1986) events were earlier than those in this study. However, they show that, with a few exceptions, a predominant thrust source mechanism for earthquakes in the Main Zagros thrust zone. The strike of the focal planes tends to parallel the trend of the Zagros mountains, although there are variations in strike. The pressure axis tends to directed vertically, or somewhat the northeast or southwest.

The two bold arrows in **Figure 31(b)** show the two approximate directions to the two stations. With some exceptions, the path to KEG tends to parallel strike or fall at an oblique angle to strike of the thrust mechanism of the earthquakes. The path to ABKT tends to fall more normal to the strike. The maximum P wave excitation for the thrust mechanism, assuming a double-couple, would tend to be directed near the vertical. If the takeoff angle relative to the vertical of Pn waves from the sources in the Zagros is smaller than 45 degrees, i.e., close to the pressure axis, the radiation will strongest for the compressional waves and weaker

58
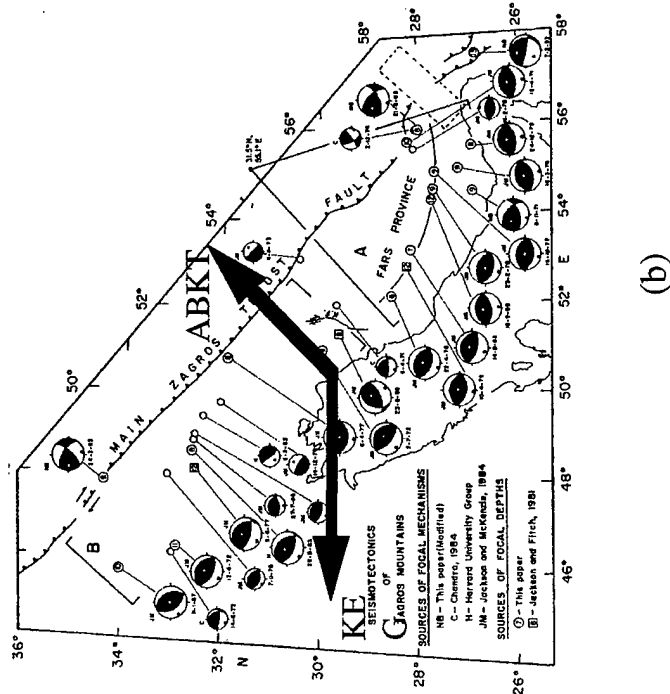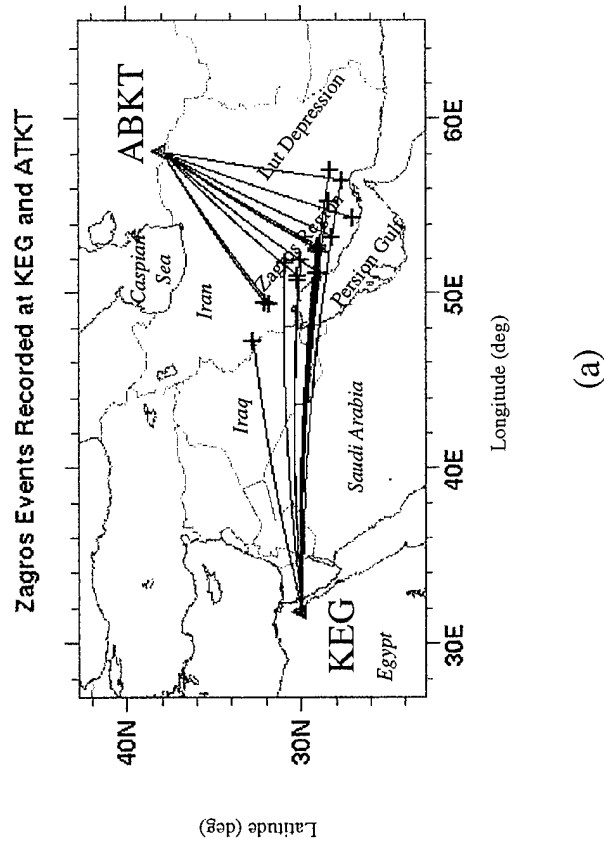
Figure 32: (a) Locations and paths from the Zagros earthquakes studied in this report to the stations KEG and ABKT. (b) Focal mechanisms for earthquakes in the Zagros from Ni and Barazangi (1986). The directions to the two stations are shown. The path to ABKT is approximately normal to the strike of the predominant thrust mechanisms where as the path to KEG is oblique to the strike.

59

for the shear waves. Thus, if *Lg* predominantly comes from shear waves taking off at steep angles, the thrust source mechanisms may tend to under-excite shear waves to the northeast and hence *Lg* may be underexcited. The path to KEG may be such that the *Pn* takeoff angles are closer to one of the nodal planes and the shear wave excitation to the west may be stronger. Thus, the variation in *Pn/Lg* ratios apparent in **Figure 27** may be due to the differences in radiation patterns of *P* and *S* waves at high frequency.

The source radiation pattern explanation assumes that source mechanisms of the Zagros earthquakes in this study are similar to those in Ni and Barazangi (1986) and that radiation patterns of point double-couple mechanisms are not canceled out by scattering at high frequency. A number of the earthquakes in this study were large enough to produce CMT solutions, so the first assumption can be checked. As for the second, it should be noted that the signals in **Figures 25, 26**, and **27** are low frequency (< 1 Hz), which may be low enough that radiation patterns may still be observed. A confirmation of this idea must await closer examination of the actual source mechanisms of these events and evaluation with synthetic seismograms.

3.7 Discriminants for Middle East Earthquakes - Inter Region Comparisons with Explosions

The earthquakes recorded at KEG and ABKT were processed through ISEIS to extract frequency-dependent regional *P/S* ratios and compared with events in other regions. The amplitude ratios, *Pn/Sn* and *Pn/Lg*, were computed for all the events were computed from RMS envelopes shown in **Figure 33**. These envelopes were computed by averaging the root-mean-square (RMS) amplitude in adjacent 1 second windows shifted down the traces. Both the unlogged and logged envelopes were computed, as shown in **Figures 33(a)** and **(b)**, respectively. The time-picks for the phases, picked on waveforms, are shown on the envelope traces in **Figure 33**. In the case of the Gulf of Aqaba events in **Figure 32**, only *Pn*, *Pg*, and *Lg* were picked. The maximum RMS
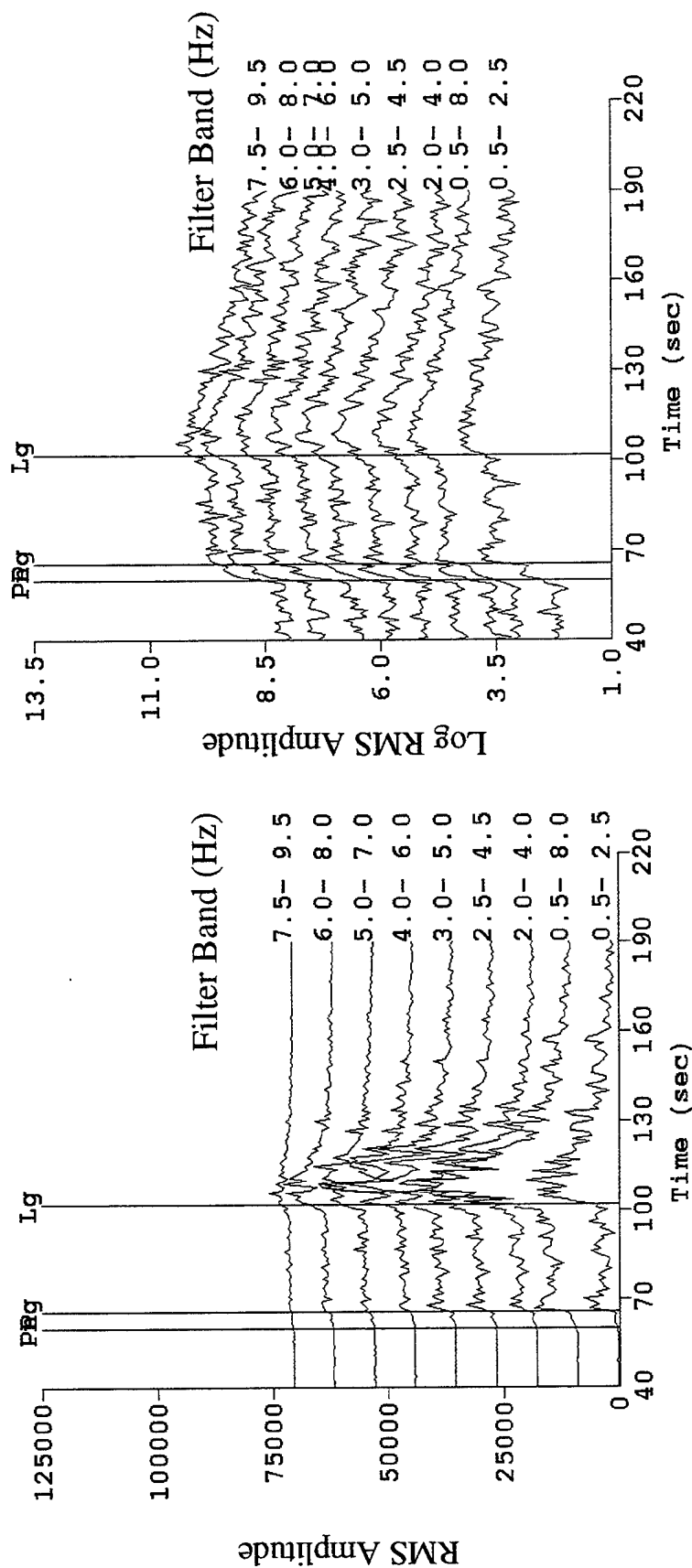
Figure 33: RMS-amplitude waveform envelope traces computed on bandpass filtered waveforms for a Gulf of Aqaba event recorded at KEG. The phase picks were made on waveforms. The envelope traces have been shifted for display purposes.

amplitudes on each of the envelopes were then computed for each of the phases in each of the nine frequency bands shown in **Figure 33**. From these envelope traces, amplitude ratios were computed.

Figure 34 shows plots versus distance of 6 to 8 Hz *Pn/Sn* ratios for the earthquakes on the Dead Sea transform where the *Lg* wave was blocked. Also plotted are ratios for Kola Peninsula mine blasts and Novaya Zemlya earthquakes. Of course, the Kola/Novaya Zemlya source region is much different from the Middle East, both tectonically and geophysically. However, they are similar in that both the Novaya Zemlya and Dead Sea transform earthquakes had blocked *Lg*. The curve in **Figure 33(a)** is the distance correction trend for *Pn/Sn* determined by Sereno (1991). The trend clearly increases distance, and **Figure 34(b)** shows the same data but with the Sereno (1991) distance trend removed. The distance corrected points for the Dead Sea transform earthquakes clearly fall below both mine blasts and nuclear explosions, indicating that Middle East earthquakes produce much stronger *Lg* waves, relative to *Pn*, than do blasts in Russia recorded in Scandinavia

Finally, **Figure 35** shows plots versus distance of *Pn/Lg* amplitude ratios, corrected for distance, for the Zagros earthquakes recorded at both KEG and ABKT compared with the Kazakh nuclear explosions and Chinese earthquakes recorded at WMQ, studied by Baumgardt and Der (1995). These two regions may be more similar tectonically. However, the ABKT waveforms had blocked or underexcited *Lg* waves from the Zagros. In the 2 to 4 Hz band in **Figure 35(a)**, the ABKT ratios at around 1000 to 1200 km distance have high scatter and higher ratios that fall close to those of nuclear explosions at Kazakh. The KEG recordings of the same region earthquakes have somewhat lower values of ratios, which seems consistent with the earlier comparison of the waveforms. Lower ratios indicate large *Lg* relative to *Pn*. However, as a group, the KEG and ABKT ratios are close. At higher frequency, 4 to 6 Hz, the earthquake points clearly fall well below the nuclear explosions and are more consistent with the Chinese earthquakes.
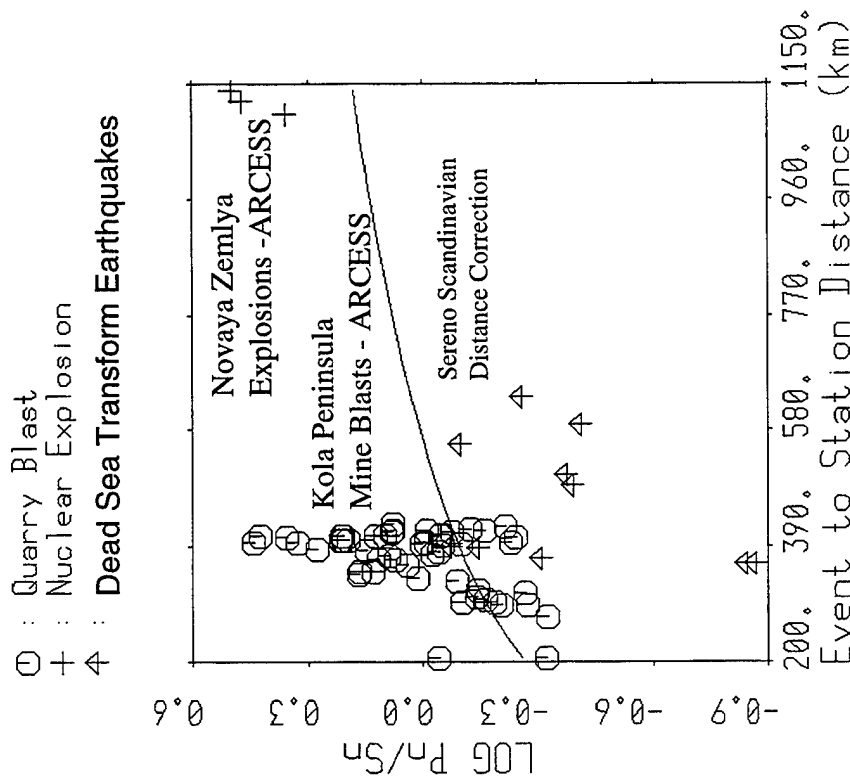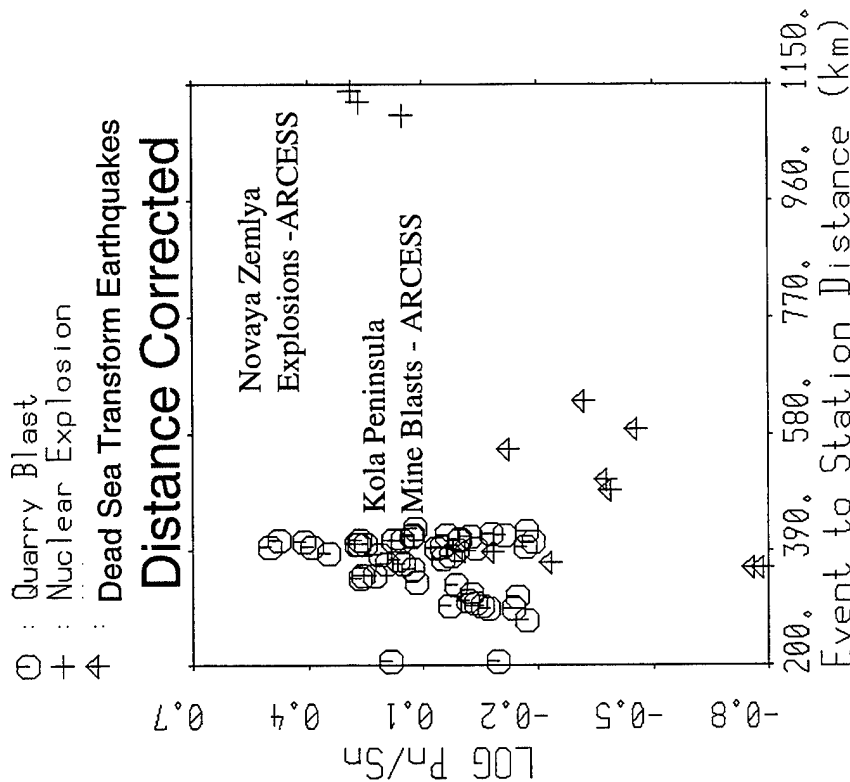
Figure 34: Pn/Sn ratios for earthquakes on the Jordan/Dead Sea transform, recorded at KEG, plotted as a function of distance along with nuclear explosions in Russia and mine blasts in Scandinavia recorded at the ARCESS array. (a) Original data with the Sereno (1991) distance correction curve for Scandinavia. (b) Data corrected for distance using the Sereno (1991) curve.

63
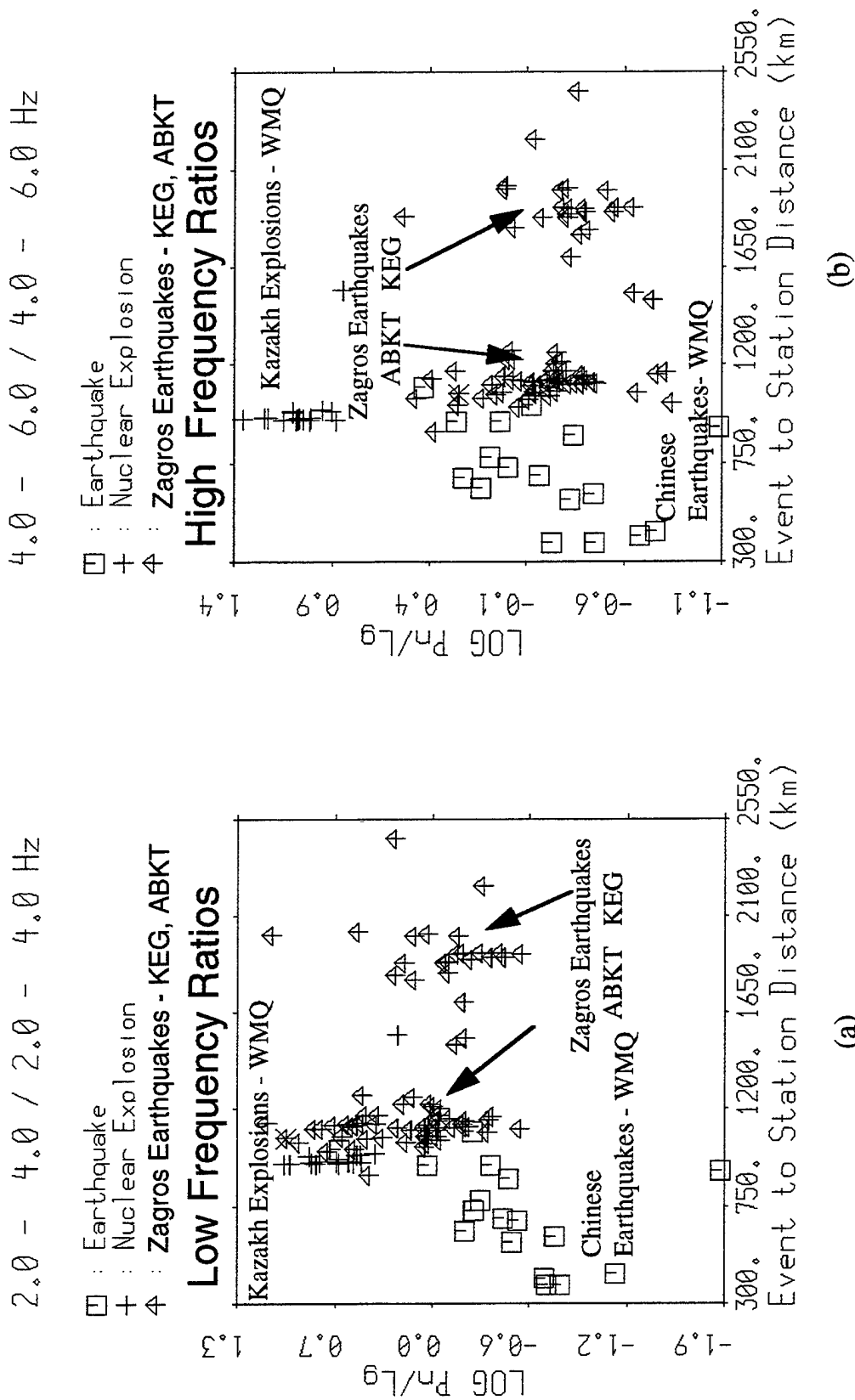
Figure 35: Pn/Lg ratios for earthquakes in the Zagros, recorded at KEG and ABKT, plotted as a function of distance along with earthquakes in China and nuclear explosions in Russia recorded at WMQ. (a) 2-4 Hz. (b) 4- 6 Hz. Both sets of data are corrected for distance using the Sereno (1991) curve.

These results indicate that, for the unblocked paths, earthquakes in the Middle East can be discriminated from blasts in other regions. However, at low frequency, the results are more problematic, particularly for blocked paths. Because of the high attenuation in the Middle East, high frequency discriminants may not be usable. Generally, it appears that, at low frequency, earthquakes in the Middle East produce much stronger shear energy, either *Sn* or *Lg,* than do nuclear explosions in other regions. It is likely that if a nuclear explosion occurred in the Middle East, it may also underexcite shear waves relative to compressional waves even at low frequency. The only problematic discrimination would be earthquakes along blocked paths, such as Zagros to ABKT. However, large shear waves would still be observed for the other station, KEG.

4. SUMMARY AND CONCLUSIONS

The systematic seismological monitoring of the CTBT and NPT will likely encounter the requirement to characterize events in parts of the world where there is limited historical data for nuclear explosions or similar type sources. The Middle East poses a particular challenge to the monitoring system because of the high seismicity of the region, the complex propagation conditions, and the currently limited quantity of regional seismic data for small events in the region. Because of the presence of countries in the Middle East that aspire to become nuclear powers, a capability must be developed to reliably identify possible "first test" nuclear explosions in these countries. The approach taken in this study to address this problem has been to characterize the effects of complex heterogeneous crustal structure on regional *P/S* ratio discriminant feature, using crustal structure information available from GIS databases, and to compare these features of earthquakes in the Middle East with nuclear explosions and mine blasts in other regions. Correct discrimination between earthquakes and any possible "first test" nuclear explosions must account for the effects of differences in geology and geophysics of the Middle East and the other regions containing historical nuclear explosions.

The well-recognized problem of "*Lg* blockage" was reexamined in terms of the effect on discrimination capability in the Middle East. Following up on earlier work on *Lg* blockage in the Barents Sea, where the *Lg* was found to be blocked by the Barents Sedimentary Basin, blockages of similar origin have been found in the Middle East in the Caspian Sea north of Iran and in the Leventine Basin of the Mediterranean Sea. Comparison of crustal cross sections, derived from GIS databases, for blocked and unblocked paths, it was found that *Lg* blockage is associated with the presence of an enclosed sedimentary basin along the path, and that this feature may be a predictor of *Lg* blockage. *Lg* blockages in these regions can be explained by the "basin capture" idea, where the shear-waves composing the *Lg* wavetrain are captured by the lower velocities of the sediments in the basins and perhaps diverted into other propagation modes, such as *Sn*, by the laterally heterogeneous velocity variations. A corre-

sponding crustal thinning does not seem to be required to block Lg, since no such thinning appears in the Barents and Caspian Sea Basins.

Obviously, P/Lg amplitude-ratio discriminants cannot be used if Lg is blocked by the propagation path. However, this study has shown that when Lg is blocked, Sn has greater energy. In fact, earthquakes can be identified on the basis of small P/Sn amplitude ratio when weak or no Lg is recorded. Often, however, when Lg propagates with high energy, Sn is not well observed. Other studies have usually explained inefficient Sn propagation as being caused by high anelastic attenuation. However, this tradeoff between Sn and Lg amplitudes may be explained by the "shear-wave energy balance" idea in which seismic source produces a certain amount of shear wave energy that must either propagate as Sn or Lg modes. If one mode is blocked, the shear-wave energy will be partitioned into the other mode.

Moreover, a similar partitioning of energy has also been observed for Pn and Pg; i.e., when Pg is strong, Pn is weak and visa versa. Emergent Pn arrivals are observed when Sn is weak or not recorded above the Pg coda "noise." Whatever blocks Lg also blocks Pg and compressional-energy gets partitioned between Pn and Pg in the same way in which shear-wave energy is partitioned between Sn and Lg. Seismic events can still be identified on the basis of the relative amount of total compressional (Pn and Pg) and total shear wave energy (Sn and Lg). Thus, a total P/S amplitude ratio discriminant is now being considered.

This study has also revealed the presence of strong, low-frequency Lg waves propagating around the Red Sea, a region that was previously thought to block Lg. Also, Pn was extremely weak for earthquakes in the region and in fact non existent at frequencies above 0.5 Hz. The Lg waves are also limited in bandwidth to below 1 Hz. The attenuation of high-frequency signals in the Red Sea region may be caused by upwelling of high-temperature, low Q aesthenospheric material in the incipient spreading center as indicated by higher heatflow in the region. However, high attenuation does not kill low-frequency Lg waves from the earthquakes.

Finally, earthquakes in the Zagros Mountains indicated azimuthally dependent patterns in Pn/Lg amplitude ratio which may be due either to

differences in *Lg* blockage along different paths or source mechanism effects. It has usually been assumed that source radiation pattern effects would be washed out at high frequency by scattering in laterally heterogeneous media. However, as in other regions of the Middle East, the regional signals observed from the Zagros were found to be low-frequency, which may be more affected by radiation patterns. Also, no *Sn* phases were observed in either direction. Since this study has suggested that both *Sn* and *Lg* have usually not been observed to be blocked at the same time, the fact that both *Sn* and *Lg* are weak in a certain direction points to a possible source radiation-pattern cause. Further study of the source mechanisms of these events and modeling studies are planned to investigate this idea further.

The Zagros results point out the need for multiple station recordings of earthquakes in order to confidently identify them. Most of the Zagros earthquakes could be identified on the basis of high *Pn/Lg* amplitudes at KEG, except for the events in the southern most part of the range, where the Lg waves were not observed (See **Figure 25**, where there is strong Lg attenuation). Beyond about 2400 km, attenuation appears to kill the propagation of most shear waves at high frequency in this region. Thus, having two stations recording the Zagros earthquakes would identify most of them, whereas if only the ABKT station were available, positive identification of the earthquakes may not be possible on the basis of *Pn/Lg* amplitude ratios alone.

Another example of where more than one station would be helpful is the case of the November 16, 1978 earthquake in the Caspian region recorded at ILPA. The ILPA array element, IR1, recorded waveforms that looked very explosion-like because of the high *Pn/Sn* ratios and that both *Pn* and *Sn* were large at high frequency, which is uncharacteristic of earthquakes in the region. However, the weak *Sn* waves and strong *Pn* waves from this event may have been caused localized path blockages of *Sn* or radiation pattern effects that excite strong *Pn* and weaker *Sn* waves in the direction of ILPA. Having another station that recorded this event at a different azimuth than the ILPA azimuth would have been very helpful in its identification. A single observation of high *Pn/Sn* ratio, which is what was

found for the ILPA IR1 recording, is not sufficient information to identify the event as an explosion. Additional observations of high Pn/Sn ratios would still be insufficient to positively identify the explosion, although the probability of explosion might be increased. On the other hand, a <u>single</u> station recording a <u>larger</u> Sn than Pn at high frequency at a different azimuth would be sufficient to identify the event as an earthquake with high probability.

In spite of tectonic complexity of the regions studied in this report and all the variations of Sn and Lg excitation, comparison of most of the Pn/Sn and Pn/Lg amplitude ratios features of the Middle Eastern earthquakes with those of nuclear explosions in Russia recorded in Scandinavia and China showed that the Middle Eastern earthquakes usually had lower ratios than nuclear explosions. However, the question of whether a nuclear explosion near the Jordan/Dead Sea transform, in the Red Sea region or in the Zagros Mountains, would look like explosions at Kazakh and Novaya Zemlya, recorded at comparable distances, remains unanswered. If propagation path blockages are the only effect, then it is likely that nuclear explosions in the Middle East should clearly be discriminated from earthquakes, since any blockage effects should be the same for explosions as for earthquakes. Since most earthquakes observed in the Middle East have some kind of large shear excitation, either Sn or Lg, compared with some kind of compressional wave excitation, either Pn or Pg, any nuclear explosion in the regions studied so far should be identifiable.

The overall conclusion of this study is that discrimination between explosions and earthquakes in the Middle East should be feasible assuming adequate signals are detected. However, perhaps the greatest discrimination problem for small events will be detection of weak signals. The station in Egypt, KEG, appears to be adequate for monitoring within 600 km with high frequency discriminants, which covers most of Israel, Saudi Arabia, and other parts of northern Africa. However, the lowest magnitude in this distance range for which usable signals were recorded at KEG was body-wave magnitude of 3.5. This is well above the threshold of Scandinavian arrays and the desired threshold for monitoring a low yield CTBT, which is on the order of 2.5. The proposed LUXESS array may improve the de-

tection threshold with improved instrumentation, better deployments of sensors, and the use of beamforming methods to lower detection thresholds.

However, even after the LUXESS array is installed, discrimination in other critical areas, such as Iraq and Iran, may be problematic if high-frequency discriminants are required because high frequency signals above 1 to 2 Hz are strongly attenuated. Although large earthquakes in regions like the Zagros thrust produce large shear waves, large nuclear blasts can also produce large shear waves at low frequency. Small nuclear explosions, including possible decoupled explosions, may require higher frequency discriminants for confident identification (Bennett et al, 1995). As this study has shown, important phases, such as *Pn* can be eliminated by anelastic attenuation at high frequencies. Thus the most important challenge to discrimination in the Middle East may not be blockage of certain regional phases, such as *Lg*, but rather the elimination by anelastic attenuation of all high frequencies in certain important phases. Future assessments of network performance for discrimination in critical regions like the Middle East need to include the detectability of high-frequency signals above and beyond the usual low-frequency detection thresholds.

REFERENCES

Ambraseys, N.N. and M. Barazangi (1989). The 1759 earthquake in the Beak Valley: implications for earthquake hazard assessment in the eastern Mediterranean region, *J. Geophys. Res.*, **94**, 4007-4013.

Barazangi, M., E. Fielding, B. Isacks, and D. Seber (1996). Geophysical and geological databases and CTBT monitoring: a case study of the Middle East, in *Monitoring a Comprehensive Test Ban Treaty*, E.S. Husebye and A.M. Dainty, 197-224, NATO ASI Series, Kluwer Academic Publishers.

Baumgardt, D.R. (1990). Investigation of teleseismic *Lg* blockage and scattering using regional arrays, *Bull. Seism. Soc. Am.*, **80**, 2261-2281.

Baumgardt, D.R. (1991). High frequency array studies of long range *Lg* propagation and the causes of *Lg* blockage and attenuation of the Eurasian continental craton, PL-TR-91-2059(II), 21 March 1991, ADA236984.

Baumgardt, D.R. (1993). Seismic waveform feature analysis and discrimination of the December 31, 1992 Novaya Zemlya event, in *The Novaya Zemlya Event of 31 December 1992 and Seismic Identification Issues, 15 th Annual Seismic Research Symposium, ARPA Report*, 30pp., PL-TR-93-2160. ADA271458.

Baumgardt, D.R. (1995). Case studies of seismic discrimination problems and regional discriminant transportability, *PL-TR-95-2106*, Final Report, ENSCO, Inc., Springfield, VA, ADA302362.

Baumgardt, D.R. and Z. Der (1994). Investigation of the transportability of the P/S ratio discriminant to different tectonic regions, *Scientific Report No. 1*, PL-TR-94-2299, 6 December 1994, ENSCO, Inc., ADA292944.

Baumgardt, D.R. and Z. Der (1996). Identification of presumed shallow underwater chemical explosions using land-based regional arrays, submitted to *Bull. Seism. Soc. Am.*

Baumgardt, D.R. and K.A. Ziegler (1988). Spectral evidence of source multiplicity in explosions: application to regional discrimination of earthquakes and explosions, *Bull. Seism. Soc. Am.*, **78**, 1773-1795.

Baumgardt, D.R. and G. Young (1990). Regional seismic waveform discriminants and case based event identification using regional arrays, *Bull. Seism. Soc. Am.*, **80**, Part B, 1874-1892.

Baumgardt, D.R., G.B. Young, and K. A. Ziegler (1991a). Design and Development of the Intelligent Event Identification System: Design Considerations and Processing for Regional Event Identification, Scientific Report No. 1, *PL-TR-91-2211*, 29 August 1991, ENSCO, Inc., Springfield, VA., ADA244503.

Baumgardt, D.R., S. Carter, M. Maxson, J. Carney, K. Ziegler, and N. Matson (1991b). Design and development of the intelligent event identification system, *PL-TR-91- 22298(I)*, Final Report, Volumes I,II, and III, ENSCO, Inc., Springfield, VA, ADA248381.

Ben-Avraham, Z. and A. Ginzburg (1990). Displaced terranes and crustal evolution of the Levant and the Eastern Mediterranean, *Tectonics*, **9**, 613-622.

Ben-Avraham, Z. and V. Lyakhovsky (1992). Faulting processes along the northern Dead Sea transform and the Levant margin, *Geology*, **20**, 1139-1142.

Bennett, T. J., B.W. Barker, M.E. Marshall, J.R. Murphy (1995). Detection and identification of small regional seismic events, Final Report, *PL-TR-95-2125*, S-Scubed, La Jolla, CA, ADA305536.

Berberian, M. (1983). The southern Caspian: a compressional depression floored by a trapped, modified oceanic crust, *Can. J. Earth Sci.*, **69**, 163-183.

Berberian, M. and G. King (1981). Towards a paleography and tectonic evolution of Iran, *Can. J. Earth Sci.*, **18**, 210-265.

Beydoun, Z. R. (1989). Hydrocarbon potential of the deep (pre-Mesozoic) formation in the Middle-East Arab countries, in *Technical Papers Presented at the Seminar on Deep Formations in the Arab Countries: Hydrocarbon Potential and Exploration Techniques*, Abu Dhabi National Oil Company, Abu Dhabi, UAE.

Fielding, E.J., M. Barazangi, and B.L. Isacks (1993). A geological and geophysical information system for Eurasia, Final Technical Report, Phil-

lips Laboratory, Contract No. F29601-91-F-DB08, Cornell University, Ithaca, New York.

Giese, P., J. Makris, B. Akashe, P. Röwer, H. Letz, M. Mostaanpour (1983). Seismic crustal studies in Southern Iran between the Central Iran and the Zagros belt, in *Geodynamic Project (geotraverse) In Iran*, Final Report, Report No. 51.

Ginzburg, A. and Y. Folkman (1990). The crustal structure between the Dead Sea rift and the Mediterranean Sea, Earth. Planetary Sci. Letters, 51, 181-188.

Gitterman, Y. and A. Shapira (1993). Spectral characteristics of seismic events off the coast of the Levant, *Geophys. J. R. Ast. Soc.*, **83**, 1799-1812.

Goldstein, P., C. Schultz, S. Larsen, and L. Minner (1996). Modeling of regional wave propagation phenomena in the Middle East and North Africa and New analysis Capabilities in Proceedings of the 18th Annual Seismic Research Symposium on Monitoring a Comprehensive Test Ban Treaty, 4-6 September 1996, *PL-TR-96-2153*, Environmental Research Papers, No. 1195, J.F. Lewkowicz, J.M McPhetres, D.T Reiter, eds., pp 165-171, ADA313692.

Grant, L., F. Ryall, I. Henson, and W. Rivers (1996). Ground truth database for seismic discrimination research, Proceedings of the 18th Annual Seismic Research Symposium on Monitoring a Comprehensive Test Ban Treaty, 4-6 September 1996, *PL-TR-96-2153*, Environmental Research Papers, No. 1195, J.F. Lewkowicz, J.M McPhetres, D.T Reiter, eds., pp 997-1006, ADA313692.

Jih, R.S. (1995). Waveguide effects of large-scale structural variation, anelastic attenuation, and random heterogeneity on SV, *Lg* Propgation: A finite-difference modeling study, *PL-TR-96-2016*, Environmental Research Papers, No. 1186, Phillips Laboratory, Hanscom, AFB, MA, ADA310774.

Kadinski-Cade, K., M. Barazangi, J. Oliver, and B. Isacks (1981). Lateral variations of high-frequency seismic wave propagation at regional distances across the Turkish and Iranian plateaus, *J. Geophys. Res.*, **86**, 9377-9396.

Kennett, B.L.N. (1986). *Lg* waves and structural boundaries, *Bull. Seism. Soc. Am.*, **76**, 1133-1142.

Kennett, B.L.N. (1996). Understanding seismic wave propagation at regional and teleseismic distance, Proceedings of the 18th Annual Seismic Research Symposium on Monitoring a Comprehensive Test Ban Treaty, 4-6 September 1996, *PL-TR-96-2153*, Environmental Research Papers, No. 1195, J.F. Lewkowicz, J.M McPhetres, D.T Reiter, eds., pp 997-1006, ADA313692.

Makris, J., C.H. Henke, F. Egloff and T. Akamaluk (1991). The gravity field of the Red Sea and East Africa, *Tectonophys*, **198**, 369-381.

Ni, J. and M. Barazangi (1983). High-frequency seismic wave propagation beneath the Indian Shield, Himalayan Arc, Tibetan Plateau and surrounding regions: high uppermost mantle velocities and efficient *Sn* propagation beneath Tibet, *Geophys. J. R. astr. Soc*, **72**, 665-689.

Ni, J. and M. Barazangi (1986). Seismotectonics of the Zagros continental collision zone and a comparison with the Himalayas, *J. Geophys. Res.*, **91**, 8205-8218.

Pollack, H.N., S.J. Hurter, and J.R. Johnson (1993). Heat flow from the earth's interior: analysis of the global data set, *Rev. of Geophys.*, **31**, 267-280.

Rodgers, A. J., J.F. Ni, and T. M. Hearn (1996). Propagation characteristics of short-period *Sn* and *Lg* in the Middle East, submitted to *Bull. Seism. Soc. Am.*

Ruzaikin, A., I. Nersesov, V. Khalturin, and P. Molnar (1977). Propagation of *Lg* and lateral variations in crustal structure of Asia, *J. Geophys. Res.*, **82**, 307-316.

Ryall, A.S., D.R. Baumgardt, M.D. Fisk, F. Riviere-Barbier (1996). Resolving regional discrimination problems: some case histories, in *Monitoring a Comprehensive Test Ban Tready*, E.S. Huysebye and A.M. Dainty, 721-741, NATO ASI Series, Kluwer Academic Publishers.

Sato, H., I. S. Sacks, T. Murase, G. Muncill, and H. Fukuyama (1989). *Qp* melting temperature relation in peridotite at high pressure and temperature: attenuation mechanism and implications for the mechanical properties of the upper mantle, *J. Geophys. Res.*, **94**, 10,647-10,661.

Sereno, T.J. (1991). Simulation of the detection and location capability of regional seismic networks in the Soviet Union, Final Report, *SAIC-91/1061*, SAIC, San Diego, CA.

Shishkevish, C. (1979). Propagation of *Lg* seismic waves in the Soviet Union, *N-1014-ARPA*, February 1979, Rand, Santa Monica, CA.

Sikharulidzhe, I.I. (1964). The nature of *Lg* and Rg and the investigation of the structure of the earth's crust, *AS Georgian SSR, Transactions of the Geophysical Institute*, **22**, 57-70.

Teng, Y.C. and J.T. Kuo (1993). Finite-element modeling of the blockage and scattering of *Lg* wave propagation, *15th Annual Seismic Research Symposium, Proceedings*, 8-10 September 1993, Vail, Co., 391-397, PL-TR-93-2160, ADA271458.

Texas Instruments (1977). Iranian Long-Period Array, Final Report, Equipment Group, Texas Instruments, Inc., 8 April 1977.

Walley, C. (1988). A braided strike-slip model for the northern continuation of the Dead Sea fault and its implications for Levantine tectonics, *Tectonophys*, **145**, 63-72.

Wessel, P. and W.H.F. Smith (1995). The Generic Mapping Tools (GMT) version 3.0, Technical Reference and Cookbook, SOEST/NOAA.

Zhang, T.R. and T. Lay (1995). Why the *Lg* phase does not traverse oceanic crust, *Bull. Seism. Soc. Am.*, **85**, 1665-1678.

Zhang, T., S. Y. Schwartz, and T. Lay (1994). Multivariate analysis of waveguide effects on short-period regional wave propagation in Eurasia and its application in seismic discrimination, *J. Geophys. Res.*, **99**, 21929-21945.

Zonenshain, L.P. and X. Le Pichon (1986). Deep basins of the Black Sea and Caspian Sea as remnants of Mesozoic back-arc basins, *Tectonophys*, **123**, 181-211.

THOMAS AHRENS
SEISMOLOGICAL LABORATORY 252-21
CALIFORNIA INSTITUTE OF TECHNOLOGY
PASADENA, CA 91125

SHELTON ALEXANDER
PENNSYLVANIA STATE UNIVERSITY
DEPARTMENT OF GEOSCIENCES
537 DEIKE BUILDING
UNIVERSITY PARK, PA 16801

RICHARD BARDZELL
ACIS
DCI/ACIS
WASHINGTON, DC 20505

DOUGLAS BAUMGARDT
ENSCO INC.
5400 PORT ROYAL ROAD
SPRINGFIELD, VA 22151

WILLIAM BENSON
NAS/COS
ROOM HA372
2001 WISCONSIN AVE. NW
WASHINGTON, DC 20007

ROBERT BLANDFORD
AFTAC
1300 N. 17TH STREET
SUITE 1450
ARLINGTON, VA 22209-2308

RHETT BUTLER
IRIS
1200 NEW YORK AVE., NW
SUITE 800
WASHINGTON, DC 20005

CATHERINE DE GROOT-HEDLIN
UNIVERSITY OF CALIFORNIA, SAN DIEGO
INSTITUTE OF GEOPHYSICS AND PLANETARY PHYSICS
8604 LA JOLLA SHORES DRIVE
SAN DIEGO, CA 92093

SEAN DORAN
ACIS
DCI/ACIS
WASHINGTON , DC 20505

RICHARD J. FANTEL
BUREAU OF MINES
DEPT OF INTERIOR, BLDG 20
DENVER FEDERAL CENTER
DENVER, CO 80225

RALPH ALEWINE
NTPO
1901 N. MOORE STREET, SUITE 609
ARLINGTON, VA 22209

MUAWIA BARAZANGI
INSTITUTE FOR THE STUDY OF THE CONTINENTS
3126 SNEE HALL
CORNELL UNIVERSITY
ITHACA, NY 14853

T.G. BARKER
MAXWELL TECHNOLOGIES
P.O. BOX 23558
SAN DIEGO, CA 92123

THERON J. BENNETT
MAXWELL TECHNOLOGIES
11800 SUNRISE VALLEY DRIVE SUITE 1212
RESTON, VA 22091

JONATHAN BERGER
UNIVERSITY OF CA, SAN DIEGO
SCRIPPS INSTITUTION OF OCEANOGRAPHY IGPP, 0225
9500 GILMAN DRIVE
LA JOLLA, CA 92093-0225

STEVEN BRATT
NTPO
1901 N. MOORE STREET, SUITE 609
ARLINGTON, VA 22209

LESLIE A. CASEY
DOE
1000 INDEPENDENCE AVE. SW
NN-20
WASHINGTON, DC 20585-0420

STANLEY DICKINSON
AFOSR
110 DUNCAN AVENUE, SUITE B115
BOLLING AFB
WASHINGTON, D.C. 20332-001

DIANE I. DOSER
DEPARTMENT OF GEOLOGICAL SCIENCES
THE UNIVERSITY OF TEXAS AT EL PASO
EL PASO, TX 79968

JOHN FILSON
ACIS/TMG/NTT
ROOM 6T11 NHB
WASHINGTON, DC 20505

1

MARK D. FISK
MISSION RESEARCH CORPORATION
735 STATE STREET
P.O. DRAWER 719
SANTA BARBARA, CA 93102-0719

ROBERT GEIL
DOE
PALAIS DES NATIONS, RM D615
GENEVA 10, SWITZERLAND

LORI GRANT
MULTIMAX, INC.
311C FOREST AVE. SUITE 3
PACIFIC GROVE, CA 93950

HENRY GRAY
SMU STATISTICS DEPARTMENT
P.O. BOX 750302
DALLAS, TX 75275-0302

I. N. GUPTA
MULTIMAX, INC.
1441 MCCORMICK DRIVE
LARGO, MD 20774

DAVID HARKRIDER
PHILLIPS LABORATORY
EARTH SCIENCES DIVISION
29 RANDOLPH ROAD
HANSCOM AFB, MA 01731-3010

JAMES HAYES
NSF
4201 WILSON BLVD., ROOM 785
ARLINGTON, VA 22230

THOMAS HEARN
NEW MEXICO STATE UNIVERSITY
DEPARTMENT OF PHYSICS
LAS CRUCES, NM 88003

MICHAEL HEDLIN
UNIVERSITY OF CALIFORNIA, SAN DIEGO
SCRIPPS INSTITUTION OF OCEANOGRAPHY IGPP, 0225
9500 GILMAN DRIVE
LA JOLLA, CA 92093-0225

DONALD HELMBERGER
CALIFORNIA INSTITUTE OF TECHNOLOGY
DIVISION OF GEOLOGICAL & PLANETARY SCIENCES
SEISMOLOGICAL LABORATORY
PASADENA, CA 91125

EUGENE HERRIN
SOUTHERN METHODIST UNIVERSITY
DEPARTMENT OF GEOLOGICAL SCIENCES
DALLAS, TX 75275-0395

ROBERT HERRMANN
ST. LOUIS UNIVERSITY
DEPARTMENT OF EARTH & ATMOSPHERIC SCIENCES
3507 LACLEDE AVENUE
ST. LOUIS, MO 63103

VINDELL HSU
HQ/AFTAC/TTR
1030 S. HIGHWAY A1A
PATRICK AFB, FL 32925-3002

ANTHONY IANNACCHIONE
BUREAU OF MINES
COCHRANE MILL ROAD
PO BOX 18070
PITTSBURGH, PA 15236-9986

RONG-SONG JIH
PHILLIPS LABORATORY
EARTH SCIENCES DIVISION
29 RANDOLPH ROAD
HANSCOM AFB, MA 01731-3010

THOMAS JORDAN
MASSACHUSETTS INSTITUTE OF TECHNOLOGY
EARTH, ATMOSPHERIC & PLANETARY SCIENCES
77 MASSACHUSETTS AVENUE, 54-918
CAMBRIDGE, MA 02139

LAWRENCE LIVERMORE NATIONAL LABORATORY
ATTN: TECHNICAL STAFF (PLS ROUTE)
PO BOX 808, MS L-200
LIVERMORE, CA 94551

LAWRENCE LIVERMORE NATIONAL LABORATORY
ATTN: TECHNICAL STAFF (PLS ROUTE)
PO BOX 808, MS L-207
LIVERMORE, CA 94551

LAWRENCE LIVERMORE NATIONAL LABORATORY
ATTN: TECHNICAL STAFF (PLS ROUTE)
PO BOX 808, MS L-221
LIVERMORE, CA 94551

LAWRENCE LIVERMORE NATIONAL LABORATORY
ATTN: TECHNICAL STAFF (PLS ROUTE)
LLNL
PO BOX 808, MS L-175
LIVERMORE, CA 94551

2

LAWRENCE LIVERMORE NATIONAL LABORATORY
ATTN: TECHNICAL STAFF (PLS ROUTE)
PO BOX 808, MS L-208
LIVERMORE, CA 94551

LAWRENCE LIVERMORE NATIONAL LABORATORY
ATTN: TECHNICAL STAFF (PLS ROUTE)
PO BOX 808, MS L-202
LIVERMORE, CA 94551

LAWRENCE LIVERMORE NATIONAL LABORATORY
ATTN: TECHNICAL STAFF (PLS ROUTE)
PO BOX 808, MS L-195
LIVERMORE, CA 94551

LAWRENCE LIVERMORE NATIONAL LABORATORY
ATTN: TECHNICAL STAFF (PLS ROUTE)
PO BOX 808, MS L-205
LIVERMORE, CA 94551

THORNE LAY
UNIVERSITY OF CALIFORNIA, SANTA CRUZ
EARTH SCIENCES DEPARTMENT
EARTH & MARINE SCIENCE BUILDING
SANTA CRUZ, CA 95064

ANATOLI L. LEVSHIN
DEPARTMENT OF PHYSICS
UNIVERSITY OF COLORADO
CAMPUS BOX 390
BOULDER, CO 80309-0309

DONALD A. LINGER
DNA
6801 TELEGRAPH ROAD
ALEXANDRIA, VA 22310

LOS ALAMOS NATIONAL LABORATORY
ATTN: TECHNICAL STAFF (PLS ROUTE)
PO BOX 1663, MS F659
LOS ALAMOS, NM 87545

LOS ALAMOS NATIONAL LABORATORY
ATTN: TECHNICAL STAFF (PLS ROUTE)
PO BOX 1663, MS F665
LOS ALAMOS, NM 87545

LOS ALAMOS NATIONAL LABORATORY
ATTN: TECHNICAL STAFF (PLS ROUTE)
PO BOX 1663, MS D460
LOS ALAMOS, NM 87545

LOS ALAMOS NATIONAL LABORATORY
ATTN: TECHNICAL STAFF (PLS ROUTE)
PO BOX 1663, MS C335
LOS ALAMOS, NM 87545

GARY MCCARTOR
SOUTHERN METHODIST UNIVERSITY
DEPARTMENT OF PHYSICS
DALLAS, TX 75275-0395

KEITH MCLAUGHLIN
MAXWELL TECHNOLOGIES
P.O. BOX 23558
SAN DIEGO, CA 92123

BRIAN MITCHELL
DEPARTMENT OF EARTH & ATMOSPHERIC SCIENCES
ST. LOUIS UNIVERSITY
3507 LACLEDE AVENUE
ST. LOUIS, MO 63103

RICHARD MORROW
USACDA/IVI
320 21ST STREET, N.W.
WASHINGTON, DC 20451

JOHN MURPHY
MAXWELL TECHNOLOGIES
11800 SUNRISE VALLEY DRIVE SUITE 1212
RESTON, VA 22091

JAMES NI
NEW MEXICO STATE UNIVERSITY
DEPARTMENT OF PHYSICS
LAS CRUCES, NM 88003

JOHN ORCUTT
INSTITUTE OF GEOPHYSICS AND PLANETARY PHYSICS
UNIVERSITY OF CALIFORNIA, SAN DIEGO
LA JOLLA, CA 92093

PACIFIC NORTHWEST NATIONAL LABORATORY
ATTN: TECHNICAL STAFF (PLS ROUTE)
PO BOX 999, MS K6-48
RICHLAND, WA 99352

PACIFIC NORTHWEST NATIONAL LABORATORY
ATTN: TECHNICAL STAFF (PLS ROUTE)
PO BOX 999, MS K7-34
RICHLAND, WA 99352

PACIFIC NORTHWEST NATIONAL LABORATORY
ATTN: TECHNICAL STAFF (PLS ROUTE)
PO BOX 999, MS K6-40
RICHLAND, WA 99352

PACIFIC NORTHWEST NATIONAL LABORATORY
ATTN: TECHNICAL STAFF (PLS ROUTE)
PO BOX 999, MS K5-12
RICHLAND, WA 99352

KEITH PRIESTLEY
DEPARTMENT OF EARTH SCIENCES
UNIVERSITY OF CAMBRIDGE
MADINGLEY RISE, MADINGLEY ROAD
CAMBRIDGE, CB3 OEZ UK

PAUL RICHARDS
COLUMBIA UNIVERSITY
LAMONT-DOHERTY EARTH OBSERVATORY
PALISADES, NY 10964

CHANDAN SAIKIA
WOOODWARD-CLYDE FEDERAL SERVICES
566 EL DORADO ST., SUITE 100
PASADENA, CA 91101-2560

SANDIA NATIONAL LABORATORY
ATTN: TECHNICAL STAFF (PLS ROUTE)
DEPT. 5791
MS 0567, PO BOX 5800
ALBUQUERQUE, NM 87185-0567

SANDIA NATIONAL LABORATORY
ATTN: TECHNICAL STAFF (PLS ROUTE)
DEPT. 5704
MS 0655, PO BOX 5800
ALBUQUERQUE, NM 87185-0655

THOMAS SERENO JR.
SCIENCE APPLICATIONS INTERNATIONAL
CORPORATION
10260 CAMPUS POINT DRIVE
SAN DIEGO, CA 92121

ROBERT SHUMWAY
410 MRAK HALL
DIVISION OF STATISTICS
UNIVERSITY OF CALIFORNIA
DAVIS, CA 95616-8671

DAVID SIMPSON
IRIS
1200 NEW YORK AVE., NW
SUITE 800
WASHINGTON, DC 20005

PACIFIC NORTHWEST NATIONAL LABORATORY
ATTN: TECHNICAL STAFF (PLS ROUTE)
PO BOX 999, MS K6-84
RICHLAND, WA 99352

FRANK PILOTTE
HQ/AFTAC/TT
1030 S. HIGHWAY A1A
PATRICK AFB, FL 32925-3002

JAY PULLI
BBN
1300 NORTH 17TH STREET
ROSSLYN, VA 22209

DAVID RUSSELL
HQ AFTAC/TTR
1030 SOUTH HIGHWAY A1A
PATRICK AFB, FL 32925-3002

SANDIA NATIONAL LABORATORY
ATTN: TECHNICAL STAFF (PLS ROUTE)
DEPT. 5704
MS 0979, PO BOX 5800
ALBUQUERQUE, NM 87185-0979

SANDIA NATIONAL LABORATORY
ATTN: TECHNICAL STAFF (PLS ROUTE)
DEPT. 9311
MS 1159, PO BOX 5800
ALBUQUERQUE, NM 87185-1159

SANDIA NATIONAL LABORATORY
ATTN: TECHNICAL STAFF (PLS ROUTE)
DEPT. 5736
MS 0655, PO BOX 5800
ALBUQUERQUE, NM 87185-0655

AVI SHAPIRA
SEISMOLOGY DIVISION
THE INSTITUTE FOR PETROLEUM RESEARCH AND
GEOPHYSICS
P.O.B. 2286, NOLON 58122 ISRAEL

MATTHEW SIBOL
ENSCO, INC.
445 PINEDA COURT
MELBOURNE, FL 32940

JEFFRY STEVENS
MAXWELL TECHNOLOGIES
P.O. BOX 23558
SAN DIEGO, CA 92123

4

BRIAN SULLIVAN
BOSTON COLLEGE
INSITUTE FOR SPACE RESEARCH
140 COMMONWEALTH AVENUE
CHESTNUT HILL, MA 02167

NAFI TOKSOZ
EARTH RESOURCES LABORATORY, M.I.T.
42 CARLTON STREET, E34-440
CAMBRIDGE, MA 02142

GREG VAN DER VINK
IRIS
1200 NEW YORK AVE., NW
SUITE 800
WASHINGTON, DC 20005

TERRY WALLACE
UNIVERSITY OF ARIZONA
DEPARTMENT OF GEOSCIENCES
BUILDING #77
TUCSON, AZ 85721

JAMES WHITCOMB
NSF
NSF/ISC OPERATIONS/EAR-785
4201 WILSON BLVD., ROOM785
ARLINGTON, VA 22230

JIAKANG XIE
COLUMBIA UNIVERSITY
LAMONT DOHERTY EARTH OBSERVATORY
ROUTE 9W
PALISADES, NY 10964

OFFICE OF THE SECRETARY OF DEFENSE
DDR&E
WASHINGTON, DC 20330

TACTEC
BATTELLE MEMORIAL INSTITUTE
505 KING AVENUE
COLUMBUS, OH 43201 (FINAL REPORT)

PHILLIPS LABORATORY
ATTN: GPE
29 RANDOLPH ROAD
HANSCOM AFB, MA 01731-3010

PHILLIPS LABORATORY
ATTN: PL/SUL
3550 ABERDEEN AVE SE
KIRTLAND, NM 87117-5776 (2 COPIES)

DAVID THOMAS
ISEE
29100 AURORA ROAD
CLEVELAND, OH 44139

LAWRENCE TURNBULL
ACIS
DCI/ACIS
WASHINGTON, DC 20505

FRANK VERNON
UNIVERSITY OF CALIFORNIA, SAN DIEGO
SCRIPPS INSTITUTION OF OCEANOGRAPHY IGPP, 0225
9500 GILMAN DRIVE
LA JOLLA, CA 92093-0225

DANIEL WEILL
NSF
EAR-785
4201 WILSON BLVD., ROOM 785
ARLINGTON, VA 22230

RU SHAN WU
UNIVERSITY OF CALIFORNIA SANTA CRUZ
EARTH SCIENCES DEPT.
1156 HIGH STREET
SANTA CRUZ, CA 95064

JAMES E. ZOLLWEG
BOISE STATE UNIVERSITY
GEOSCIENCES DEPT.
1910 UNIVERSITY DRIVE
BOISE, ID 83725

DEFENSE TECHNICAL INFORMATION CENTER
8725 JOHN J. KINGMAN ROAD
FT BELVOIR, VA 22060-6218 (2 COPIES)

PHILLIPS LABORATORY
ATTN: GPBP
29 RANDOLPH ROAD
HANSCOM AFB, MA 01731-3010

PHILLIPS LABORATORY
ATTN: RESEARCH LIBRARY/TL
5 WRIGHT STREET
HANSCOM AFB, MA 01731-3004